2015

Mechanical Properties of Cold-drawn Steel Strand at Elevated Temperatures

Conor Thompson
Lehigh University

Mechanical Properties of Cold-drawn Steel Strand at Elevated Temperatures

By

Conor Thompson

A Thesis
Presented to the Graduate and Research Committee
of Lehigh University
in Candidacy for the Degree of
Master of Science

in
Structural Engineering

Lehigh University
August 2015

This thesis is accepted and approved in partial fulfillment of the requirements
for the Master of Science

_____
Date

_____
Dr. Spencer Quiel, Thesis Adviser

_____
Dr. Panos Diplas, Department Chairperson

Acknowledgements

First, I would like to thank my family. Without their love and support this thesis would not have been possible. My parents' interest in my work and their reassurance helped me to stay positive throughout the process. Lunch trips and weekend visits with my extended family provided me with additional motivation and encouragement.

I would also like to thank Lehigh University for being my home for the past five years and for providing me with the Presidential Scholarship, which paid for my graduate school tuition. Thanks to the PITA program (www.pitapa.org) for providing funding for the experimental portion of this study.

The professors and staff at Lehigh's Civil Engineering Department have had a huge impact on my life. I would like to thank you all for you not only providing me with my engineering background but also for my professional development. Many of you have gone above and beyond the call of a professor, and I am extremely grateful for your mentorship. I also would like to acknowledge Dr. Moyer and the Material Science Department at Lehigh for the help with the microstructure analysis.

I would like to thank the staff at ATLSS Lab. Darrick Fritchman and Peter Bryan all took interest in my research and provided support. I owe great thanks to Carl Bowman for his help and guidance during instrumentation, testing, and problem solving. Andrew Hansen and Sarah Dudney were extremely helpful during the experimental testing. Thanks to both of you for volunteering your time and waking up early on Friday mornings.

Lastly, I would like to thank my thesis adviser Dr. Quiel for his role in this project. His calm demeanor and constant reassurance kept me grounded and on track during this process. I am very grateful for his guidance in this project and in my professional life.

Table of Contents

List of Tables

List of Figures

Abstract

Fire is a one of the most serious threats that a structure may experience during its service life. Thermal expansion, extreme temperature gradients, and degrading material properties can lead to structural failure. Structural fire resistance is addressed in building codes; however fire resistance for bridge structures is not subject to the same standards. Past researchers have shown that while bridge fires are a low probability event, the outcome is often of high consequence. Recent fires on cable-stayed bridges have led to stay cable loss. Past research has shown that cold-drawn steel is more susceptible to mechanical property degradation compared to hot-rolled steel. To ensure that the current standards of practice accurately predict the behavior of cold-drawn steel at elevated temperature, an experimental study was conducted at Lehigh University. Samples of 7-wire ASTM A416-12a steel strand were tested in tension using an electrically heated ceramic furnace and a universal testing machine. The stress strain behavior along with the ultimate strength and elastic modulus were determined through constant temperature testing. The rupture temperature was determined through a series of transient temperature tests. A metallurgical microstructure analysis was conducted on samples from the constant temperature testing to observe changes in the steel microstructure. The test methods were modelled after past research and the rate of loading and sample sizes conformed to current ASTM standards. The test results showed good agreement with the current reduction values for ultimate strength found in ACI 216 (2014). Faster heating rates provide a more conservative rupture temperature due to incomplete microstructure reorganization in the absence of an extended thermal soak. And the current data also shows that the Eurocode material model for cold-drawn steel at elevated temperature does not accurate predict the stress-strain behavior of these strands. Modifications to the Eurocode material model are proposed. This model is more suitable for a performance based approach to structural fire resistant design of cable-stayed bridges.

Chapter 1 Introduction

1.1 General

This thesis presents the results of an experimental investigation of the tensile properties of cold-drawn steel cable at elevated temperature. The program includes tests at both constant and transient temperature along with a metallurgical microstructure analysis of the steel after heating. In this chapter the motivation for research is presented as well as the objectives and scope of the project.

1.2 Motivation for Research

Structures subject to fire experience large thermal strains, reductions in material properties, and, in some cases, irrecoverable losses. Fire can be the most extreme hazard that a structure experiences in its life. For this reason, extensive fire resistance is put in place for buildings. However, bridges do not have the same level of detail in prescribed fire protection. Giuliana (2012) refers to bridge fire as a low probability / high consequence (LPHC) event. When bridge fire is compared to other LPHC events, such as earthquake or large vessel impact, there is little to no design concern. As stated by Giuliana, "the design against fire and explosion in particular is mostly limited to the case of buildings and hardly considered in the design of bridges." A literature review by Garlock et al. (2012) outlined recent bridge fire events and outlines a need for studying the 'high temperature properties of the new construction materials used in bridges'. In the same paper, a New York Department of Transportation survey from 2008 listed fire as the fourth most likely cause of bridge failure. Bridge failure often involves many casualties and is associated with a high economic cost. The United States economy is reliant upon the transportation infrastructure. The cost in repairs for the MacArthur Maze bridge fire was estimated at $9 million USD and the economic loss was close to $6 million USD per day of to the San Francisco area (Garlock et al. 2012).

Zoli (2007) points out that the design of bridges for member loss is only typical of cable-stay bridges. The Post-Tensioning Institute (PTI) publishes the *PTI Recommendations for Stay Cable Design* (2012), in this manual, cable-stay bridges are to consider the abrupt loss of a member. This is done by including dynamic increase factors and alternate load path analysis. The design of cable loss is not a federal standard and is not included in AASHTO. Further, the PTI manual suggests a cable loss dynamic factor (CLDF) of 0.0, suggesting that the event of fire is considered a gradual process producing no dynamic forces at the alternate load path.

Two recent cable-stay bridge events highlight the concern for fire hazard. The Mezcala Bridge in Mexico was closed after a fire resulted in the loss of a stay cable (Zoli and Steinhouse 2007). An accident involving a school bus and a truck transporting coconuts ignited the fire. The stay cable was replaced and the bridge was later reopened. While this bridge was designed to handle the loss of a single cable, Zoli (2007) poses the question, "would this bridge have survived the loss of two or three adjacent cables?" Another event occurred 2005 in Greece (Zoli and Steinhouse 2007) The Rion Antirion Bridge was struck by lightning six months after opening. The lightning strike ignited a fire and caused socket failure, resulting in the loss of a single stay cable.

To ensure that bridges are able to survive these LPHC fire events, Gross and Cauffman (2011) suggest treating fire as a design load. This is accomplished during the analysis and design of bridges in a performance based design approach. Building fire design is typically handled using prescriptive ratings based on the length of exposure to the ASTM E119 fire curve (Gross and Cauffman 2011; PTI 2006) however the type of fire that would occur on a bridge is different than a building fire. Building fires are typically compartment fires that consume the combustible materials in the room. Bridge fires typically involve vehicles and, potentially, hydrocarbon fuels. These incidents result in plume fires

where a building fire is usually considered as a confined compartment fire (Gross and Cauffman 2011). Figure 1 shows that the hydrocarbon curve experiences a more rapid rise to a higher maximum temperature than the E119 curve for building fires. The structural elements in bridge systems are also different than building systems. Bridges, for instance, may have long spanning steel girders, prestressed concrete beams, stay cables, or suspension cables. The non-standard design of bridges does not allow for the same type of single component based fire testing that building systems have used for decades. Thus, performance based approach is more suitable for bridge fires.

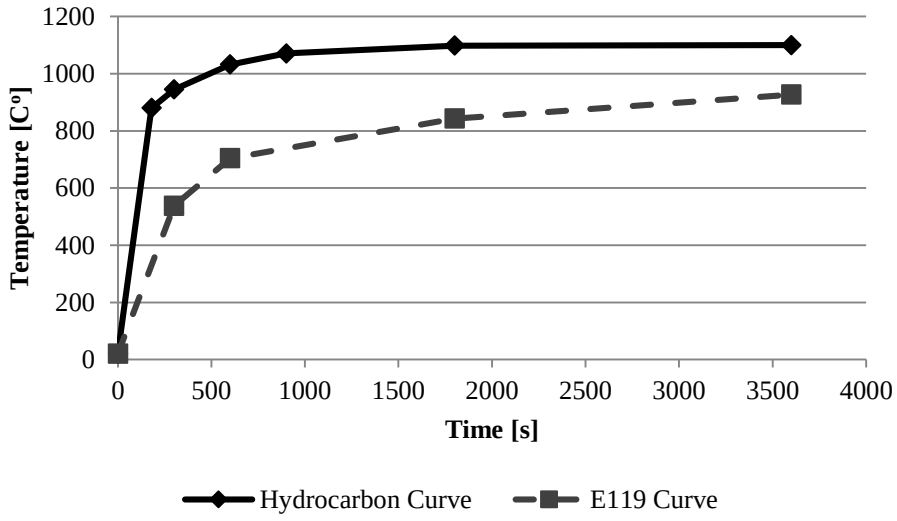

Figure 1: Standard Fire Curves

In this type of design, the interaction between a proposed fire and the structural members is explicitly analyzed, rather than using a prescriptive fire resistance rating approach. Gross and Cauffman conclude that for performance based design to be implemented, experiments must be conducted to verify bridge fire response.

The mechanical properties of steel are known to decrease with temperature. The properties of cold-drawn steel are more susceptible to elevated temperature and degrade at an earlier rate when compared to hot-rolled mild steel. Elevated temperature essentially works against the material microstructure of cold-working by allowing the stacked discontinuities to slip more easily. For this

reason, it is imperative that the correct strength curve be selected when designing steel structures. The cold-drawn steel curve found in ACI 216 (ACI 216.1-14) is based on research performed in 1961 by Abrams and Cruz. The steel used in that experimental study was commercially available grade 250 ksi 7-wire strand, equivalent to ASTM A416 strand (The earliest ASTM A416 is from 1974). The 1961 study was conducted for applications of prestressed concrete. Thus, the researchers chose heating rates and service level stresses that were applicable to prestressed concrete beams. Today, we are using the same ACI 216 curve yet the applications are not limited to prestressed concrete. As the chemical and mechanical properties of structural steel have changed over time, it is important to ensure that the past standards of practice still apply.

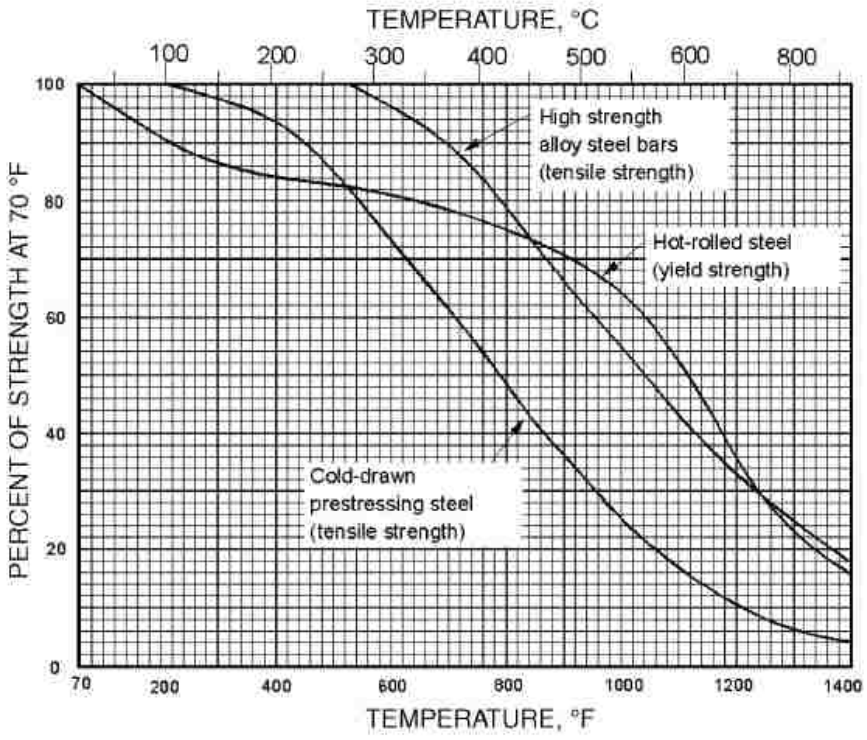

Figure 2: ACI 216 Steel Strength Curves (ACI 2014)

1.3 Research Objectives

The objective of the research program is to determine the tensile properties of commercially available cold-drawn steel strand at elevated temperature. The focus of this thesis will be ASTM A416 7-wire strand, which is commonly used in stay cables for bridge applications. The results from the experimental program will be compared to the existing standards in practice, and recommendations for further study will be presented. The testing objectives are as follows:

1. Create a test set-up and procedure that can be easily replicated for repetition and future study
2. Determine the mechanical properties of the steel strand specimens, including:
    2.1. The reduction in ultimate strength at elevated temperature
    2.2. The rupture temperature of steel strand when held at a constant stress level
    2.3. The reduction in the elastic modulus at elevated temperature
3. Determine the temperature effects on the microstructure of cold-drawn steel cable
4. Determine the effect of the heating rate of the mechanical properties of cold-drawn steel cable
5. Compare the result to data in existing standards and other references

1.4 Scope of Research

The remainder of the thesis is divided into five chapters. Chapter 2 is focused on the background of the behavior of structural steel at elevated temperature along with a literature review of the past research on the mechanical properties of cold-drawn steel cable at elevated temperature. Chapter 3 outlines the testing program and the experimental setup and procedures. Chapter 4 presents the results of the testing program. Chapter 5 provides an evaluation of the test results. Chapter 6 summarizes the results of the thesis, and also provides conclusions and recommendations for future research on this topic.

Chapter 2 Background

2.1 General

In this chapter the background of this research topic is presented. The background includes information about the cold-drawn fabrication process used to make steel strand. The mechanical properties of cold drawn steel are presented alongside the properties of mild steel. The current practice of fire protection engineering as it relates to cold-drawn strand and bridge engineering is discussed. Lastly, a literature review is presented which details the work previously completed on the mechanical properties of cold drawn steel strand at elevated temperatures.

2.2 Mechanical Properties of Steel

Steel is an alloy consisting of iron and carbon (carbon being between 0.002% and 2.1% weight). Some steel grades known as carbon steels (ASTM A36 for example) consist entirely of these two elements. Other steels consist of various combinations of other alloy metals in order to achieve desired characteristics like higher strength or hardness (ASTM A992 for example). Steel is a popular construction material due to its high tensile strength, ease of construction, and lower cost relative to other metallic construction materials. Steel has a wide variety of structural uses such as wide flange steel beams, rebar, and cable tension elements to name a few.

The two main types of steel are mild steel and cold-worked steel. The two names come from the processes used to manufacture the steel. Mild steel is produced by working the steel at temperatures above the recrystallization temperature. To ensure that the metal is above the recrystallization temperature a safety factor 50^{o}C to 100^{o}C above the recrystallization temperature is typical

(DeGarmo and Kohser 1988). Cold-worked steel, on the other hand, is formed at temperatures below the recrystallization temperature.

Cold-working is the process of plastically deforming the alloy in order to increase the hardness and strength. The increase in strength and hardness also leads to a decrease in the ductility of the alloy. This phenomenon can also be referred to as strain-hardening. The process of cold-working is explained by Callister and Rethwisch (2008) as an increase in the dislocation density which in turn increases the stress required to deform the metal. The strength required to deform the alloy increases with the amount of cold-working performed. The cold-working properties can be removed by subjecting the steel to elevated temperature through a process known as recovery.

Mild and cold-worked steel have some properties that vary. Some thermal and mechanical properties are relatively unaffected by the metalworking process such as the elastic modulus, the temperature varying specific heat, and the thermal conductivity. However, the mechanical properties at ambient and elevated temperature of mild and cold-drawn steel are significantly different.

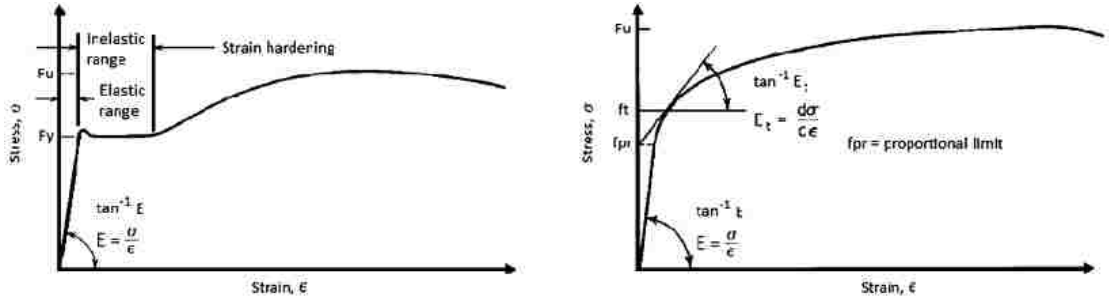

[redacted]

[redacted]

Figure 3 shows the stress strain behavior of mild steel (A) and cold-drawn steel (B). The mild steel has a distinctive yield point followed by a yield plateau. The yield plateau transitions to a nonlinear strain hardening zone before the ultimate strain is reached. The cold-drawn steel does not have a distinctive yield peak and transitions directly from the linear elastic zone to a nonlinear strain hardening zone.

Cold-worked steels typically have higher strength and lower ductility compared to mild steels. As mentioned, the mechanical properties that are changed during the cold-working process can be recovered at elevated temperature. Cold-worked steels will therefore experience greater reductions in mechanical properties at elevated temperatures. Figure 4 shows the Eurocode (2004) reduction factors for the design yield stress. The reduction factor for cold-drawn steel forms an S-shaped curve which begins to decrease at 200ºC. The decrease is constant until approximately 600ºC where the curve begins to flatten out. The reduction for cold-drawn steel is always greater than the reduction for mild steel, and it is essential that the appropriate reduction factor is used in practice.

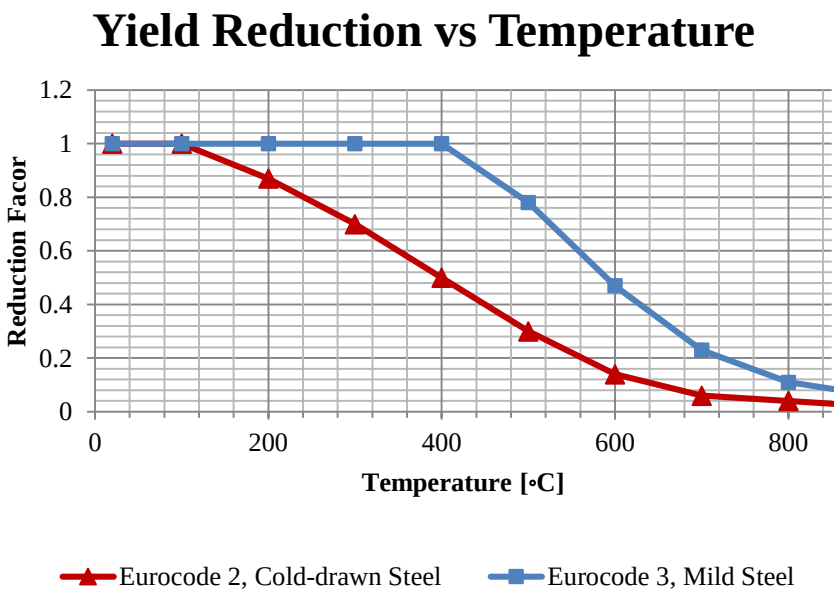

Figure 4: Eurocode Material Model Yield Reduction Factors

These reduction values are used in the Eurocode (2004) stress-strain model for mild and cold-drawn steel at elevated temperature. This material model modifies the assumed elastic-perfectly plastic model that is commonly used for steels at room temperature (Franssen and Zaharia (2005)). The elevated temperature model is made up of a linear elastic region, a parabolic region, a perfectly plastic region, and a linearly declining region that models the decline in strength at very high strains. Figure 5 shows the stress strain model that can be modified to represent both mild and cold-drawn steels at temperatures between 20ºC and 1200ºC. The equation parameters and reduction values are provided in Table 2 and Table 3. This material model uses the same equation for both cold-drawn and mild steel but the reduction values are different. As shown above, the yield reduction is more severe for cold-drawn steel. The proportionality limit (Figure 8) follows a similar trend and the proportionality limit reduction is more severe for the cold-drawn steel. However, the elastic modulus is relatively the same for mild and cold-drawn steel at elevated temperature as shown in Figure 7.Figure 8

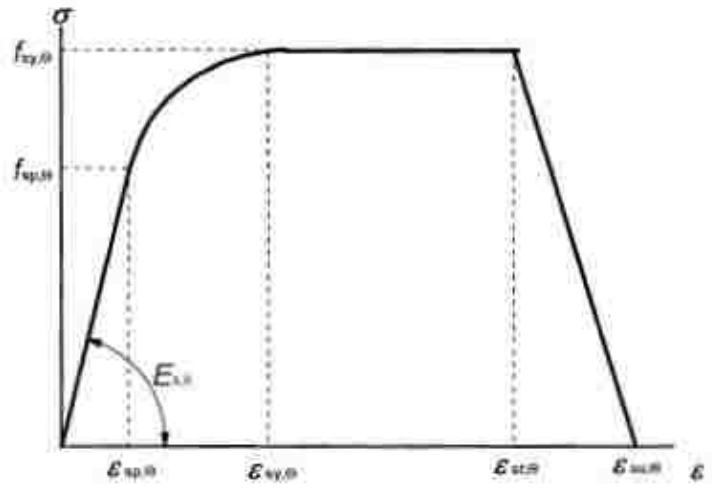

Figure 5: Eurocode (2004) Stress-Strain Material Model for Mild Steel

The stress-strain models of cold-drawn steel between 20°C and 800°C are shown in Figure 6. This material model does not include the strain-hardening effects of cold-drawn steel. The model assumes that once the yield stress is reached, the steel will behave perfectly plastic until it reaches the ultimate strain limit. At that point, the steel stress declines until rupture. One of the goals of the current study is to update this stress-strain model to include the strain-hardening zone. For a performance-based design for fire-resistant structures, it is important to use a model that predicts the actual behavior of the material. For this reason, modifications to the Eurocode (2004) material model are presented in Chapter 5.

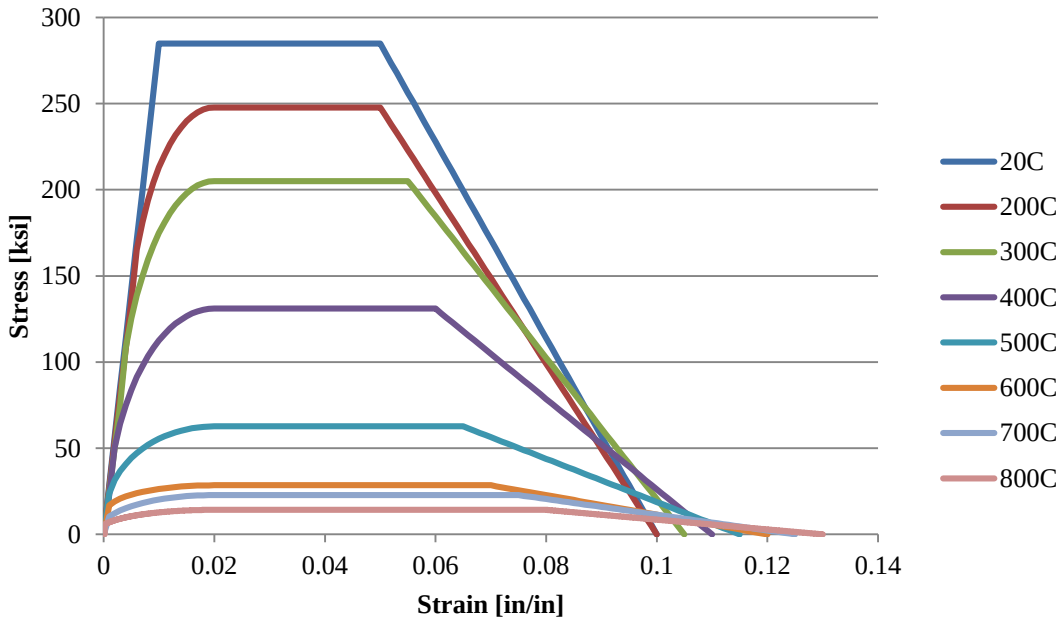

Figure 6: Eurocode Stress-Strain Model for Cold-drawn steel

2.3 7-Wire Strand Manufacturing Process

The production of multi-wire steel strand begins with the descaling of hot-rolled wire rod. The wire-rod (now free of mill scale) is then lubricated in order to protect the wire from wear and failure during the cold drawing process. The lubricated wire-rod is drawn through a series of carbide dies until it achieves the desired mechanical properties. A416 7-wire strand (ASTM A416-12a) used in this study was manufactured by Sumiden Wire Products Corporation (SWPC). The SWPC process uses 8 or 9 carbide dies, reduces the original cross section area by approximately 85%, and increases the tensile strength from ~172 ksi to the minimum required strength of 270 ksi (SWPC 2015). The chemical composition of the steel wires must meet the requirements of Table 1. The individual steel wires are stranded by wrapping six wire strands helically around a central core wire. The difference in measured diameter between the core wire and any of the strand wires must be within the tolerance required by ASTM A416 specifications for 7-wire steel strand. For the 0.6 diameter strand used in this testing program, the maximum difference in diameter is 0.004 inches (ASTM A416-12). Once the steel wires are stranded it is then stress relieved and stretched by applying a tensile load at elevated temperature. This process removes residual stresses created during the manufacturing process and also gives the strand the low-relaxation property.

Table 1: Sumiden Wire Products Base Chemistry Specifications

Chemistry- Base specification ASTM A510-1080 Modified per SWPC Specification

Element	C Carbon	Mn Manganese	P Phosphorus	S Sulfur	Cr Chromium	V Vanadium	Cu Copper	Si Silicon
Min (%)	0.81	0.75	N/A	N/A	N/A	N/A	N/A	0.15
Max (%)	0.84	0.85	0.020	0.020	0.15	0.05	0.15	0.35

2.4 Structural Fire Engineering

It is well known that fire is a severe hazard and poses a threat to both buildings and bridges. Fire subjects the structure to thermal elongation and weakened material properties. Because fire is such a severe threat, codes and specifications have been put in place to minimize its potential. The basic concepts of structural fire engineering are to prevent structural collapse, contain the spread of fire, and to limit the damage. Life safety and economic impact are the primary factors that govern the required fire resistance. Fire resistance is provided through passive and active systems. Passive systems, such as intumescent paints and sprayed on fire resistant materials, are always in place. Active systems, such as sprinkler systems, fire extinguishers, or oxygen suppression systems, require a triggering mechanism before they provide fire suppression. Fire resistant design of structures can be simply expressed as followed:

$$Required\ Fire\ Resistance \leq Provided\ Fire\ Resistance \quad (1)$$

For buildings, the required fire resistance is a function of the type of construction, type of structural element, the importance factor, and the height or area. The provided fire resistance is a function of the structural member's ability to maintain its function at elevated temperature. Structural fire resistance for buildings is required by the International Building Code (IBC 2012). Specifications often provide guidance in terms of what is required and how to achieve that resistance (AISC 2011; ACI 216.1-14).

Building fire resistance is typically achieved via a prescriptive approach (Gross and Cauffman 2011; PTI 2006). In the prescriptive approach to fire resistance, engineers determine the required fire resistance based on building and construction classifications and then select building materials and/or fire suppression systems that provide the required fire resistance rating.

Historically, both the required fire resistance and provided fire resistance are derived in units of hours. The provided fire resistances are based on the ASTM E-119 Standard Fire Test (ASTM 2014). To date, a wide range of E-119 tests have been performed for a variety of building assemblies, and the results are published to help engineers choose structural components (reference UL standards). The time ratings are loosely correlated to the time of egress in the event of a fire and can be generally used to ensure the safety of the fire-fighters who attempt to suppress the fire.

There are three categories for which specimens are assessed: load bearing capacity, integrity, and temperature on the unexposed side (ASTM E-119-14). Specimens do not necessarily need to pass all three categories for the test to be a success. For example, beams and columns are only required to maintain the load bearing capacity while a non-load bearing wall may be required to maintain integrity and meet a maximum temperature requirement for the unexposed side.

Fire protection for bridges is specified by the National Fire Protection Association (NFPA) 502, *Standard for road tunnels, bridges, and other limited access highways* (NFPA 2001). The three categories required by NFPA 502 are as follows:

1. Maintain life safety
2. Mitigate structural damage and prevent progressive structural collapse
3. Minimize economic impact

The standard does not provide guidance on how to meet the requirements, and the engineer must decide what level of protection to provide.

The Post-Tensioning Institute (PTI) published a document called the Recommendations for Stay Cable Design (PTI 2012). In this reference book, minimum fire resistance for stay cables is specified as follows: "Fire rating requirements will be established by the Owner if these are to be a project criterion." In lieu of Owner requirements, a 30-minute minimum time rating based on the E-119 fire curve is required. The stay strand and stay system are subject an external heat source of 1100^{o}C (The furnace must be capable of reaching 1100^{o}C within the first five minutes of testing and maintain this temperature throughout the test) and must maintain a temperature below 300^{o}C for at least 30 minutes. If the stay cable and stay system meet the temperature requirements, the test shall be repeated in a tension frame where the tension element is placed at 45% minimum ultimate tensile strength (MUTS). The stay cable must maintain the load without slip for at least 30 minutes. The 300^{o}C temperature is chosen because it is known that the cold-drawn steel used in cable stay design enters the plastic domain at 400^{o}C and the HDPE material used to prevent cable corrosion ignites at 330^{o}C. When the HDPE ignites, there is a sudden increase in cable temperature (PTI, 2012).

The PTI required resistance is based on the E-119 fire curve and is a prescriptive design approach. Performance based fire design is an alternative to the prescriptive approach. Performance design still needs to meet the same basic objects as prescriptive design, but it is not limited to the published E-119 test results. In this type of structural fire design, the engineer selects the design fire that the structure is exposed to, performs a heat transfer analysis, and then calculates the structural response.

2.5 Past Research

Many previous experimental studies examined the tensile properties of mild steel at elevated temperature. Cold-drawn steel strand has received less attention, and most test programs were performed prior to 1970. The results from past experiments have not been verified in recent years, and the composition of steel may change depending on the country of origin and the year of manufacturing. The data from the Abrams and Cruz experiment is used in ACI, PCI, and PTI for the tensile strength reduction curves of prestressed steel. Other researchers have shown interest in the mechanical properties of single tendons from the 7-wire strand, residual strength testing, and the mechanical properties of similar steels (A421). Due to the difficult nature of gripping 7-wire strand for a tensile test, many researcher chose to experiment using the single wire approach. This section outlines the past work done on this topic in chronological fashion.

1.4.1 Abrams and Cruz, 1961

Abrams and Cruz performed two series of tensile tests on heated specimens consisting of commercially available 7-wire stress-relieved Grade 250 ksi strand. Both sets of tests were performed using 3/8-inch diameter strand, a universal testing machine, and an electric furnace. During the first phase of testing, the strand was initially loaded to a set stress level and then heated until failure. The initial prestress was selected at 55 and 70% minimum ultimate tensile strength (MUTS) and the heating rates were chosen at a rate 5, 10, and 15 ^{0}F/min (2.8, 5.5, and 8.3 ^{0}C/min) to mimic the heating rate of prestressed strands imbedded in concrete. The prestressing level was maintained during the test and the temperature at rupture was recorded. The rupture temperature for the 55% and 70% MUTS prestressing was approximately 800^{0}F and 600^{0}F, respectively (426^{0}C and 315.5^{0}C). It was found that the heating rate had only a slight effect on the rupture temperature. Prolonged heating tests were also performed to determine

whether sustained exposure to elevated temperature changes the rupture temperature. During the sustained heating tests, the 3/8-inch diameter strand was stressed to 55% MUTS and heated to 400^0F and 600^0F. After being held constant for an increment of either 30 or 60 minutes, the temperature was increased until rupture. Abrams and Cruz found that prolonged heated did not change the rupture temperature.

The tensile strength testing was conducted on the 3/8-inch diameter strand to determine the reduction in ultimate strength at elevated temperature. The specimen was placed in the test frame and heated at 10^0F/minute (5.5^0C/minute) until the specimen reached its desired level. Once the set temperature was reached the breaking strength was determined. This experiment was repeated for set temperatures between 200^0F and 1400^0F at 200^0F intervals. The test results showed that at temperature of 400^0F (204.4^0C), less than 10% ultimate strength was lost, while 50% ultimate strength is lost at 800^0F (427^0C). The test was also carried out on strands of ¼ and 7/16-inch diameter and it was found that the strand size does not affect the percent loss of ultimate strength.

Metallurgy was conducted on samples that were heated for longer periods. It was observed that spheroidization of the carbide took place in a strand that was heated to 1300^0F for 6 hours, and to a lesser extent when only heated for 2 hours. A specimen heated to 800^0F for 6 hours had maintained a similar microstructure to that of the unheated strand.

1.4.2 Harmathy and Stanzak, 1970

Harmathy and Stanzak tested the tensile properties of A421 prestressing steel wire and presented the results. The goal of the test program was to determine the tensile properties at elevated temperature. The authors also examined the microstructure of the steel specimens after heating

and cooling. The wires tested were 0.794% carbon A421-65 steel wire. The test was carried out using a 30-kip universal testing machine with a cylindrical tube furnace.

The tensile test procedure was to heat the specimen to the desired temperature, wait for the specimen to reach steady state, and then test the specimen in tension. During the tensile test, the furnace temperature was raised to the target level and maintained once the specimen thermocouple reached a quasi-steady-state status. This status was generally reached 60 to 90 minutes after the start of heating. The results provided complete stress-strain curves which the authors mention as being "of some interest to design engineers concerned with rapid plastic deformations," because "such complete stress-strain curves are generally not available." The test procedure did not include a direct measurement of the elastic modulus of the steel because the modulus is known to remain independent of the steel microstructure as shown by past research. The temperature-induced modulus decrease for cold-drawn strand would therefore be expected to be similar to that of mild steel. The testing was carried out at three separate strain rates and it was concluded that for temperature below 700^0F, the strain rate did not considerably affect the shape of the stress-strain curves. The authors make note that the spheroidization of the pearlite lamellae microstructure may take several days to occur at temperatures of 800^0F, however, at 1200^0F this process can occur within hours. This phenomena is important for prestressing steel because the high strength properties are a function of the lamellar pearlite structure. When spheroidization occurs, the pearlite loses its lamellar structure as the lamellae of cementite form into globules. When the steel is heated above 732°C (1350^0F), known as the eutectoid temperature, the original microstructure is completely changed from the initial cold-worked state.

The results show that up to temperatures of 400^0F, there is no significant loss in ultimate strength. Past 400^0F, there is a sharp decrease in ultimate strength as the specimen temperature increases.

The yield stress data show a more significant decline in the yield limit up to 500^0F when compared to the initial ultimate strength loss. Past 500^0F, the yield stress rapidly decreases with temperature.

1.4.3 Holmes et al., 1982

Holmes et al. performed three series of experiments to determine the yield stress, ultimate strength, and elastic modulus of prestressing steel at elevated temperature. The specimens were manufactured to British Standard specifications BS 2691 and BS 3617 for steel wire and steel strand respectively. The steel specimens were placed into a specially built load frame. Three types of experiments were carried out.

Constant heat tests were performed in which the specimen was heated to its desired temperatures, soaked for 30 minutes, and then tested in tension. Heating-cooling tests were also performed in which the same procedure was used but the specimen was allowed to cool after the 30 minute heat soak. Once the temperature reached room temperature it was tested in tension. For the constant heat and heating-cooling tests the set temperature ranged from 100^0C to 700^0C with testing at 100^0C increments. The specimens were heated at an unspecified load rate. The third series consisted of transient heat tests, in which the specimen was prestressed to 70% MUTS and then heated until either rupture or a maximum temperature was reached.

The constant temperature results indicate a 50% reduction in yield stress and ultimate strength for temperatures between 370^0C and 420^0C and between 510^0C and 530^0C for the modulus of elasticity. At 325^0C, the prestressing steel lost 30% of the ultimate tensile strength. The heat-cooling test showed that until 300^0C there were no significant loss in residual yield stress or

ultimate strength. At 610 to 650^{0}C there was 50% loss in residual yield stress. The residual elastic modulus remained unaltered during the heating-cooling test. The transient temperature tests resulted in a rupture temperature of 300^{0}C for all of the prestressing steel testing. Holmes et al. recommended using a value between 50% and 60% MUTS instead of 70% in order to give a better representation of in-service use that accounts for prestress loss over time.

1.4.4 Neves et al., 1996

Neves et al. performed a series of tests to determine the effects of the heating-cooling process have on the tensile strengths and the rupture strain of commonly used 0.824% carbon prestressing steel. The focus of the research was to characterize the residual properties of the steel after cooling. To test the prestressing steel, the center tendon was cut from the strand. In batches of 10 single strands, the specimens were heated at a rate of 10^{0}C/minute until reaching the desired temperature. The set temperature was maintained for one hour as it was "considered to be enough to achieve temperature uniformity in the steel mass and to allow all possible transformations to take place in the steel structure." After heating, five samples were rapidly cooled using water jet or water immersion and five samples were air cooled. The test specimens were then tested in tension and a metallographic analysis was performed to determine the microstructure. The test results show residual strength loss occurs at maximum temperature between 300 and 400^{0}C. Up to 300 and 400^{0}C the residual strength remains almost constant as the strand gains back all of the initial strength. The experiments also show that for temperatures above 700^{0}C strength losses of up to 60% are expected. Also, for fires of 800 and 900^{0}C it was found that cooling by water jet causes the tendon to become brittle which increases the tensile strength while decreasing the strain at rupture.

1.4.5 Hertz 2004

Hertz proposed a simple mathematical model (See Equation 2) to predict the reduction in mechanical properties for several steel types at elevated temperatures based on the experimental results of previous studies by other researchers. The author bases the work from the idea that an S-shaped curve is capable of describing 'almost any material'. The paper briefly describes the cold-working process and that as temperature increases, the energy needed to yield the material is reduced. This phenomena allows for mild steel to have an increase in its initial yield stress for temperatures within 200-300^{0}C because the lattice slipping process essentially cold-works the steel. For cold worked bars the crystalline structure loosens above 300^{0}C. At 600^{0}C the effects of cold-working are removed and the steel behaves like mild steel. The residual properties of cold worked steel suffer irrecoverable losses if subject to temperatures over 400^{0}C. If the steel is subject to temperatures above 800^{0}C the cold-working properties are removed entirely and the residual steel behaves as mild steel.

The mathematical model uses four temperature constants: T_1, T_2, T_8, T_{64} and the symbol *k* which describes the ratio between the maximum and minimum value of the parameter being represented and is shown below. The Greek symbol ξ represents the ratio between the property at temperature *T* and the property at temperature *T*=20^{0}C.

$$\xi(T) = k + \frac{1-k}{1+(T/T_1)+(T/T_2)^2+(T/T_8)^8+(T/T_{64})^{64}} \qquad (2)$$

For prestressing steel wire, the values of the constants for ultimate strength:

T_1=100,000 T_2=750 T_8=430 T_{64}=100,000 k=0

For yield stress the values:

T_1=2000 T_2=360T_8=430T_{64}=100,000 k=0

The model was compared to Harmathy and Stanzack (1970) where the reduction function showed good agreement with past testing results for both yield stress and ultimate strength values of A421 prestressing wire.

1.4.6 MacLean et al., 2008

MacLean et al. published research based on experimental testing of the residual effects of prestressing steel wire after elevated temperature and relaxation testing under transient thermal exposure. The test specimen was chosen based on commonly used prestressing steel for unbonded prestressing applications in building floor slabs. Commercially available ASTM A416-03 ½-inch diameter Grade 270 low relaxation strand was chosen for testing. The steel was 0.8% carbon by weight and was manufactured from "pearlitic steel, having a fine-grained microstructure… which permits large amounts of cold-working and is essential for attaining 270 ksi." MacLean et al. also point out that older steel designations may contain varying carbon compositions and have different strengths.

For the high temperature residual tension tests, a total of 41 samples were used in the test matrix. The samples were heated in batches of 6. The specimens were heated at a rate of 10^0C per minute to the desired set point. In accordance with typical fire endurance testing standards (reference), a soak time of 1.5 hours was chosen to ensure thermal equilibrium and constant temperature through the specimen thickness. The specimens were then cooled to room temperature in the furnace and then tested in tension. Because of the common difficulty in testing steel strand, only the core wires were tested in tension. A metallographic mount was prepared using 1 sample from each batch.

The results of the experiment were in agreement with past research. There was no loss in residual strength for specimens heated to temperature below 300^0C. At 400^0C microstructure changes were evident along with 7% loss in residual yield stress and ultimate strength. For steel exposed to 700^0C the ultimate strength was reduced to 38% of the unheated steel. The results also show that the elastic modulus is unaffected by exposure temperature, again in agreement with the past research. MacLean et al. state that the steel used in the test performed similarly to steels used in Europe, China, and 1960's America and that the curves introduced by Hertz appear slightly conservative when measuring the residual properties of prestressing steel at high temperature.

During the high temperature relaxation testing eight specimens were tested. The 7-wire strand was prestressed to 55% ultimate, a typical strength expected of in service unbonded tendons. Furnace set points were chosen at 200, 300, 400, 500, and 700^0C and the specimen was heated at a rate of 10^0C/min. The specimen temperature and stress level was monitored throughout the process and each sample was held at the set point temperature for 90 minutes. In addition to the eight samples, three additional samples were heated to 400^0C but only held for 5, 45, and 90 minutes. All specimens were cooled to room temperature while the temperature stress profile was continuously recorded.

The results show significant irreversible losses occur for specimens subjected to temperatures above 400^0C. For temperatures of less than 300^0C a prestress loss of less than 5% was recorded. The results found by the authors were consistent with past research. MacLean et al. point out that the percentage of stress loss is dependent upon the ratio of heated to unheated length of the strand and because the tendons used in unbonded construction are typically long strands additional study is required (e.g. heating a small portion of the strand may cause a reduction in strength but no

overall prestress loss, while heating a large portion of the strand can cause a total loss in prestress due to thermal elongation).

1.4.7 Gales et al., 2009

Using the experimental data from MacLean et al. a computer model was created to predict the prestress loss at various prestressing levels. The model predicted that after being exposed to a standard ASTM E119 fire for one hour, strands initially prestressed to 55-65% MUTS would experiences a 50% reduction in the initial prestressing force.

1.4.8 Atienza and Elices, 2009

Atienza and Elices performed two sets of experiments using prestressing steel. The two types of testing were tensile and relaxation tests at high temperature and relaxation tests after a simulated fire. For every test, 5mm commercial 0.77% Carbon prestressing steel wires were used. The test was conducted using an Instron tensile testing machine with an attached furnace.

For the tensile testing at high temperature the specimen was placed in the testing machine and heated to the set temperature. Set temperature ranged from 100 to 600^0C at intervals of 100^0C. The test results showed a strong correlation to British Standard and Eurocode2 recommended standards. From 100^0C onward there is a progressive decrease in the ultimate strength of the wire. The relaxation tests at high temperature showed that there is significant prestress loss as the temperature increases. The results also show that the percentage of prestress loss is dependent upon the initial prestress level. The study included initial prestress loads from 10 to 90% of the wire strength.

The 'behavior after fire' testing show that after 250^{0}C the mechanical properties decrease. At 400^{0}C this decrease "is very important". Above 400^{0}C recrystallization of the steel microstructure occurs and the properties created during the cold-working process are lost. Atienza and Elices did not perform a metallurgical analysis but note that the results are a conservative estimate and the exact assessment requires more variables. The recrystallization processes is dependent upon both time and temperature and this work presented by the author is conservative.

2.6 Summary

Past studies have shown that both the yield stress and ultimate strength of cold-drawn steel begin to decrease around 200^{0}C. At 200^{0}C, prestressing steel loses approximately 10% of its ultimate strength (Abrams and Cruz 1961). Past 200^{0}C, both the yield stress and ultimate strength begin to decrease rapidly (Harmathy and Stanzak 1970). Holmes et al. (1982) found that between 370^{0}C and 420^{0}C the ultimate strength and yield stress are reduced by 50% while Abrams and Cruz found the 50% reduction to occur at 427^{0}C. For prestressing levels of 55 and 70% the rupture temperature was close to 425^{0}C and 315^{0}C respectively (Abrams and Cruz 1961). Holmes et al. reported a rupture temperature of 300^{0}C for cold-drawn steel prestressed to 70% MUTS. Holmes et al. also found that between 510^{0}C and 530^{0}C the elastic modulus is half of the unheated modulus. There is not a significant amount of data for the elastic modulus at elevated temperature due to the difficulty of measuring strains for heated strand and wire specimens.

While the residual properties are an important design consideration, they are not the scope of this research. Many of the previous studies performed both residual testing and elevated temperature tests, and therefore some discussion of the existing residual test data has been included in this thesis. Steel temperatures up to 300^{0}C produce no significant reduction in the residual yield

stress or ultimate strength (Holmes et al. 1982; Neves et al. 1996). Holmes et al. found that temperature between 610^0C and 650^0C will result in near 50% loss in yield stress. Neves et al. report that temperature over 700^0C will result in permanent strength loss of at least 60% ultimate.

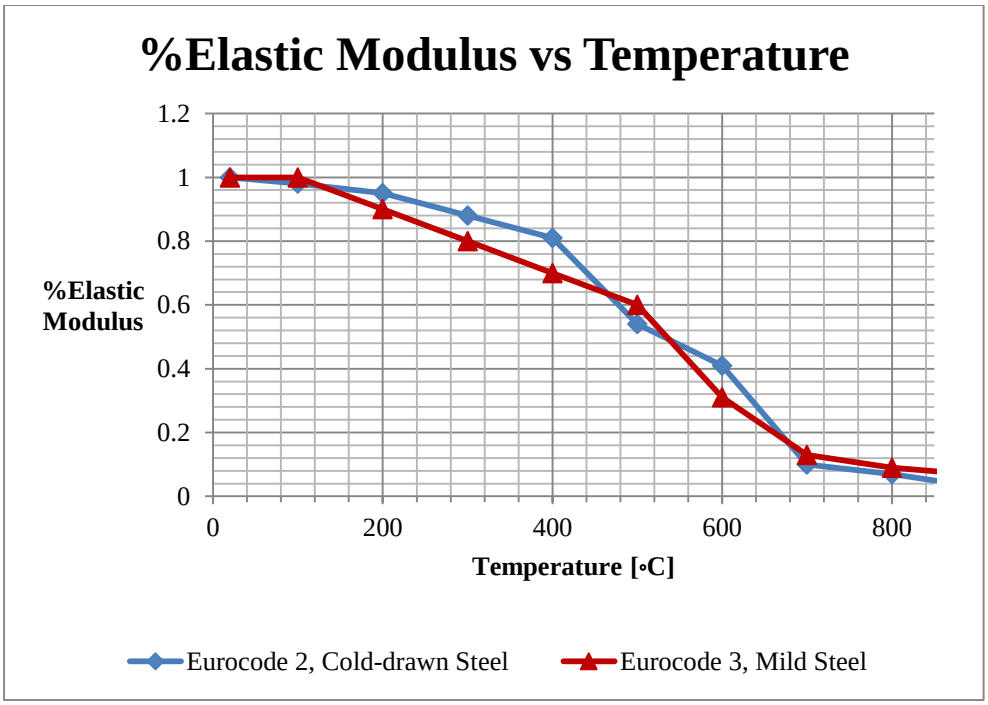

Figure 7: Eurocode Elastic Modulus Reduction

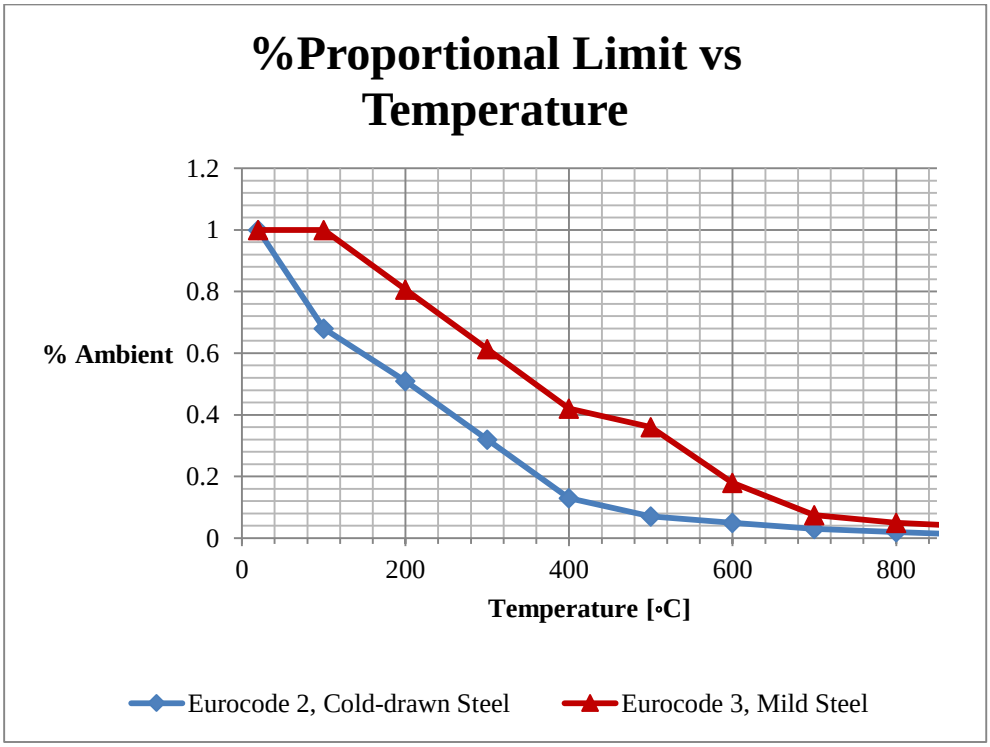

Figure 8: Eurocode Proportional Limit Reduction

Table 2: Eurocode (2004) Stress-Strain Equation Parameters

Range	Stress $\sigma(\theta)$	Tangent modulus
$\varepsilon_{sp,\theta}$	$\varepsilon E_{s,\theta}$	$E_{s,\theta}$
$\varepsilon_{sp,\theta} \le \varepsilon \le \varepsilon_{sy,\theta}$	$f_{sp,\theta} - c + (b/a)[a^2 - (\varepsilon_{sy,\theta} - \varepsilon)^2]^{0.5}$	$\frac{b(\varepsilon_{sy,\theta} - \varepsilon)}{a\left[a^2 - \left(\varepsilon - \varepsilon_{sy,\theta}\right)^2\right]^{0.5}}$
$\varepsilon_{sy,\theta} \le \varepsilon \le \varepsilon_{st,\theta}$	$f_{sy,\theta}$	0
$\varepsilon_{st,\theta} \le \varepsilon \le \varepsilon_{su,\theta}$	$f_{sy,\theta}[1-(\varepsilon - \varepsilon_{st,\theta})/(\varepsilon_{su,\theta} - \varepsilon_{st,\theta})]$	-
$\varepsilon = \varepsilon_{su,\theta}$	0,00	-
Parameter *)	$\varepsilon_{sp,\theta} = f_{sp,\theta} / E_{s,\theta}$ $\varepsilon_{sy,\theta} = 0,02$ $\varepsilon_{st,\theta} = 0,15$ $\varepsilon_{su,\theta} = 0,20$ Class A reinforcement: $\varepsilon_{sp,\theta} = 0,05$ $\varepsilon_{su,\theta} = 0,10$	
Functions	$a^2 = (\varepsilon_{sy,\theta} - \varepsilon_{sp,\theta})(\varepsilon_{sy,\theta} - \varepsilon_{sp,\theta} + c/E_{s,\theta})$ $b^2 = c\,(\varepsilon_{sy,\theta} - \varepsilon_{sp,\theta})\,E_{s,\theta} + c^2$ $c = \frac{(f_{sy,\theta} - f_{sp,\theta})^2}{(\varepsilon_{sy,\theta} - \varepsilon_{sp,\theta})E_{s,\theta} - 2(f_{sy,\theta} - f_{sp,\theta})}$	

Table 3: Eurocode (2004) Reduction Factors for Cold-drawn Steel

Steel temp. θ [°C]	$f_{sy,\theta} / (\beta f_{yk})$			$f_{su,\theta} / (\beta f_{yk})$		$E_{s,\theta}/E_s$		$\varepsilon_{sp,\theta}$ [-]	$\varepsilon_{sy,\theta}$ [-]
	cw		q & t	cw	q & t	cw	q & t	cw, q&t	cw, q&t
	Class A	Class B							
1	2a	2b	3	4	5	6	7	8	9
20	1,00	1,00	1,00	1,00	1,00	1,00	1,00	0,050	0,100
100	1,00	0,99	0,98	0,68	0,77	0,98	0,76	0,050	0,100
200	0,87	0,87	0,92	0,51	0,62	0,95	0,61	0,050	0,100
300	0,70	0,72	0,86	0,32	0,58	0,88	0,52	0,055	0,105
400	0,50	0,46	0,69	0,13	0,52	0,81	0,41	0,060	0,110
500	0,30	0,22	0,26	0,07	0,14	0,54	0,20	0,065	0,115
600	0,14	0,10	0,21	0,05	0,11	0,41	0,15	0,070	0,120
700	0,06	0,08	0,15	0,03	0,09	0,10	0,10	0,075	0,125
800	0,04	0,05	0,09	0,02	0,06	0,07	0,06	0,080	0,130
900	0,02	0,03	0,04	0,01	0,03	0,03	0,03	0,085	0,135
1000	0,00	0,00	0,00	0,00	0,00	0,00	0,00	0,090	0,140
1100	0,00	0,00	0,00	0,00	0,00	0,00	0,00	0,095	0,145
1200	0,00	0,00	0,00	0,00	0,00	0,00	0,00	0,100	0,150

Note: For intermediate values of temperature, linear interpolation may be used.

Chapter 3 Test Program

3.1 General

Chapter 3 presents the experimental test program that performed for this research project. Specifically, this chapter describes the goals, specimens, setup, and procedure.

3.2 Test Matrix

Two series of tensile tests were performed for this project for steel strands exposed to high temperature: constant temperature and transient temperature testing. The constant temperature test is carried out by heating a steel strand, which is held taut in a universal testing machine, to a target temperature and allowing 30 minutes of heat soak at that temperature - the cable is then pulled until yielding and tensile failure occur. The constant temperature tests are used to evaluate the cable performance at a defined elevated temperature. These tests are commonly used to establish the material performance at a range of temperatures; however, they are not realistically representative of actual fire exposure, during which an element is exposed to variable temperatures. The transient temperature test is carried out by initially loading the cable to a desired level of stress (typical stress levels for cable-stay bridges and post tension concrete were chosen) - once the strand is at the stress level, the furnace is turned on and the increasing temperatures are recorded. The strand is maintained at the desired stress level until the specimen ruptures due to temperature increase. This goal of this type of testing is to replicate the realistic scenario of a hydrocarbon bridge fire and to evaluate the relationship between the constant and transient test results. Additionally, elastic modulus testing was performed using string pot displacement sensors to measure the deformation of the heated cable portion. To ensure reliability in the results, two experiments were carried out at every instance.

3.3 Test Specimen

Cold-drawn A416 7-wire strand was used as the test specimen for this experiment. The grade 270-ksi strand was 0.6 inches in diameter and was manufactured by Sumiden Wire Products Corporation. The 7-wire strand was chosen because of its availability and application to cable-stay bridge design. Two unused spools of the 0.6 inch diameter strand were leftover from previous testing at Lehigh University. The two spools had slightly different chemical composition as shown in Table 4. The specimens used were fresh from the spool, which had been stored indoors at Lehigh University's Mountaintop Campus. Table 4 also shows the chemical composition that was used in similar studies.

Table 4: Chemical Composition of Steel

	Current Study	Current Study	MacLean	Neves	Harmathy
Origin	USA	USA	Canada	Portugal	Canada
Date	2012	2012	2006	1996	1970
ASTM	ASTM A416	ASTM A416	ASTM A416	--	ASTM A421
C (%wt.)	0.79	0.84	0.8	0.824	0.794
Cr(%wt.)	0.14	0.12	0.04	0.237	--
Mn(%wt.)	0.71	0.82	0.868	0.712	0.78
P(%wt.)	0.009	0.01	0.023	0.02	0.012
Si(%wt.)	0.25	0.22	0.45	0.235	0.187
S(%wt.)	0.012	0.01	0.012	0.013	0.031

The two spools of 7-wire strand had similar mechanical properties. The strands were low-relaxation strand. The elastic modulus ranged from 28,200 ksi to 28,400 ksi. The yield point ranged from 55,806 lbf to 56,097 lbf. The area of the strand ranged from 0.2216 in^2 to 0.2221 in^2. The breaking strength of the cable ranged from 61,802 lbf to 61,994 lbf.

As recommended by ASTM A931-08 (ASTM A931-08, 2013), the test length of cable should exceed 3ft between the grips for wire ropes up to one inch in diameter. In order to ensure that the grips were close to ambient temperature and not effected by the heat transfer during testing, a 5 ft. test length between the grips was chosen.

3.4 Test Setup and Procedures

Three types of tests were performed: constant temperature, transient temperature, and elastic modulus testing. The following section outlines the equipment and procedures that were used for each type of testing. All tests were completed at Lehigh University's ATLSS Laboratory between December 2014 and July 2015. The testing procedures were in accordance with the applicable ASTMs for multi-wire steel strand and are consistent with those used in previous studies.

3.4.1 Test Apparatus

Testing was performed using a SATEC 600-kip universal testing machine at Lehigh University's ATLSS Lab. The universal testing machine is shown in Figure 9A. The machine operated using a hydraulic-powered screw driven top head. The bottom head does not move during the test. The test specimen was clamped at each end inside the top and bottom heads. The SATEC testing machine is controlled using Partner – Materials Testing Software for Windows (Figure 9B).

Figure 9: Universal Testing Machine

The electric furnace, an Instron SF-16 furnace with extensometer port (Catalog no. W-8711-F), is shown in Figure 10. The split tube furnace has a 3 inch radius 11 inch tall interior heated dimensions and 10 inch radius 13 inch tall exterior dimensions. The furnace has three independently heated zones that are controlled using the SATEC Model TCS 3202 three zone temperature control system, as shown in Figure 11. Each furnace zone has a type K thermocouple mounted to the exterior of the ceramic heating panels. The furnace control temperature ranges from 300^{o}C to 1200^{o}C. During testing, it was found that the furnace was capable of maintain a 200^{o}C specimen temperature even though 300^{o}C was the recommended low-point.

Figure 10: Electric Furnace

Figure 11: Furnace Controller

When testing 7-wire strand at elevated temperatures, past researchers have commented on the difficulty in gripping 7-wire strand. Many researchers opted to remove the exterior strands and perform testing on only the central strand (Maclean, 2008; Neves et al., 1996). Initially, wedge-

in-barrel ‘open grip’ prestressing grips were attempted for testing the strand. Using this grip, the strand failed before reaching the minimum ultimate tensile strength (MUTS) during preliminary tensile tests at ambient temperature. A method presented by Preston (1990) was adopted and adapted for testing. A custom aluminum grip was created for the test program and is displayed in Figure 12. The grips were machined from an 8 inch by 1 inch by 1 inch rectangular block of aluminum. A 0.6-inch diameter hole was drilled through the center of the block. The block was cut into two halves. An epoxy/grit mixture was applied to the inside of the aluminum in order to provide grip and shear strength. The mixture was composed of #80 Silicon Carbide grit manufactured by AGSCO Corporation and 3M Scoth-Weld DP 420 epoxy. The epoxy was had a shear strength of 4.5 ksi at room temperature. Using this setup, the strand was able to reach over 1.05% MUTS during preliminary tensile tests at ambient temperature.

Figure 12: Custom Aluminum Grips

3.4.2 Instrumentation

The 7-wire strand was instrumented with 4 type-K thermocouples. The thermocouple locations are displayed in Figure 13. Two thermocouples were placed inside the furnace. One was attached at the midpoint of the furnace, referred to as TCM, and the second was placed 3.5 inches above

TCM, referred to as TCMT. The location of TCMT was chosen during the preliminary testing phase. 3.5 inches above the furnace midpoint was found to be the hottest part of the cable and the failure location for almost all heated specimens. Two additional thermocouples were placed at 18 inches below and above the furnace midpoint, referred to as TCB and TCT respectively.

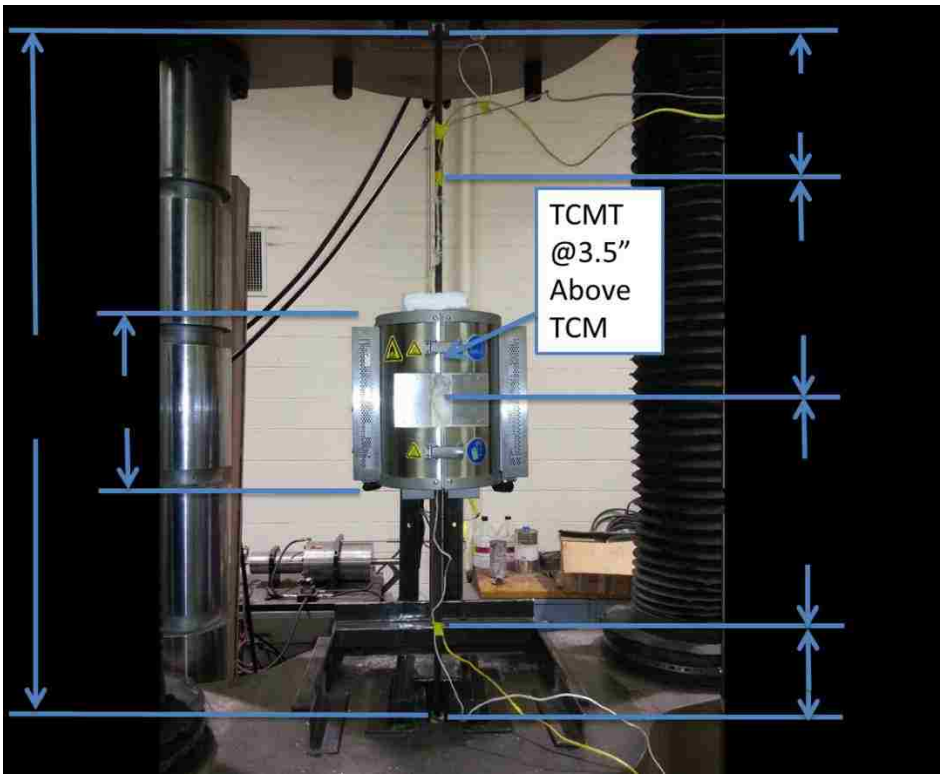

Figure 13: Test Setup

A Campbell Scientific CR9000X Data Logger was used to record the testing. The logger recorded the load, cross head displacement, and thermocouple data for all three types of testing. The data logger and laptop PC used to record the test data is shown in Figure 14.

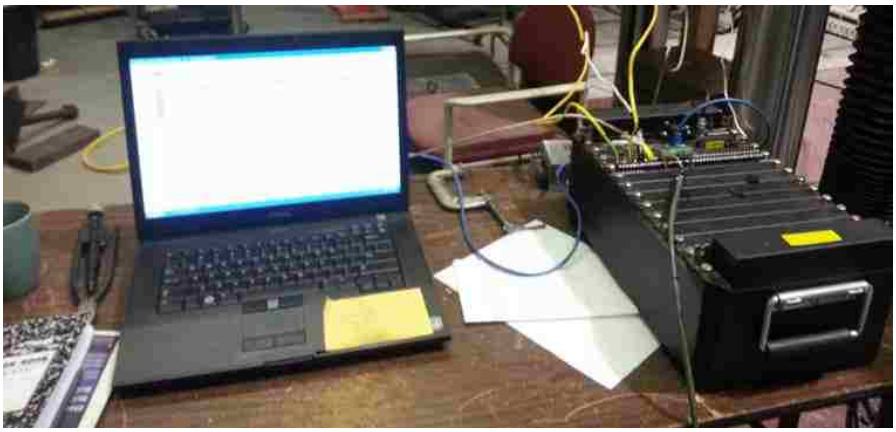

Figure 14: Data Acquisition System

3.4.3 Test Protocol

The test protocol for each type of testing is presented below. Each test followed the same basic set-up procedure. The aluminum grips were held in place using electrical tape as the strands were placed inside the SATEC. The grips were clamped into the testing machine, a process that produced a small initial compressive load. The compression in the cable was removed and the furnace was placed around the specimen. A stainless steel pipe was placed between the strand and the furnace in order to protect the ceramic furnace panels during rupture. The steel pipe was fabricated from a 2 inch radius 13.5 inch tall stainless steel pipe. The tube was vertically cut in half and mounted to the furnace through bolted stainless steel plates that were welded to the tube. In order to increase the heat flow into the specimen, holes were drilled into the steel pipe and is shown in Figure 15. This initial procedure was followed for all tests in this study.

Figure 15: Protective Steel Pipe Configuration

3.4.3.1 Constant Temperature Test

The constant temperature tests were performed at eight different temperatures: 20°C, 200°C, 300°C, 400°C, 500°C, 600°C, 700°C, and 800°C. During a typical test, the furnace was initially set 100°C above the desired temperature. All three furnace zones were used and set to the same desired temperature. The strand was initially loaded to ~1% of the MUTS (close to 600 lbf). This initial load allowed for thermal elongation during the heating phase, and ensured that the strand remained taut without causing and mechanical plastic deformation. The universal testing machine held the strand at the 1% MUTS load during the heating phase. Once the interior thermocouples indicated that the specimen had reached the desired temperature, the cable was held at that temperature for 30 minutes. This thermal soak allowed for the strand to reach a uniform equilibrium temperature and to allow for the completion of potential microstructure phase changes. A similar thermal soak approach was used in previous studies, and the 30-minute soak time was common for elevated temperature testing (Holmes et al. 1982; Abrams and Cruz 1961).

After heat soak, the specimen was placed in tension and pulled at a displacement rate of 0.25 inches/minute until rupture. Once the strand ruptured, the furnace was turned off and the split tube was opened. The specimen was cooled with a fan until it was safe to handle. Typically, the furnace panels and steel strand were adequately cool within 30 minutes to an hour following the completion of a test. A portion of the failed strand was removed and tagged for future microstructure analysis.

3.4.3.2 Transient Temperature Test

The transient temperature test provides a more realistic simulation of fire exposure on a cable tension element. The 7-wire strand was initially loaded to a predetermined stress level. Once the strand was tensioned to the desired stress level, the furnace was turned on and the strand began to heat up. The strand was held at that stress level throughout the test. The universal testing machine held that constant load by adjusting the cross heads during any thermal elongation, creep, or relaxation. The test continued until the strand ruptured, and the rupture temperature was recorded.

The two test stress levels were chosen as 45% MUTS and 70% MUTS. The 45% MUTS is a load that is typical of cable-stay bridges (PTI, 2006) practice. The 70% MUTS was chosen because it is a load that is typical of in-service stress levels for post-tensioned concrete construction and was the stress level used by Abrams and Cruz (1961) and Holmes (1982). An additional stress level of 42% MUTS was added to the test program to gather additional test data.

Data was collected using two separate heating rates, referred to as fast (20-25 $^{\circ}$C/minute) and slow (5-10 $^{\circ}$C/minute). The furnace controller did not have an explicit mechanism for implementing a specific rate of heating. However, the furnace produces a faster heating rate when a higher initial temperature is specified. To achieve the fast heating rate, the fiber

insulating material was placed over the furnace opening and the furnace controller was set to 1200°C. To achieve the slow heating rate, the insulation material was removed and the furnace set points were chosen at 200°C above the associated constant temperature rupture temperature (e.g. if the 500°C constant temperature test had a ultimate strength of 45% MUTS, then the set point was chosen at 700°C for a 45% MUTS transient test).

3.4.3.3 Modulus Test

An additional series of tests were performed to determine the reduction in the elastic modulus at elevated temperatures. The original test plan relied on an extensometer that was compatible with the built in extensometer port in the split tube furnace. A W-E418-2 high temperature extensometer was purchased from Instron. This extensometer had a 2 inch gauge length and was accurate for temperature up to 1200°C. The extensometer was attached to the specimen by way of spring loaded ceramic fiber cords. However, the knife-edge contacts at the end of the extensometer arms did not maintain constant contact with the braided 7-wire strand during preliminary heated tests, and a new method was therefore pursued to measure the elastic modulus. The cable was initially loaded to approximately 400 lbf, similar to the constant temperature test. The furnace was turned on and the cable was heated to the desire temperature and allowed to soak for 30 minutes at that temperature. After the heat soak, the cable was loaded at 0.25 inches per minute displacement until the following displacements were reached (which were sufficiently low to avoid any plastic deformation): 0.75 inches for 20°C, 0.5 inches for 200°C, 300°C, and 400°C, 0.25 inches for 500°C, 0.10 inches for 600°C, 700°C and 800°C. The same specimen was used to test temperatures all temperatures: 20°C, 200°C, 300°C, 400°C, 500°C, 600°C, 700°C, and 800°C. As for the constant and transient temperature tests, two complete test runs were performed.

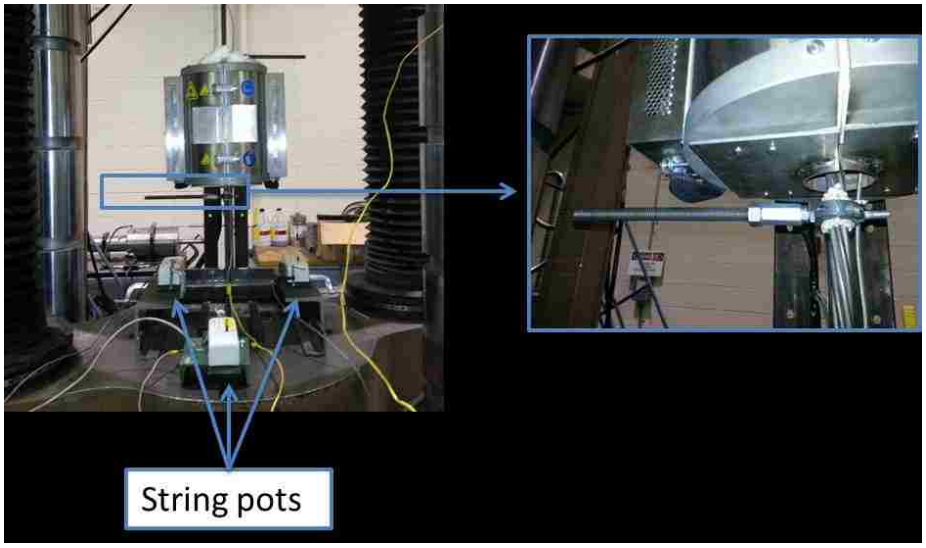

Figure 16: Elastic Modulus Gauge Length

The deformation inside the heated zone was measured using two Celesco PT510-0050-111-1120 Stringpot Displacement Sensor (20" Range), shown in Figure 16. The rods were clamped approximately ½ inch above and below the furnace. The spacing between the two arms was used as the gauge length. To determine the stress-strain relationship, the deformation recorded by the bottom swing arm was subtracted from the deformation of the top swing arm. The third stringpot was used to determine the overall cross-head displacement, however this data was not used to determine the elastic modulus. The string pots were placed on the bottom head of the SATEC and were connected to slotted rods, which were clamped directly to the 7-wire strand. A fire-retardant fabric was used to seal the connection between the circular clamp and the 7-wire strand.

Chapter 4 Test Observations

4.1 General

This chapter summarizes the observations from the test program. Both the constant temperature testing and the transient temperature testing are presented. For the tests, plots of load vs. displacement, temperature histories, and photographs of the specimens after testing have been included.

4.2 Constant Temperature Test

The constant temperature tests followed the procedure outlined above in Chapter 3. Each test (except for the ambient temperature test) followed the same procedure: load specimen, heat to desired temperature, hold the desired temperature for 30 minutes (i.e. the thermal soak), and then pull the specimen until failure. , Quantitative measurements focused on the load-displacement sequence as well as the temperature of the specimen and the furnace. Qualitative observations were made during each test in regards to thermal expansion, energy released during failure, physical changes to the specimens (e.g. color change, material flaking), reduction of cross section area, and failure surface examination.

It is important to note that all specimens experienced either a ‘cap and cone’ tensile failure type or a necking down to a point tensile failure type. These types of failure are an indication of a ductile failure and extremely ductile failure, respectively (Callister and Rethwisch, 2008). All heated specimens failed within the heated zone of the furnace, however, the ambient temperature test failed close to the grips.

4.2.1 20°C (Ambient) Tests

The ambient temperature test exceeded the minimum ultimate tensile strength (MUTS) during each test. The load displacement plot is shown below in Figure 17. The initial stiffness, from a load of 0 kips to approximately 1 kip, is less than the stiffness after 1 kip. This indicates that the grips were still settling as the universal testing machine starts to pull the specimen. Specimen 15_01_07 started to experience non-linear load-displacement behavior after exceeding a proportional limit of approximately 50.7 kips. Similarly, specimen 15_02_19 exceeded its proportional limit at approximately 46.9 kips. Both specimens failed close to the grips. The failure of the 7-wire strand was initiated by a single wire rupture that was then followed by subsequent ruptures. The failure of the strand was considered 'violent'. During the failure a large amount of potential energy in the cable was released - the strands recoiled with a load 'bang,' and the severed wires became partially unbraided from the strand.

4.2.2 200°C Tests

The load displacement plot for the 200°C constant temperature test is shown in Figure 18. At 200°C the 7-wire strand still exhibits strain hardening after the steel has yielded. This is an indication that the specimen is still below the recrystallization temperature, which is the minimum temperature at which the deformed metal grain structure is replaced by undeformed grain structures (Callister and Rethwisch 2008). The thermal expansion during the heating phase was negligible compared to the deformation during loading. As was the case for the ambient test, there was an initial loading period with a decreased stiffness while the grips settled. Specimen 15_02_23 failed at 56.3 kips with a proportional limit of 45 kips. Specimen 15_03_02 failed at 57.0 kips and had a proportional limit of 45 kips. Both specimens failed inside the furnace zone.

For both specimens, the failure was initiated by a single wire rupture that was followed by subsequent wire ruptures. The failure was accompanied by a load ‘bang’ and the potential energy was released in violent recoil of the cable upon rupture.

Figure 19 shows the temperature history for specimen 15_02_23. During this testing it was found that TCM was damaged during the prior testing. The thermocouple leads can become damaged during explosive wire recoil and need to be inspected before each test. The thermocouple was thought to be working properly prior to the testing; however when the sample was placed in tension, the thermocouple showed signs of malfunction indicated by the rapid spike in temperature shown at approximately 4000 seconds. It appears that the thermocouple leads were not fully contacted during the initial heating phase. When the tension phase started, the cable tension increased the contact of the thermocouple leads, which created the unusable temperature readings. Because the failure occurred at TCMT, the data for the sample is still valid. This test was a good reminder that a more thorough inspection of test equipment is required before the test begins. It took approximately 39 minutes for the specimen to reach 200^{o}C. The thermocouple readings for TCMT show a temperature increase close to 6.5^{o}C/minute.

The temperature history for specimen 15_03_02 is shown in Figure 20. It took approximately 38.5 minutes to heat the cable from 20^{o}C to 200^{o}C. The initial 8 minutes held a heating rate close to 10^{o}C/min. The heating rate tapered down as the furnace reached the desired temperature. The two thermocouples inside the furnace recorded a temperature differential of close to 30^{o}C. This indicates that for this temperature it is difficult for the furnace to maintain a uniform temperature over the length of the specimen within the furnace. TCMT, which is located 3.5 inches from the center of the furnace, recorded the 200^{o}C temperature for 30 minutes. During the thermal soak,

the maximum temperature varied by a maximum of ±5ºC. This temperature variation was expected as it is difficult to maintain the desired temperature on the lower end of the temperature spectrum. This furnace is not recommended for temperatures lower than 300ºC for this reason. Once the specimen failed, the thermocouple recorded an increase in temperature because it was no longer in contact with the steel specimen.

Figure 21 and Figure 22 show the failed specimens for the 200ºC test. In each photo it clear that not all wires broke during the testing. The test was stopped after the failure of the outside wires to prevent any damage to the ceramic furnace through unnecessary wire recoils. In both tests, the outside wires ruptured first. The failure surfaces indicated the cup and cone tensile fracture.

4.2.3 300ºC Tests

At 300ºC there is a change in the load displacement plot when compared to the ambient test data. Shown in Figure 23, once the proportional limit is reached and the cable begins to show non-linear behavior, there is no strain hardening region or yield plateau. Once the strand reaches the ultimate strength, the cable resistance decreases. The 300ºC tests experienced a more ductile failure and showed signs of significant necking before failure. During both tests (specimen 15_03_02_300 and specimen 15_03_06_300) strand failure was initiated by a single outside wire rupture that was followed by the progressive failure of the other strands. The test was stopped soon after the rupture of the first strand. Strand 15_03_02_300 had an ultimate strength of 45.45 kips and a proportional limit of 37.2 kips. Strand 15_03_06_300 had an ultimate strength of 43.7 kips and a proportional limit of 37.5 kips.

The temperature history for specimen 15_03_02_200 is shown in Figure 24. The strand reached 300ºC after 53 minutes of heating. There was a 17ºC temperature differential between the

thermocouple at the furnace center (TCM) and the thermocouple 3.5” above the furnace center (TCMT).

Figure 25, shown below, displays the failed specimen 15_03_02_300. The specimen shows signs of significant necking in the unbroken wires. The broken wires also display the cup and cone fracture which is an indication of a ductile failure. The black smudge marks on the strand are the result of using a high temperature braided cord to attach the thermocouple to the cable. It was discovered that the coating of the high temperature cord began to melt, although the cord still held the thermocouple in place. The failure at the 300^{o}C exhibited signs of a violent rupture. As the strand failed, a loud bang was heard and the wires recoiled. Qualitatively, the recoil appeared to have less energy than the 200^{o}C specimens.

Figure 26 shows the temperature history for specimen 15_03_06_300. Data recording started 420 seconds before the furnace as turned on. During this test, TCMT reached 318^{o}C and TCM recorded a temperature of 307^{o}C. These temperatures were reached after 41 minutes of heating. The thermocouple readings after 5000 seconds indicate that the thermocouple was no longer in full contact with the strand and was recording the hot air temperature. Those recordings came after the strand was loaded in tension.

The failed specimen 15_03_06_300 is shown below in Figure 27. The center wire was the only strand that did not rupture during testing. This wire shows signs of necking while all other wires show the cup and cone fracture. As stated for specimen 15_03_02_300, the rupture was followed by a loud popping sound and violent wire recoil.

4.2.4 400°C Tests

The load displacement curves for the 400°C tests are shown below in Figure 28. Both curves have similar thermal expansion phases and follow very similar initial slopes. The 400°C curves follow a similar shape compared to the 300°C curves with an initial elastic range, followed by brief non-linear phase before failure. There is no well-defined yield plateau or strain hardening zone. Both specimens failed soon after reaching the ultimate strength. Specimen 15_03_06_400 reached an ultimate strength of 33.85 kips and had a proportional limit of 28.07 kips. Specimen 15_03_23 reached an ultimate strength of 31.53 kips and had a proportional limit of 26.9 kips.

Figure 27 shows the temperature history for sample 15_03_06_400. The strand recorded a temperature of 400°C after 33.3 minutes of heating. TCMT recorded 404°C and TCM recorded 380°C. It appears that at higher set temperatures the furnace is better able to hold the strand at a constant temperature and also produce a faster heating rate.

Figure 30 shows the failed specimen 15_03_06_400. During this test, all seven wires failed simultaneously whereas the previous constant temperature tests resulted in the failure of a single strand that led to the progressive failure of the other wires. It is important to note the straightening of the original braid. In Figure 30(A) it is apparent that the helical structure has untwisted at the failure zone. Another interesting observation (see Figure 30(B)) was the formation of a pale blue tint on the failed cross section of the strand. The strand failure was less violent than all previous tests. For temperatures 300°C and below, the specimen failed with a loud bang and violent recoil. The 400°C specimen failed with a soft ‘ping’ sound and the wires recoiled slightly.

The temperature history for specimen 15_03_23 is shown in Figure 31. This specimen took twice as long to reach the desired temperature of 400°C compared to 15_03_06_400. For this specimen,

insulation was added to the extensometer port of the furnace. This allowed less hot air to escape the furnace and resulted in a lower ceramic panel set temperature. The ceramic panel set temperature is the temperature read by built in thermocouples at the edge of the ceramic furnace panels. Lowering the furnace set point leads to a longer heating time, but also a more uniform temperature throughout the furnace. TCMT recorded a temperature of 402^{o}C while TCM recorded a temperature of 398^{o}C. Note that previous temperature differentials were closer to 20^{o}C of separation between TCMT and TCM.

Figure 32 shows specimen 15_03_23 after failure. It is very similar to Figure 30 with regards to the oxidation layer and the cup and cone fracture. Figure 32clearly shows that the strand rupture did have some recoil as the individual wires are not neatly packed in the original hexagonal packing configuration. The shifting in the strand configuration indicates that the wires ruptured with recoil.

4.2.5 500^{o}C Tests

The 500^{o}C constant temperature tests were carried out at slightly different temperatures. The 500^{o}C test was the first 'heated' test and was used a calibration run for the furnace. Specimen 15_02_20_500 was heated to 500^{o}C and specimen 15_01_12_550 was heated to 550^{o}C. The reason specimen 15_01_12_550 was heated to 550^{o}C was to establish the 500^{o}C temperature at TCM (The thermocouple at the furnace midpoint). The test program was then adjusted to set TCMT to the desired temperature due to the temperature differential between the two interior thermocouples. The load displacement curve for that specimen shows a break in the curve near 18 kips. The break in the curve is the result of pausing the test to remove a high temperature strain gauge. As mentioned in the Chapter 3, the initial test proposal involved a high temperature extensometer which would contact the specimen within the furnace. To ensure that the strain

gauge was not damaged during cable recoil, it was removed once the strand started to show non-linear behavior. However, due to twist in the braid of the 7-wire strand during tensile testing as well as difficulties in establishing a clear contact on the wires, the strain gauge was not able to record any usable strain data. For this reason, it was not used in previous tests and the extensometer port was filled with a fiber insulation material.

Specimen 15_02_20_500 had an ultimate strength of 17.85 kips and a proportional limit of 15 kips. Specimen 15_01_12_550 had an ultimate strength of 12.84 kips with a proportional limit of 11.6 kips.

The temperature history for 15_01_12_550 is shown in Figure 34. As mentioned above, TCM was recorded at 500ºC and TCMT recorded a temperature of 550ºC. The strand reached the desired temperature after approximately 70 minutes of heating.

The rupture of specimen 15_01_12_550 was ductile. As shown in Figure 36, the individual wires exhibited extreme necking. The failure was still in the form of the cup and cone fracture. The strand failed when all seven wires failed simultaneously and produced an audible, but very quiet, 'pinging' sound. Because the failure was so quiet, it was unclear whether or not the strand had snapped. Upon opening the furnace it was discovered that the strand was ruptured.

Specimen 15_02_20_500 was set to 500ºC for TCMT. The temperature time history is shown in Figure 35. The strand reached 500ºC after 55 minutes of heating. TCMT recorded a maximum temperature of 509ºC and TCM recorded approximately 500ºC throughout the duration of the temperature soak phase.

The failed specimen 15_02_20_200 is shown in Figure 37. Figure A shows that all seven wires were ruptured simultaneously along the same plane. Figure B shows that the blue tint that was clearly visible at the 400ºC is not evident at 500ºC. This could suggest that the tinting is a function of time and temperature.

4.2.6 600ºC Tests

The load displacement curves for the 600ºC specimens started to show a new behavior that was not shown for the lower temperature specimens. Figure 38 shows that after the strand reaches the ultimate strength, the resistance decreases linearly until the load reaches approximately 1.5 kips. At that point the resistance becomes nonlinear as the strand begins to fail. Specimen 15_03_27_600(1) had an ultimate strength of 7.77 kips with a proportional limit of 6.67 kips. Specimen 15_03_27(2) had an ultimate strength of 7.12 kips with a proportional limit of 6.24 kips.

The temperature history displayed in Figure 39 shows that both the TCM and TCMT recorded temperatures of 600ºC during the heat soak phase. The strand reached the desired temperature after 50 minutes of heating. At this temperature there is almost no temperature differential between the two interior thermocouples.

Figure 40(A) shows specimen 15_03_27_600(1) after testing. The cross section area close to the failure plane has been reduced, which indicates an extremely ductile failure mode. Figure 40(B) shows the significant area reduction of the cross section compared to the original unreduced cross section.

The temperature-time history for specimen 15_03_27_600(2) is shown in Figure 41. The strand reached 600ºC after approximately 43 minutes of heating. There were slight variations in temperature during the heating phase as the TCMT ranged from 598 to 608ºC and TCM ranged from 603 to 608ºC.

The failed specimen 15_03_27_600(2) is shown below in Figure 42. The failed specimen is similar to the first 600ºC specimen. Figure 42 clearly shows the significant area reduction and failure through necking down to a point. The 600ºC specimen failure was quiet and non-violent.

4.2.7 700ºC Tests

The load displacement curves for the 700ºC constant temperature test are shown below in Figure 43. The 700ºC curves follow the same trend that was observed for the 600ºC test. It was found that at the 700ºC temperature, the initial ~1% MUTS load (applied to keep the cable taut during the thermal expansion) was too great and the strand started to go non-linear soon after the load was increased from the holding load. As a result for the 15_04_03_700 test (and both 800ºC tests), the initial load was reduced from ~560 lbf to ~250 lbf. At this low load, the universal testing machine had a difficult time maintaining exactly 250 lbf; however, the load remained within 50 lbf of the holding load. Reducing the hold load also reduced the expansion during the heating phase from 0.4 inches to approximately 0.2 inches. Specimen 15_03_30_700 reached an ultimate strength of 2.54 kips with a proportional limit of 17.5 kips.

Figure 44 shows the temperature-time history for specimen 15_03_30_700. The strand reached 700ºC after 60 minutes of heating. At such a high overall temperature, it was observed that TCM was recording higher temperatures compared to TCMT, which was closer to the non-heated steel. At 5750 seconds, the temperature decrease in TCMT indicated that the TCMT location was no

longer in the furnace due to large thermal and mechanical elongation and began to cool off as a result.

Figure 45 shows the extreme ductility of the 700ºC specimen 15_03_30_700. The cross section of failure was reduced even further than the 600ºC testing. During failure, there was a barely audible 'pinging' sound which indicated the cable had snapped. All seven strands broke simultaneously.

Figure 46 shows the temperature history for specimen 15_04_03_700. It took approximately 45 minutes for the strand to reach the desired temperature. During the tensile tests, the large thermal and mechanical elongation of the cable at this temperature again caused TCMT to lift out of the heated zone of the furnace. The thermocouple was exposed to the cool air and began to cool down as can be seen at the 88 minute mark.

The failed specimen 15_04_03_700 is shown in Figure 47. This specimen failed with a simultaneous rupture of all seven strands. The failure was extremely ductile and the cross section was reduced nearly to a fine point. The strand rupture was non-violent, and was accompanied by a barely audible pinging sound.

4.2.8 800ºC Tests

The load displacement curves from the 800ºC test are displayed in Figure 48. The curves no longer have the same bi-linear properties that were exhibited during the 600ºC and 700ºC tests. At 800ºC the shape of the load displacement curve shows a yield plateau after the maximum load is reached. The overall displacement has decreased when compared to the 600ºC and 700ºC tests; however, the failure was still ductile and the strand showed significant necking before failure. Specimen 15_04_03_800 reached an ultimate strength of 2.11 kips with a proportional limit of

1.2 kips. Specimen 15_04_06_800 reached an ultimate strength of 2.34 kips with a proportional limit of 1.2 kips. At this high temperature, it is difficult to isolate the linear elastic region of the load displacement curves. The cable is extremely ductile at 800°C and the strand begins showing non-linear behavior soon after the load is increased from the holding load.

The temperature-time history for specimen 15_04_03_800 is shown in Figure 49. The strand reaches the desired temperature of 800°C after approximately 57 minutes of heating. At this high heat, the strand temperature was increasing a rate close to 24°C/minute. The furnace panels, the protective steel pipe, and the strand were all emitting a bright orange/red glow.

The post-test specimen 15_04_03_800 is shown in Figure 50. At this temperature the exposed surfaces of the strand started to flake off as shown in Figure(A). The strand did not elongate to the extent that the 700°C strand elongated. The necking was localized to the failure cross section (Figure(A)). Figure(B) shows that the failed cross section has necked down to a point, which is highlighted by the juxtaposition of the reduced and unreduced cross sections.

4.3 Transient Temperature Test

The transient temperature test procedures are outlined in Chapter 3. For each test, the strand was held under a constant stress level typical to service level loads for cable-stay bridge structures (PTI, 2006) or post-tensioned concrete beams. Once the desired stress level was reached, the furnace was turned on while the cable maintained the stress level. The test was stopped once the cable failed and the ultimate rupture temperature was recorded. The rate of heating was obtained from the temperature history of the furnace prior to rupture. All specimen failures occurred at or very close to the location of the interior upper thermocouple (TCMT).

Qualitative observations made during the test include the strand heating rate, energy released during failure, physical changes to the specimens, cable expansion during temperature increase, failure surface examination, and the time elapsed between the first indication of failure and the moment of failure.

4.3.1 45 % MUTS

According to PTI (2006), the main tension elements of cable-stay bridges are typically stressed to 45% of MUTS. The load level was chosen to determine the rupture temperature of in-service cable elements for cable-stay bridges. The first two tests were conducted using a heating rate close to 25ºC. The second two tests were conducted using a slower heating rate.

4.3.1.1 Test 1

The time-history for the 1st 45% MUTS transient test is shown in Figure 57. The universal testing machine applied a holding load of 26.59 kips. The furnace maintained an approximate heating rate of 25ºC/minute. During the initial loading the strand was deformed 0.70 inches. During the heating phase, the strand deformed an additional 0.30 inches before rupture. The strand ruptured at a temperature of 501ºC. As the strand approached failure, the interior thermocouple (TCMT) went offline. The thermocouple went back online right before failure and the temperature was predicted by extrapolating the heating rate over the periods of missing temperature data. The strand failed 3.2 seconds after the first indication of load reduction.

Figure 58 shows the strand after testing. Four of the exterior strands ruptured simultaneously. The strand exhibited violent recoil and a loud ‘bang’ sound was heard. The strands that did not rupture

showed signs of significant necking. The ruptured strands displayed the cup and cone fracture type and there was no sign of any heat tinting along the failed cross section.

4.3.1.2 Test 2

The time-history for the 2nd 45% MUTS transient temperature test is shown in Figure 59. The strand was initially loaded to 26.42 kips. The initial loading resulted in 0.70 inches of deformation. The strand experienced a 26°C/minute heating rate. During the heating phase, the strand deformed an additional 0.39 inches and ruptured at 500.8°C. 13.2 seconds elapsed between the first indication of load reduction and cable rupture.

The post-test strand is shown in Figure 60. Five of the exterior strands ruptured simultaneously, resulting in violent recoil and a loud "bang" sound. The failed cross sections did not show any signs of discoloration. The remaining two strands were extremely necked, while the failed strands showed a cup and cone type fracture.

4.3.1.3 Test 3

The time-history for the 3rd 45% MUTS transient temperature test is displayed in Figure 61. The load was held at 26.35 kips. The initial loading produced 0.73 inches of cable deformation. During this test, the furnace insulation was removed and the heating rate was reduced. The strand temperature increased at a rate of 7°C/minute during the last five minutes of testing. There was an initial period of faster heating which transitioned to the slower rate at nearly 300°C. The strand elongated an additional 0.46 inches during the heating phase. The strand ruptured at 458°C, 7.4 seconds after the first indication of a load reduction. The thermocouple (TCMT) went offline during some parts of testing.

The cable failed when four of the exterior strands ruptured. The strands ruptured simultaneously and displayed a cup and cone type fracture. The cross section of the failed strands showed no indication of discoloration. The remaining three strands exhibited significant necking at the same location where the other strands had failed.

4.3.1.4 Test 4

The time-history for the 4th 45% MUTS transient temperature test is shown in Figure 63. The cable was held at 26.4 kips. The holding load produced an initial elongation of 0.7 inches. The furnace insulation was removed in order to create a slower heating rate (the same procedure as test 3). The cable was heated at a rate close to 9^{o}C/minute. During the heating phase, the cable elongated 0.475 inches and ruptured at a temperature of 457^{o}C. The rupture occurred 6 seconds after the first signs of a reduction in the holding load.

Figure 64 shows the cable after rupture. Four of the exterior strands ruptured simultaneously. The remaining three strands had significant necking at the same location where the other strands ruptured. The rupture cross sections did not show any signs of discoloration, and the failed surface had a cup and cone type fracture. The rupture was followed by violent recoil and produced a loud "bang" sound.

4.3.2 70% MUTS

The 70% MUTS was chosen to compare the current study to past research. Abrams and Cruz (1961) tested the rupture temperature of strands prestressed to 70% ultimate stress. In that study it was determined that the rupture temperature was not affected by the rate of heating. The heating of the Abrams and Cruz study were 5^{o}F/minute, 10^{o}F/minute, and 15^{o}F/minute. The 70% ultimate

stress level was also used in the Holmes (et al.) study is typical for post-tensioned concrete. Holmes (et al. 1982) claim that 70% was chosen to simulate the prestress level in concrete, however due to prestress losses the in-service stress level is typically lower.

4.3.2.1 Test 1

The time-history for 70% MUTS test 1 is shown in Figure 65. The load was held at 40.7 kips (500 lbf from exactly 70%). During the initial loading the cable stretched 0.97 inches and stretched an additional 0.32 inches, during the transient heating phase, before rupture. The strand experienced a heat increase rate close to 19°C/minute, and ruptured when at a temperature of 386°C. 2.2 seconds elapsed between the first indication of cable failure and rupture.

Figure 66 shows the ruptured cable. The break was considered violent and sudden. Five of the exterior cables broke simultaneously and a loud bang occurred. The wires recoiled and were no longer helically woven into the 7-wire strand configuration. The failed cross section of the strand showed a blue tint. This was the same type of discoloration that was observed in the constant heat testing for 400°C and 500°C. This discoloration did not occur for the 42% or 45% MUTS transient tests.

4.3.2.2 Test 2

The time-history for 70% MUTS test 2 is shown in Figure 67. The strand was stressed to 41.04 kips during the initial loading. This loading produced a 0.987 inch deformation in the cable. During the transient heating phase, the cable deformed an additional 0.363 inches. The strand experienced a heating rate of approximately 18°C/minute. The strand ruptured at a temperature of 395°C, where the rupture occurred 2.2 seconds from the instant the load started to drop.

Figure 68 shows the failed specimen. The strand failed when five of the exterior wires ruptured simultaneously. Necking was evident at the same location where the other wires failed. The rupture was violent and occurred suddenly. The broken wires recoiled, as can be seen in the post-test specimen, and a loud bang was heard. At the cross sections of failure, a blue tint was found. This was the same type of discoloration that was found in the 70% MUTS test 1.

4.3.2.3 Test 3

The time-history for the 3rd 70% MUTS transient test is shown in Figure 69. The load was held at a constant 41.05 kips. There was 1.04 inches of deformation during the initial loading. The furnace insulation material was removed and the cable was heated at a slower rate that the first two 70% MUTS transient tests. The furnace created two observable heating rates. The strand was initially heating at a rate of approximately 20°C/minute. The second heating rate of 7°C/minute started at approximately 290°C. This heating rate is considered the controlling heating rate. During the heating phase, the cable elongated an additional 0.46 inches. The cable failed at 350°C. The failure occurred 6 seconds after the first indication of load reduction.

Figure 70 shows the 7-wire strand after testing. Four of the exterior strands ruptured simultaneously which resulted in a violent recoil and a loud "bang". The failed cross sections showed a blue tinting and the cup and cone fracture type. The remaining three strands displayed significant necking. The necking was located in the same cable section as the ruptured cross section.

4.3.2.4 Test 4

The time-history for the 4th 70% MUTS transient test is shown in Figure 71. The constant load was held at 40.95 kips. During the initial loading the cable deformed 0.96 inches. The furnace insulation was removed and the temperature-time curve shows a bilinear heating rate. The second heating rate of 6ºC/minute begins at approximately 250ºC. The heating phase produced an additional 0.46 inches of deformation. The cable failed at a temperature of 337.5ºC. The failure occurred approximately 5.5 seconds after the first indication of load reduction.

Figure 72 shows the 7-wire strand after testing. Four of the exterior strands ruptured simultaneously. The remaining three strands show signs of significant necking. The necking in the three remaining strands is at the same location as the strand rupture. The ruptured strands exhibit a cup and cone fracture along with a blue discoloration to the steel cross section. When the cable failed, a loud "bang" was heard and the cable recoiled violently.

4.3.3 42% MUTS

Two tests were carried out at 42% MUTS at ambient temperature. This stress level was chosen to study the sensitivity of the rupture temperature. This 42% stress level would be similar to the in-service load of a cable tension element that was stressed to 45% and experienced a loss in prestressing.

4.3.3.1 Test 1

The time-history for the first 42% MUTS is shown in Figure 53. The universal testing machine was programmed to hold an initial load of 24.6 kips, and during the test the accuracy of the machine allowed for the holding load of 24.52 kips. The strand heated at a rate of approximately 24ºC/minute until failure at 515ºC. The strand displaced 0.7 inches during the loading. During the transient heating phase, the cable displaced an additional 0.38 inches before rupture. The strand

displaced 0.7 inches during the initial loading. During the transient heating phase, the cable displaced an additional 0.38 inches before rupture.

The strand failed suddenly and with violent recoil. The load started to drop from the 24.52 kip holding load, and three seconds later the outer wires ruptured instantaneously (except for one). The center wire and one of the outer wires did not rupture but displayed necking at the same location that the other wires failed. No color change was evident. The wires splayed from the center strand as shown in Figure 54.

4.3.3.2 Test 2

Figure 55 shows the time-history for the 2nd 42% MUTS transient temperature test. The load was held at 24.6 kips. The furnace created a heating rate of 22.5°C/minute and the strand failed at 513.8°C.

The strand displaced 0.727 inches during the initial loading. Before rupture, the transient heating caused an additional 0.423 in displacement. The load started to decline from the holding load at 39.33 minutes into the test. After another 3.8 seconds following the first indication of load decrease, five wires ruptured simultaneously. The failed cross sections all displayed cup and cone fractures, and the non-ruptured wires showed necking. The failed specimen is shown in Figure 56.

4.4 Elastic Modulus Test

The elastic modulus test did not provide many qualitative observations. The specimen was displaced by a predetermined length and returned to the initial undeformed length during each

loading sequence at each temperature. The largest length of displacement was 0.75 inches at a displacement rate of 0.25 in/minute. A displacement rate of 0.25 in/minute was difficult to observe with the human eye in real time. Thus, the only observations made were of the load displacement curves on the controller display monitor. Test 1 results are shown in Figure 74 through Figure 80 and Test 2 results are shown in Figure 82 through Figure 89. A linear regression line was fit through the data points and the slope of that line was accepted as the elastic modulus of the strand.

During the test, the furnace remained closed between temperature increases. The only observations of the cable occurred after the test was completed. The cable showed signs of discoloration (Figure 73and Figure 81), however, it did not exhibit the flaking of exterior metal that occurred during the constant temperature test for 800ºC. In the elastic modulus test, the strand's stress was kept below the yield limit at all times. The specimens for these tests were never tested to failure.

4.5 Summary

This chapter provided the observations and test data from the experimental testing. Three types of tests were conducted and presented: constant temperature, transient temperature, and elastic modulus. Observations were made in regards to the type of failure, cable behavior at failure, and any noticeable changes in cable properties. Load-displacement curves and time-temperature history curves were included along with photos of the failed cable sections.

For the constant temperature testing, a noticeable change in load-displacement curves was observed at 300ºC and above. At this temperature, the curve no longer resembled the ambient

temperature curve. The cable did not exhibit any significant strain-hardening or yield plateau between 300°C and 700°C. The cross section showed signs of extreme necking and area reduction at these temperatures. At 800°C, the load-displacement curves again changed shape. At this temperature, the curve resembled the 20°C ambient temperature curve and the cross section showed less area reduction when compared to the 600 and 700°C strand. The test data results are shown in Table 5.

Table 5: Ultimate Strength Data

Date	Temperature [°C]	Ultimate Strength [kips]	Percent Ultimate
15/01/07	20	61.65	100.00%
15/02/19	20	61.95	100.00%
15/02/23	200	56.33	91.15%
15/03/02	200	57.02	92.26%
15/03/02	300	45.45	73.55%
15/03/06	320	43.7	70.71%
15/03/06	400	33.85	54.77%
15/03/23	400	31.53	51.01%
15/02/20	500	17.85	28.88%
15/01/12	550	12.84	20.78%
15/03/27	600	7.77	12.58%
15/03/27	610	7.12	11.53%
15/03/30	700	2.54	4.11%
15/04/03	700	2.70	4.37%
15/04/03	800	2.11	3.41%
15/04/06	800	2.34	3.78%

The transient temperature testing showed that for a higher heating rate, the rupture temperature of the cable was approximately 10% higher than at lower heating rates. At slower heating rates, the cable had approximately a 35% greater deformation during the heating phase when compared to the faster heating rates.

Table 6: Transient Test Data

Test	Holding load [kips]	% MUTS	~ Heating Rate [^{o}C/min]	Rupture Temp [^{o}C]
15-05-01(1)	24.52	42%	24	515
15-05-01(2)	24.6	42%	22	513.8
15-06-08(1)	26.59	45%	25	501
15-06-08(2)	26.34	45%	26	500.8
15-06-09(1)	26.35	45%	7	458
15-06-09(2)	26.4	45%	9	457
15-05-08(1)	40.7	69%	19	386
15-05-08(2)	41.04	70%	18	395
15-06-05(2)	41.05	70%	7	350
15-06-09(3)	40.95	70%	6	337.5

The elastic modulus testing showed relatively no decrease from 20^{o}C to 200^{o}C. A slight linear decrease in elastic modulus was determined from 300^{o}C to 500^{o}C where 500^{o}C had approximately 82% of the ambient elastic modulus. At 600^{o}C there was a sharp decrease in the modulus and the strand was determined to have 38% of the ambient modulus. The elastic modulus was relatively unchanged between 700^{o}C and 800^{o}C having 20% and 18% of the ambient modulus respectively. The test data results are shown in Table 7 and Table 8.

Table 7: Elastic Modulus Test Data 15_05_28

Temperature [^{o}C]	Elastic Modulus [ksi]	Percent Ambient
20	28656	100%
200	28086	98%
300	28148	98%
400	24130	84%
500	20924	73%
600	7980	28%
700	6400	22%
800	5740	20%

Table 8: Elastic Modulus Test Data 15_05_29

Temperature [°C]	Elastic Modulus [ksi]	Percent Ambient
20	27358	100%
200	27100	99%
300	25850	94%
400	25850	94%
500	23954	88%
600	12700	46%
700	4698.8	17%
800	4246	16%

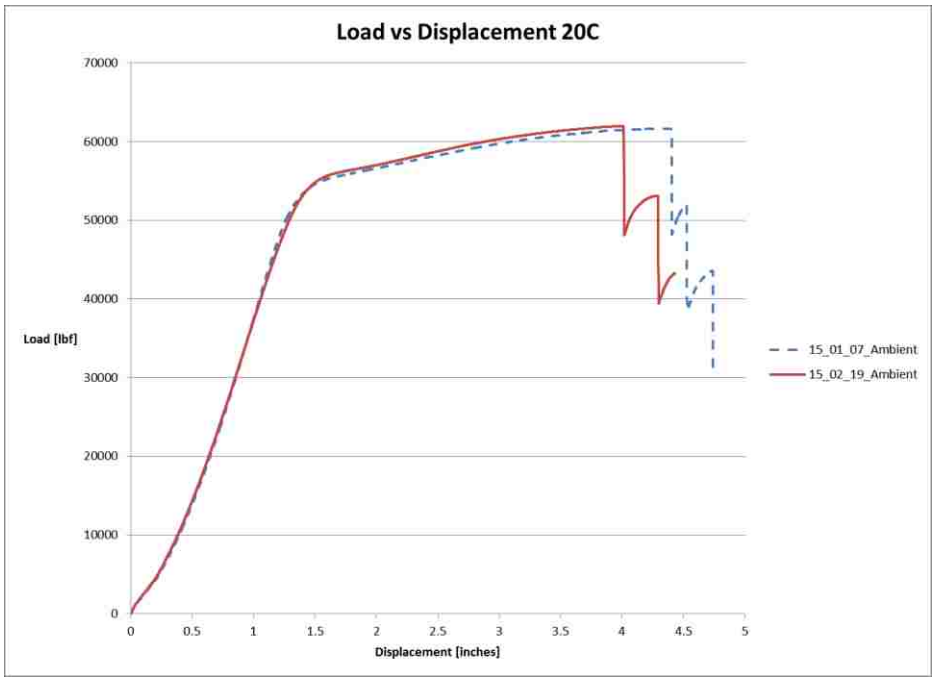

Figure 17: Load vs Displacement 20C

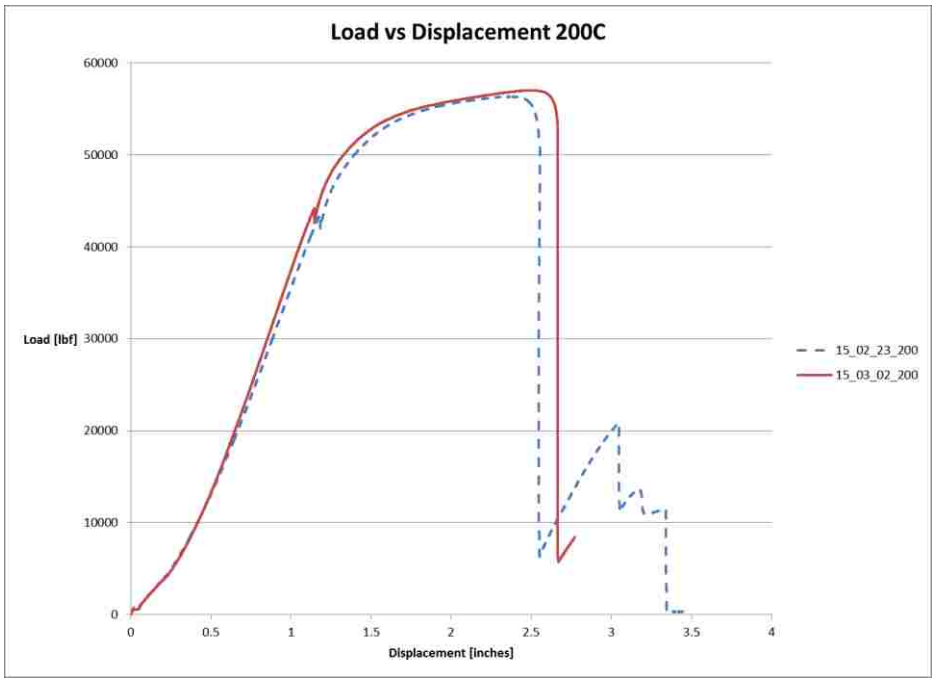

Figure 18: Load vs Displacement 200C

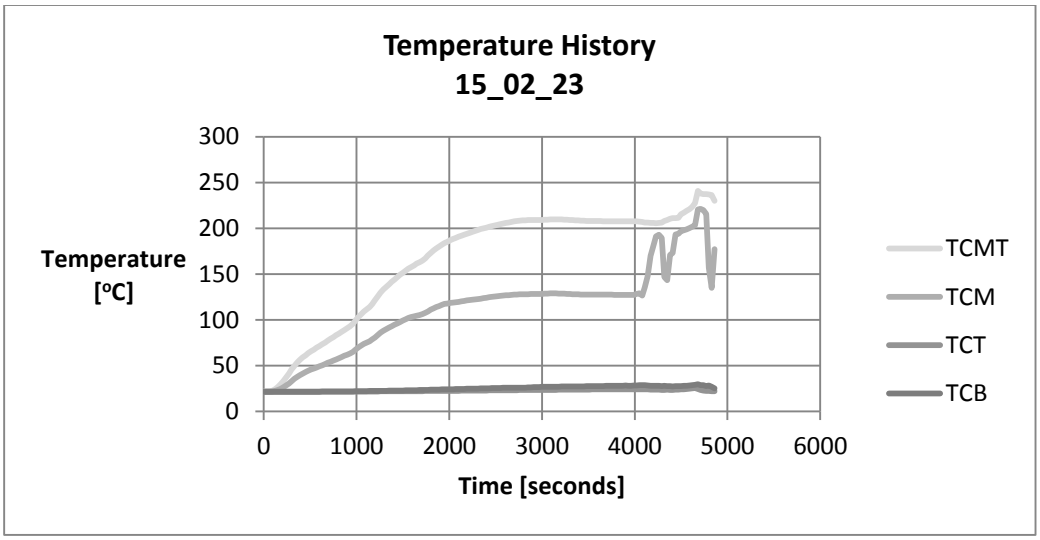

Figure 19: Temperature History 15_02_23

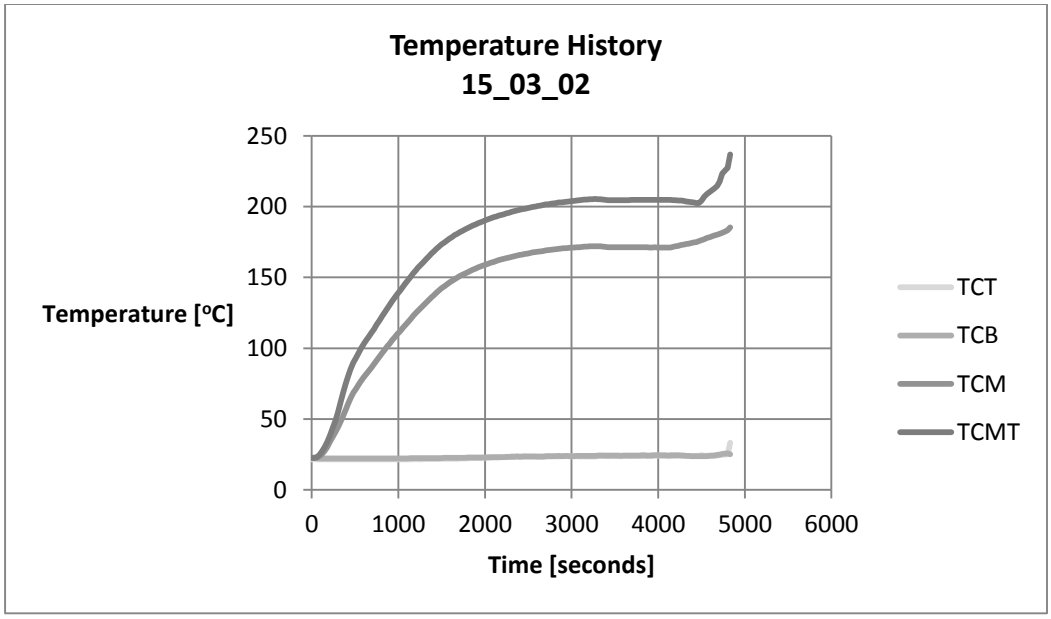

Figure 20: Temperature History 15_03_02

Figure 21: Specimen 15_02_23 Post-test

Figure 22: Specimen 15_03_02(1) Post-test

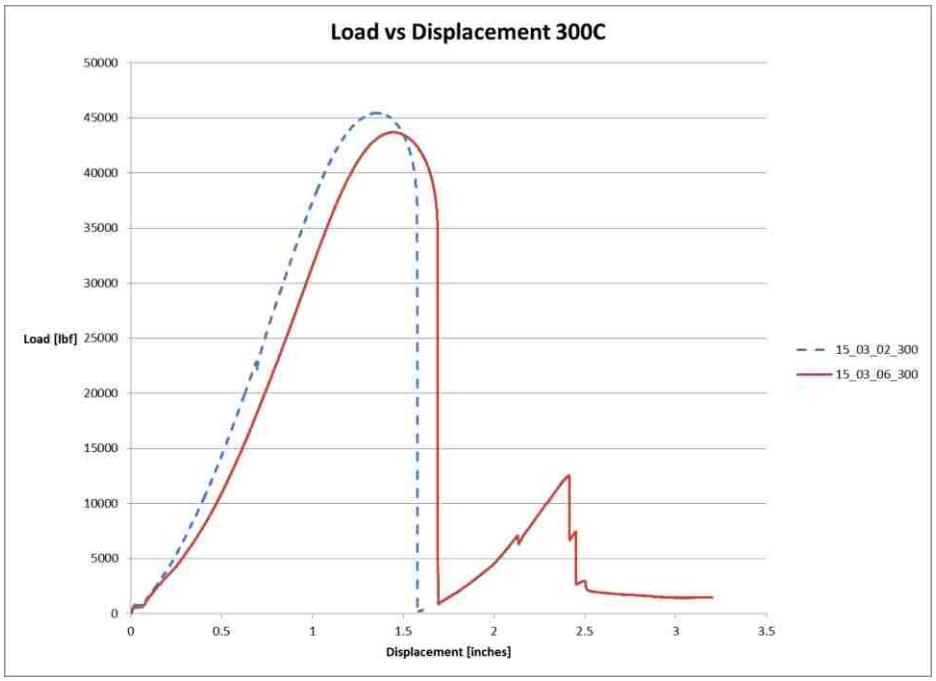

Figure 23: Load vs Displacement 300C

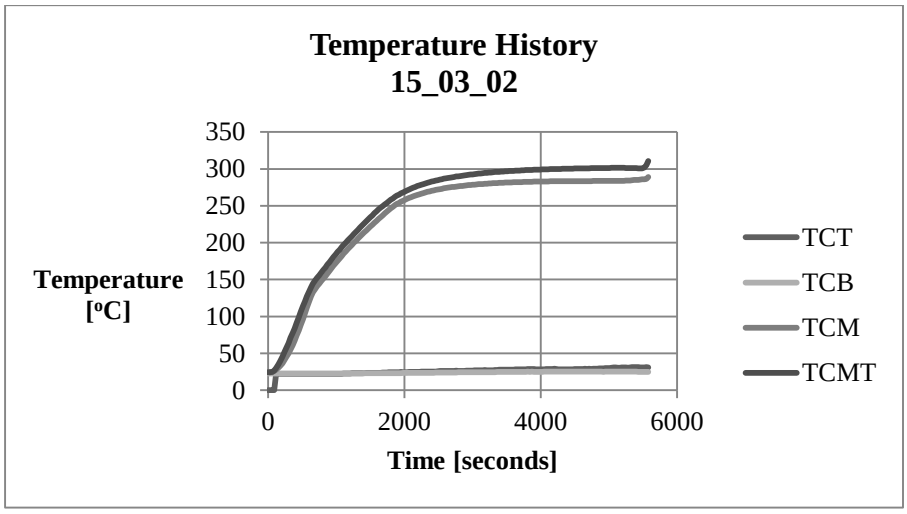

Figure 24: Temperature History 15_03_02

Figure 25: Specimen 15_03_02(2) Post-test

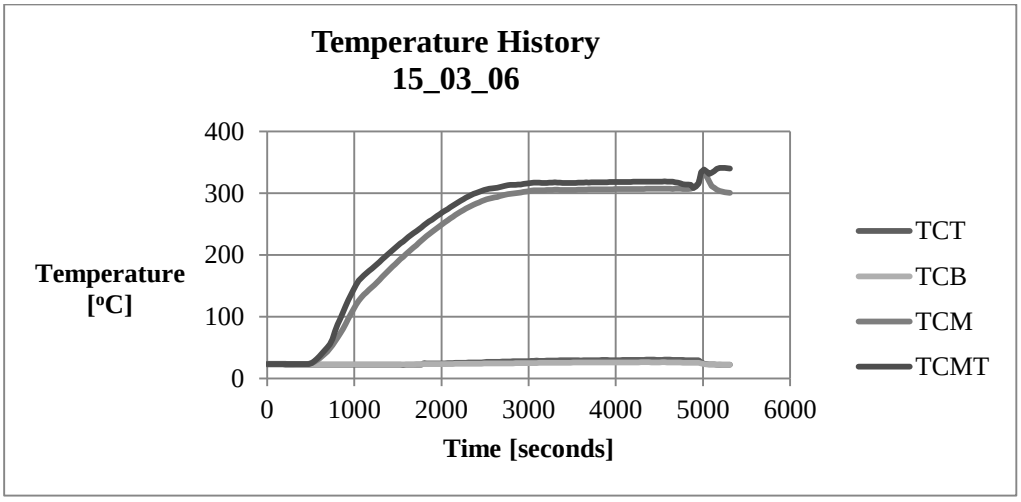

Figure 26: Temperature History 15_03_06

Figure 27: Specimen 15_03_06(1) Post-test

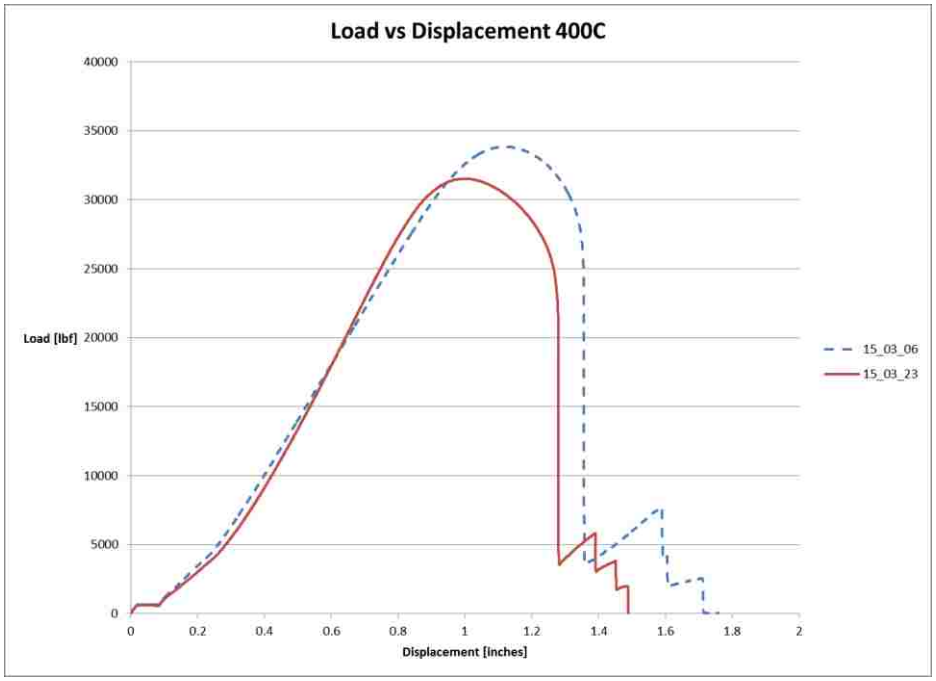

Figure 28: Load vs Displacement 400C

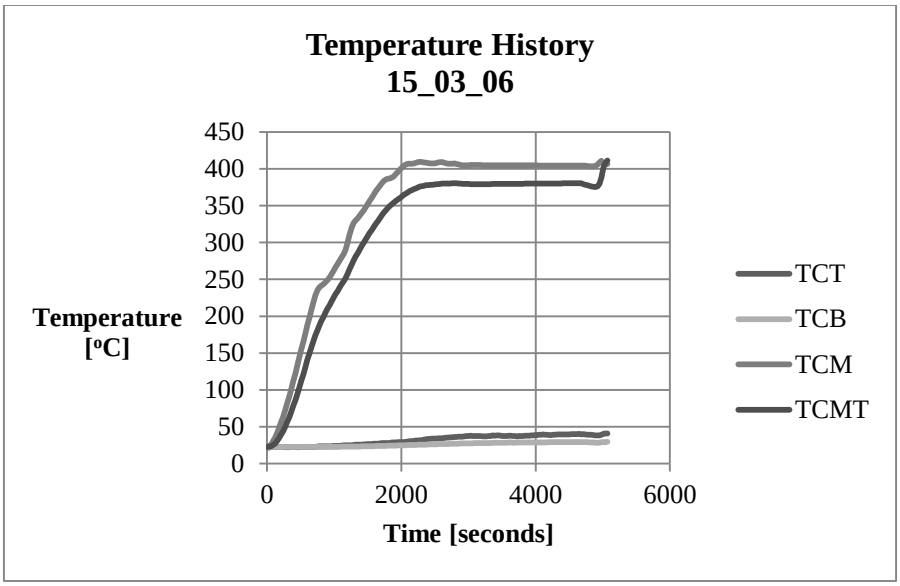

Figure 29: Temperature History 15_03_06

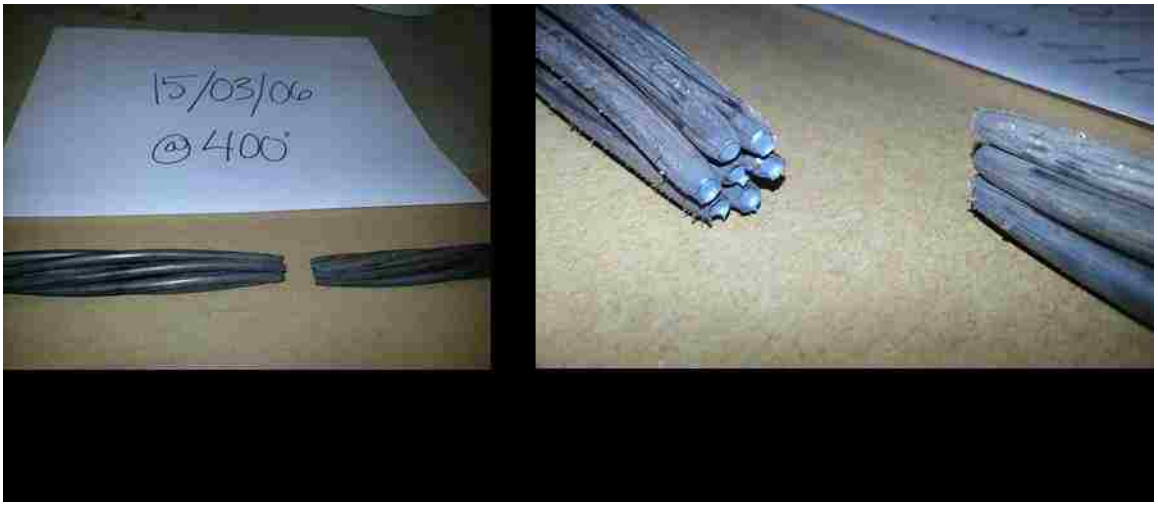

Figure 30: Specimen 15_03_06(2) Post-test

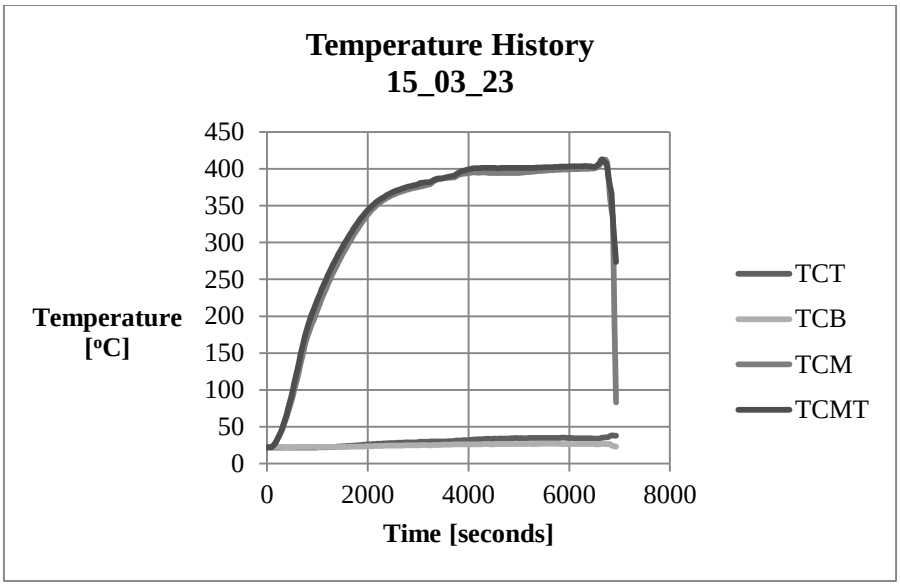

Figure 31: Temperature History 15_03_23

Figure 32: Specimen 15_03_23 Post-test

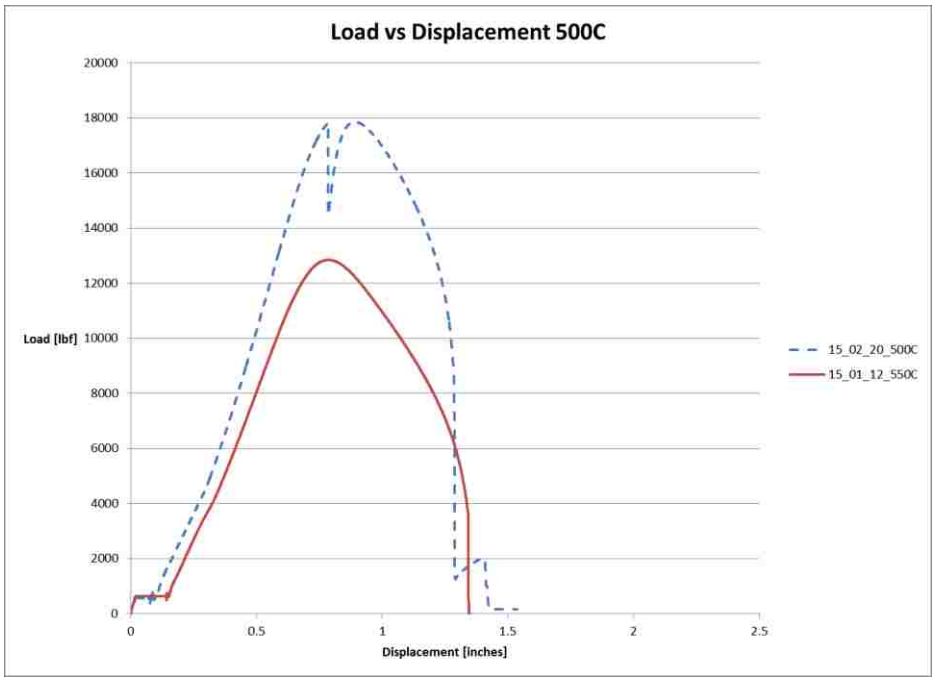

Figure 33: Load vs Displacement 500C

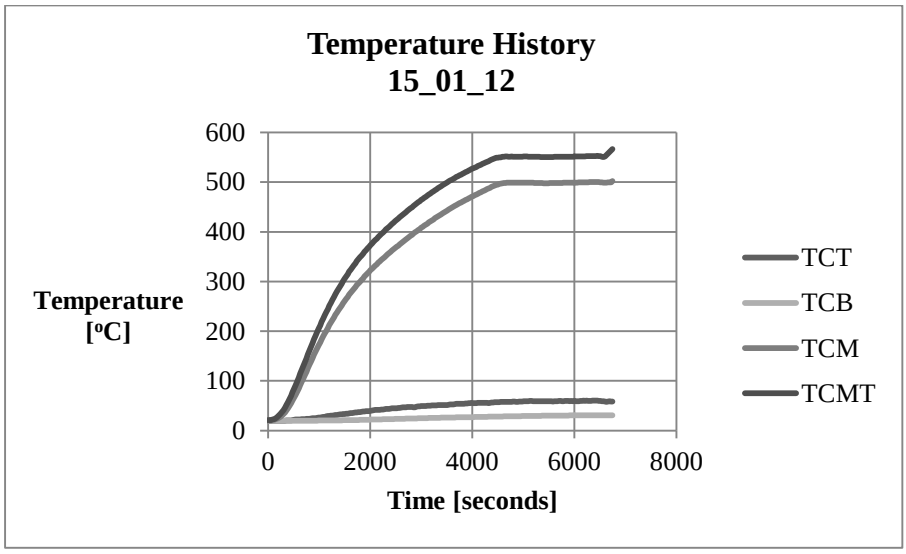

Figure 34: Temperature History 15_01_12

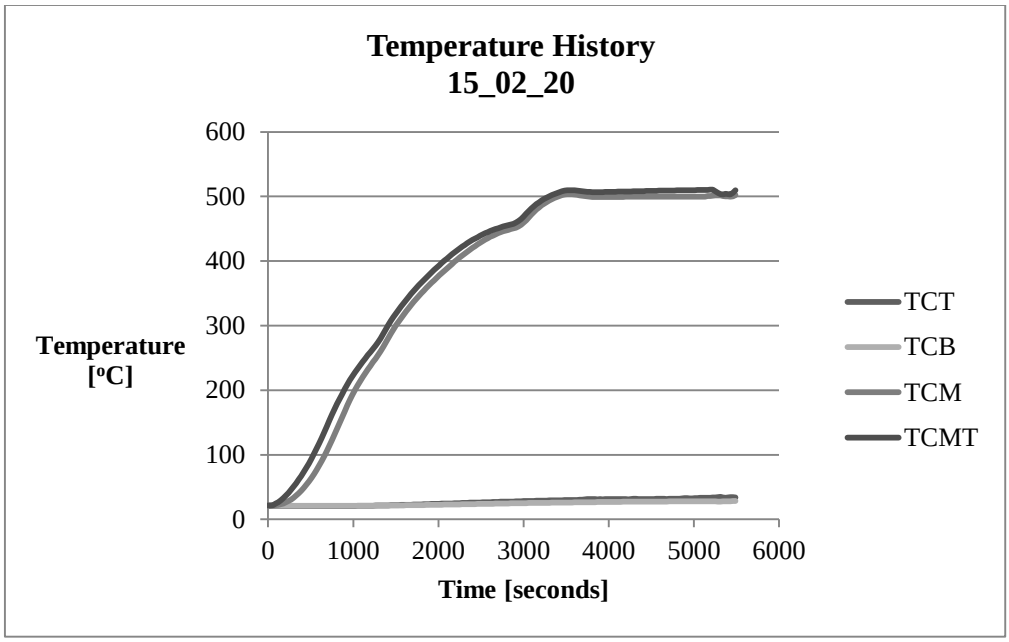

Figure 35: Temperature History 15_02_20

Figure 36: Specimen 15_01_12 Post-test

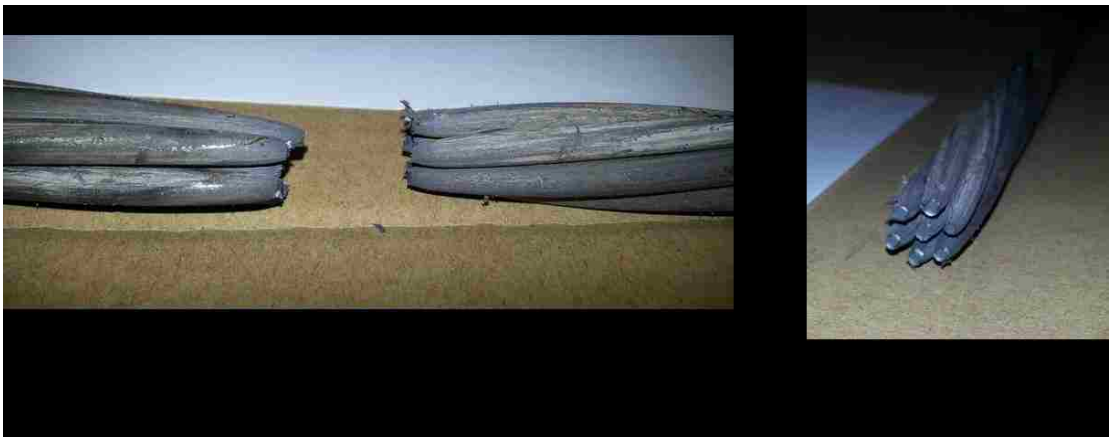

Figure 37: Specimen 15_02_20 Post-test

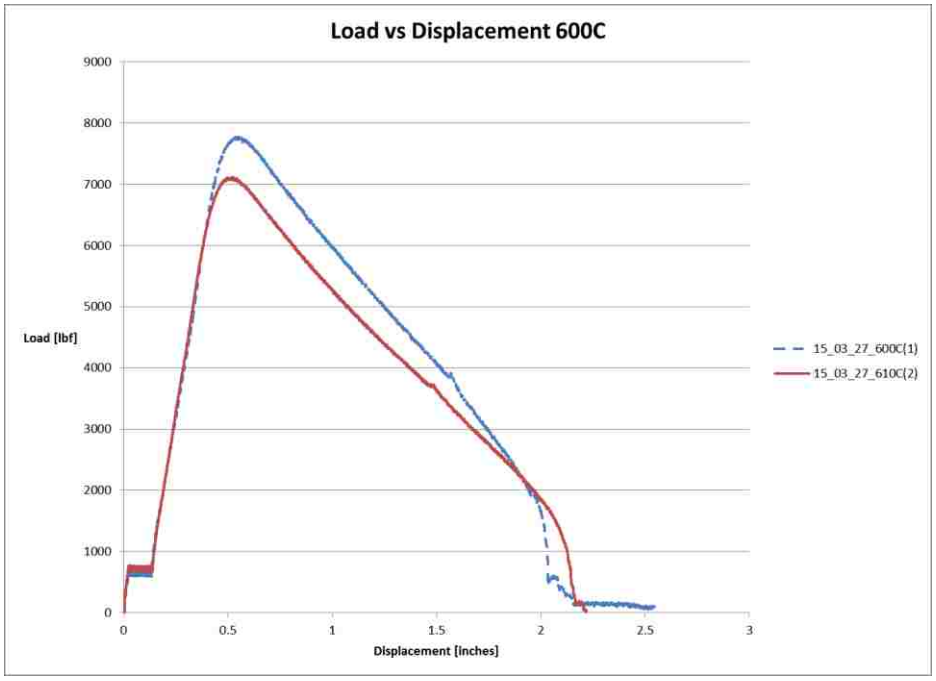

Figure 38: Load vs Displacement 600C

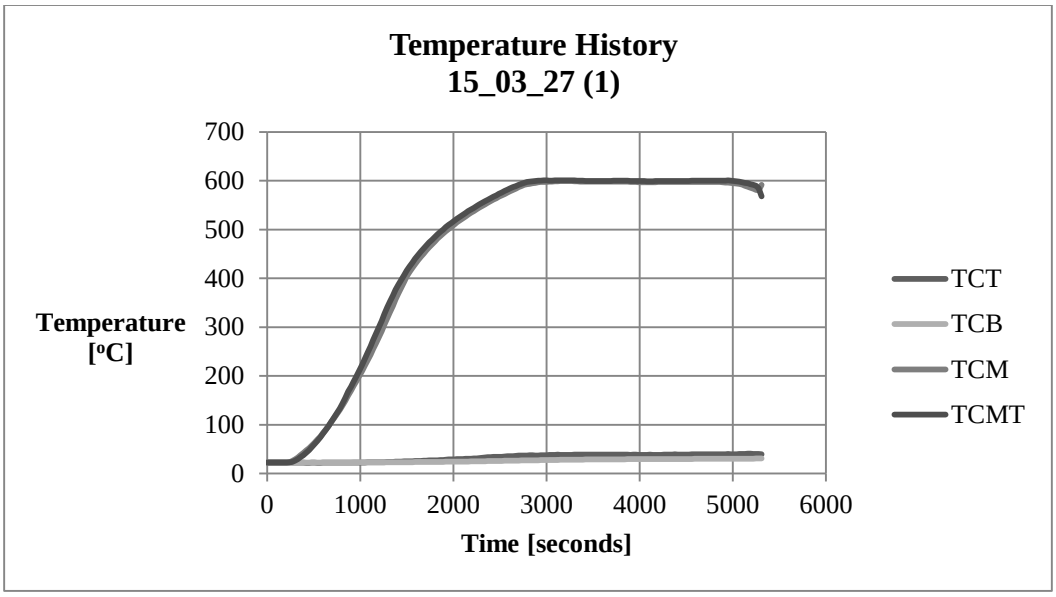

Figure 39: Temperature History 15_03_27(1)

Figure 40: Specimen 15_03_27(1) Post-test

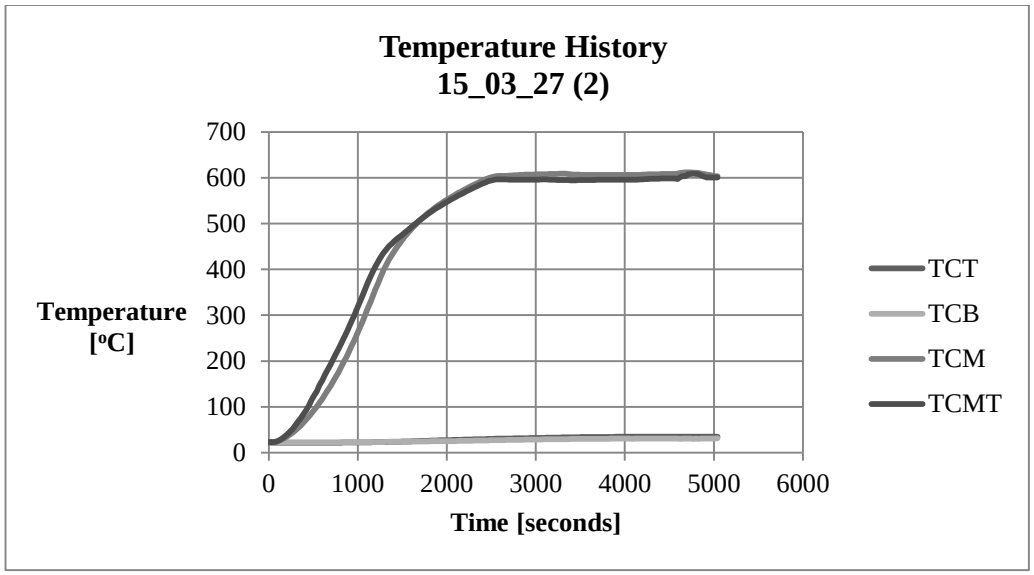

Figure 41: Temperature History 15_03_27(2)

Figure 42: Specimen 15_03_27(2) Post-test

Figure 43: Load vs Displacement 700C

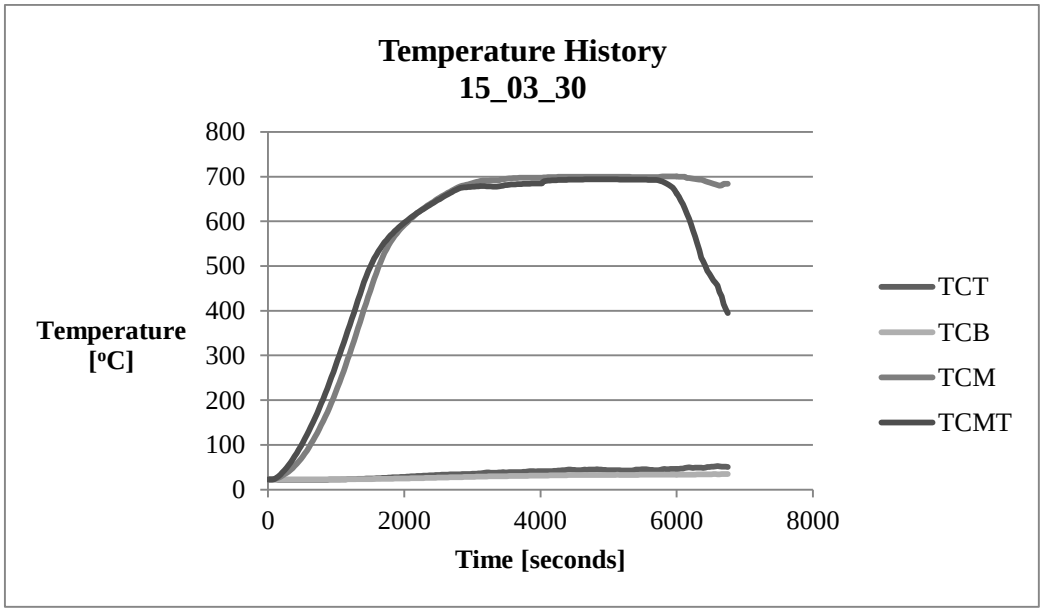

Figure 44: Temperature History 15_03_30

Figure 45: Specimen 15_03_30 Post-test

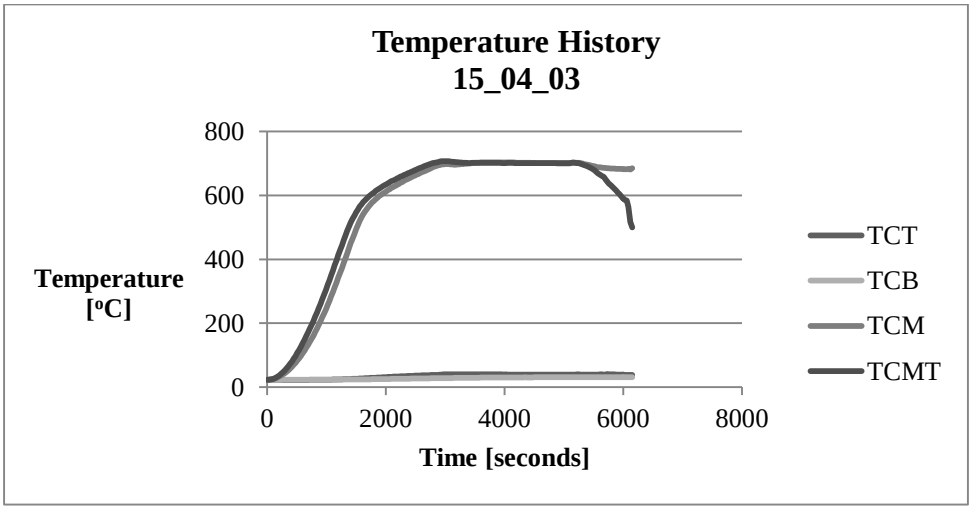

Figure 46: Temperature History 15_04_03

Figure 47: Specimen 15_04_03(1) Post-test

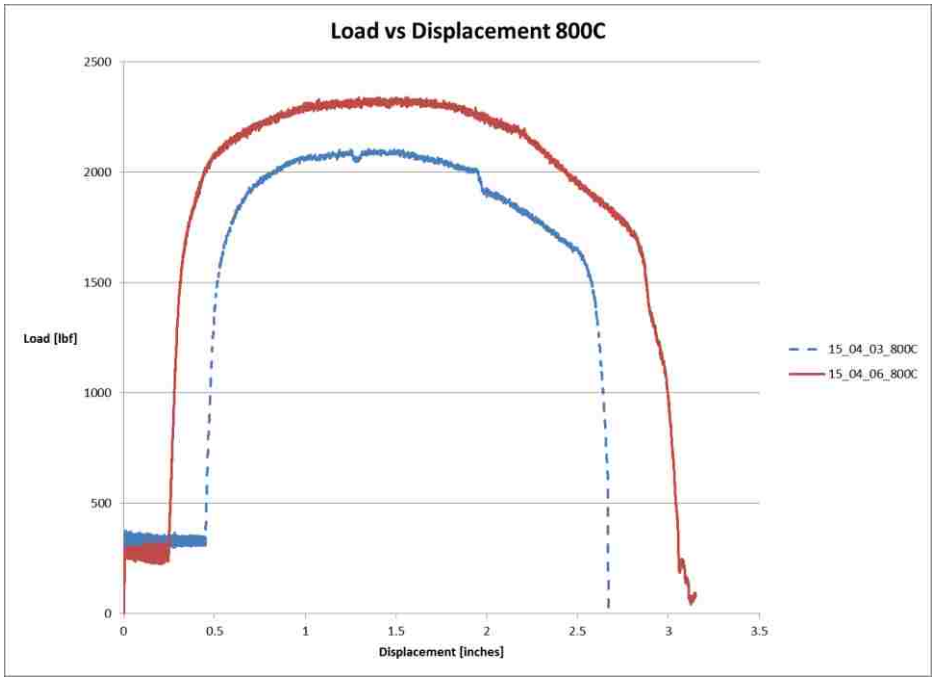

Figure 48: Load vs Displacement 800C

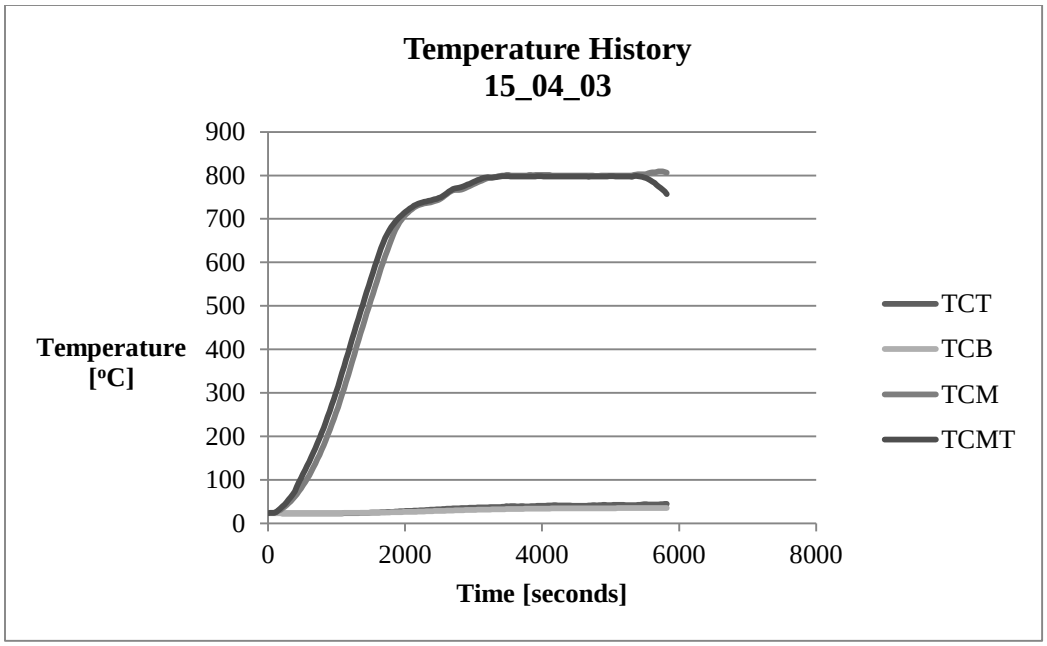

Figure 49: Temperature History 15_04_03

Figure 50: Specimen 15_04_03 Post-test

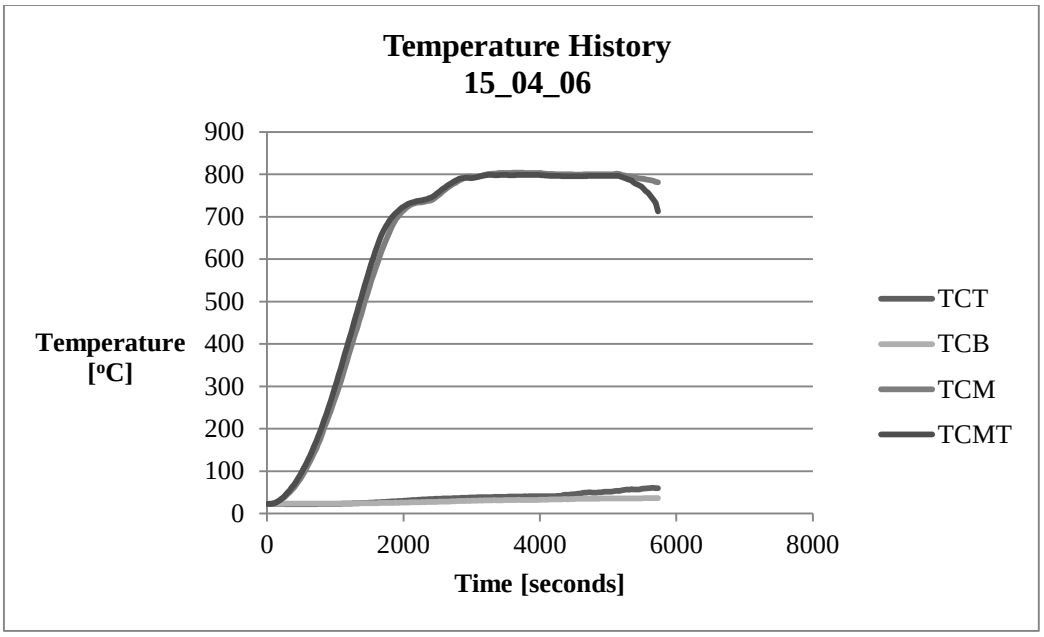

Figure 51: Temperature History 15_04_06

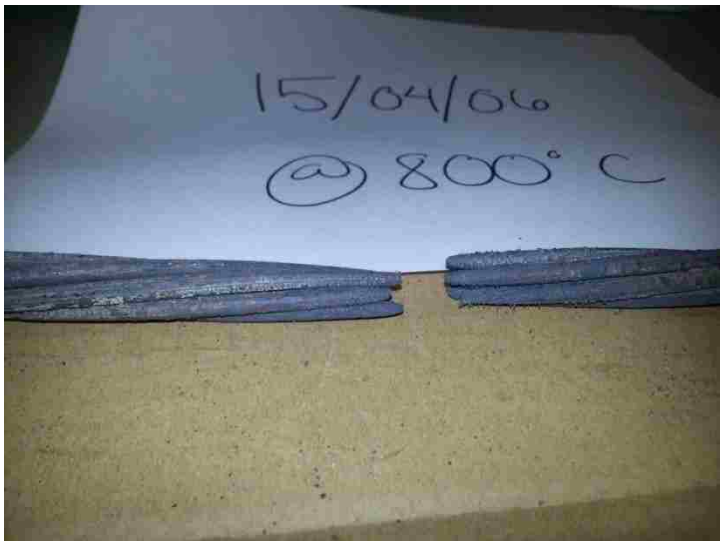

Figure 52: Specimen 15_04_06 Post-test

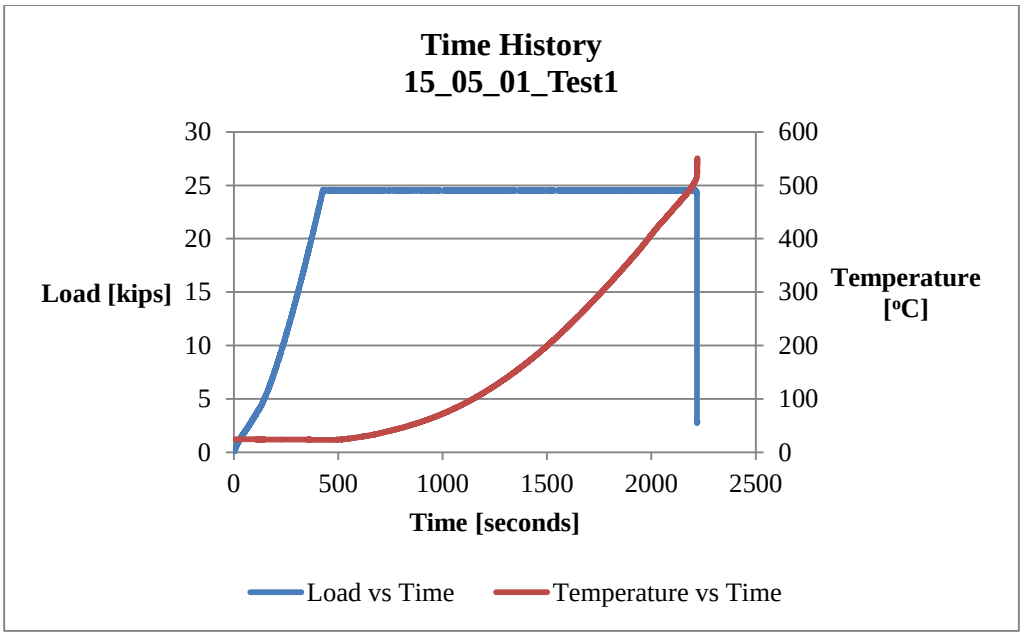

Figure 53: Time-History Specimen 15_05_01(1)

Figure 54: 42% Stress Test1 Post-test

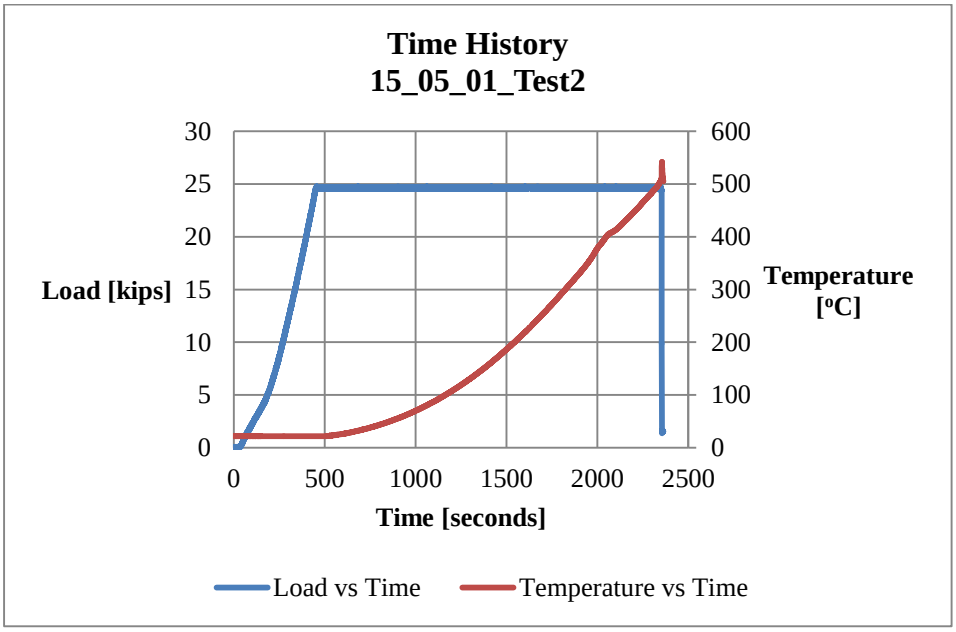

Figure 55: Time-history Specimen 15_05_01(2)

Figure 56: 42% Stress Test2 Post-test

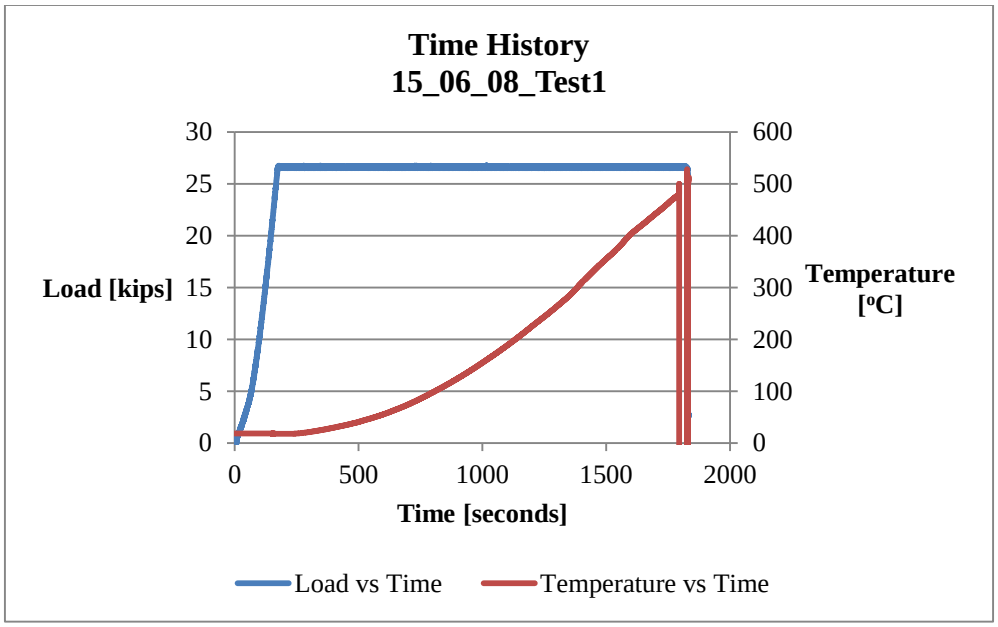

Figure 57: Time-history Specimen 15_06_08(1)

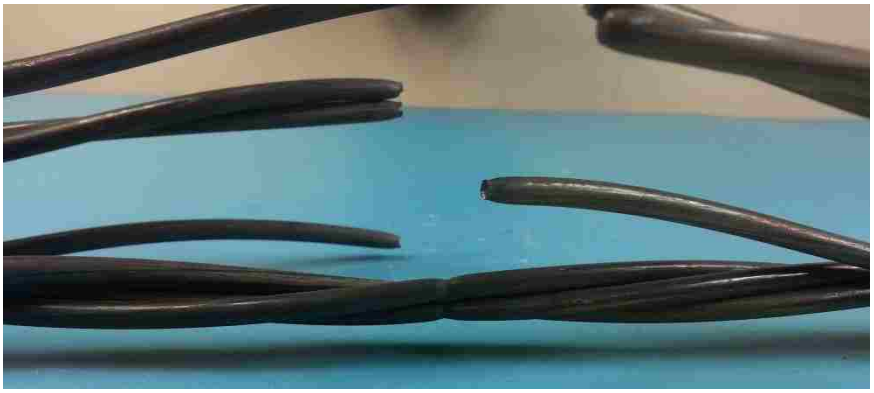

Figure 58: 45% Stress Test 1

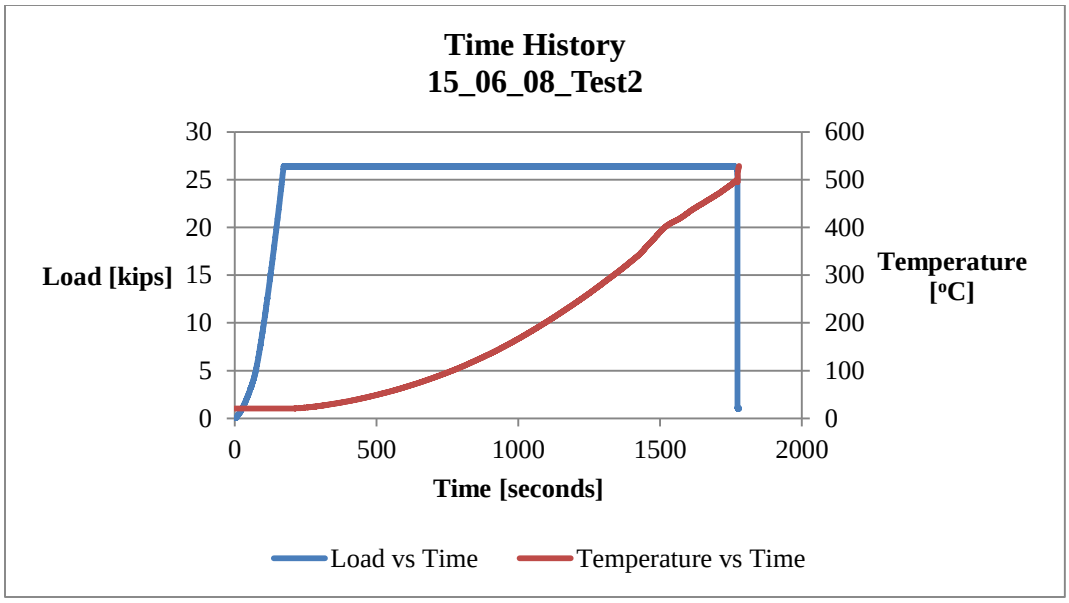

Figure 59: Time-history Specimen 15_06_08(2)

Figure 60: 45% Stress Test 2

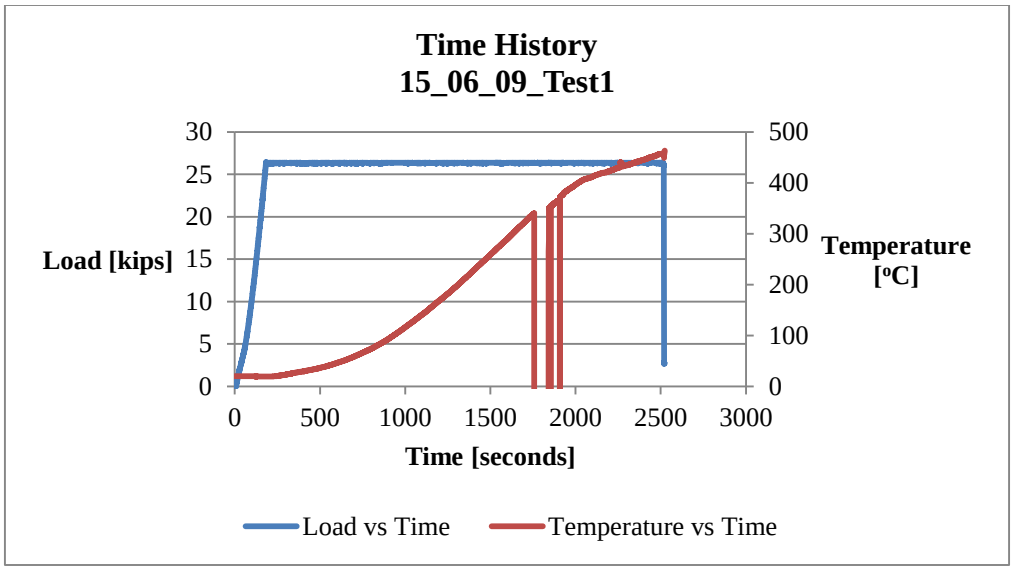

Figure 61: Time-history Specimen 15_06_09(1)

Figure 62: 45% Stress Test 3

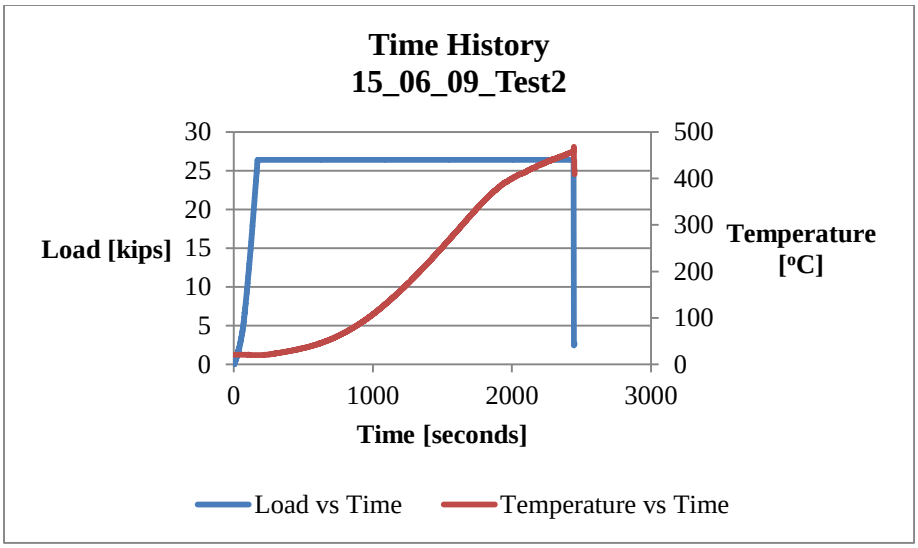

Figure 63: Time-history Specimen 15_06_09(2)

Figure 64: 45% Stress Test 4

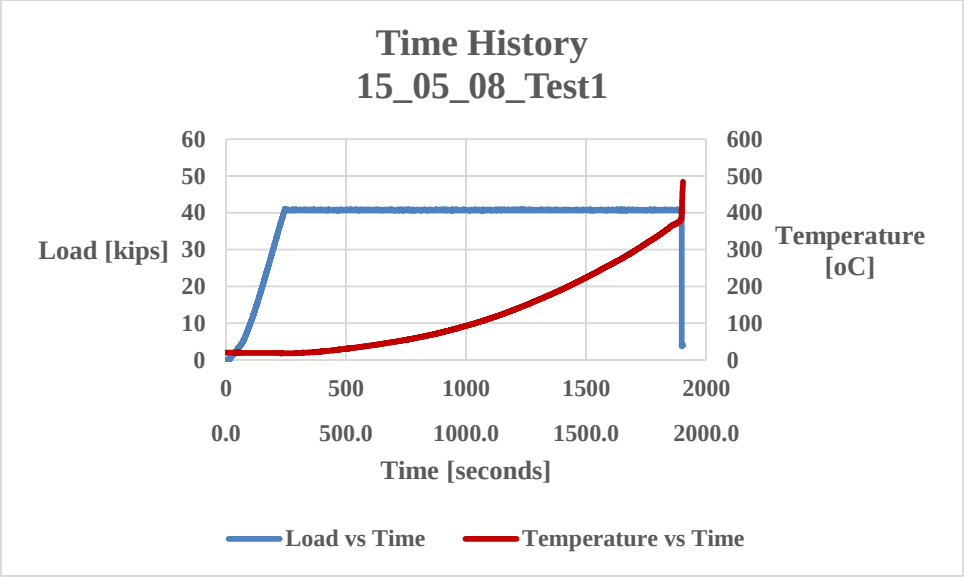

Figure 65: Time-history Specimen 15_05_08(1)

Figure 66: 70% Stress Test 1

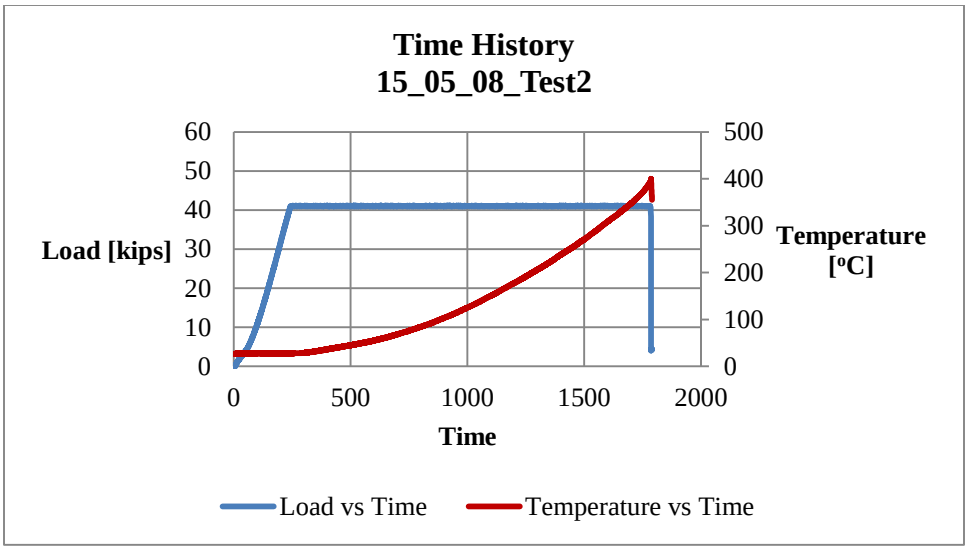

Figure 67: Time-history Specimen 15_05_08(2)

Figure 68: 70% Stress Test 2

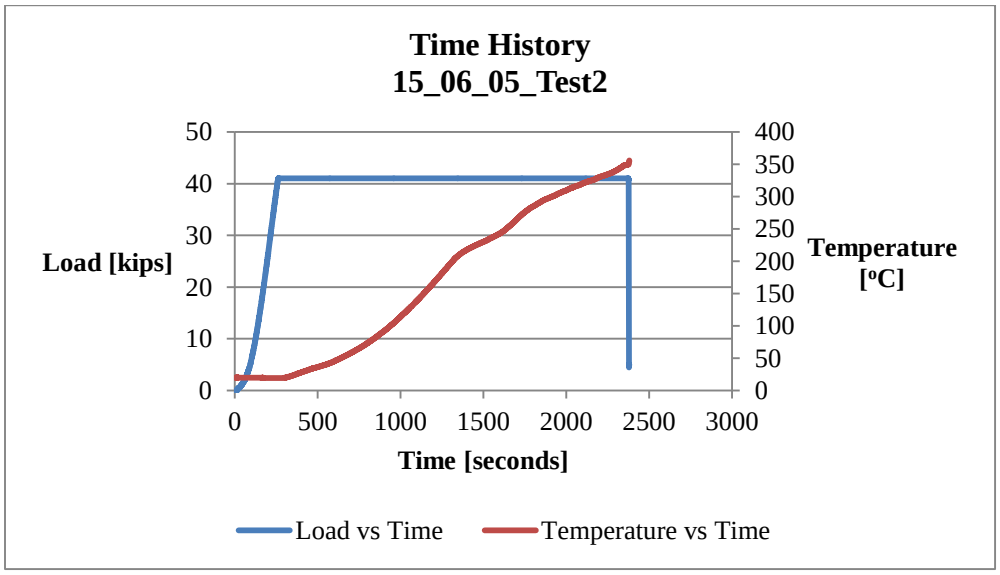

Figure 69: Time-history Specimen 15_06_05(2)

Figure 70: 70% Stress Test 3

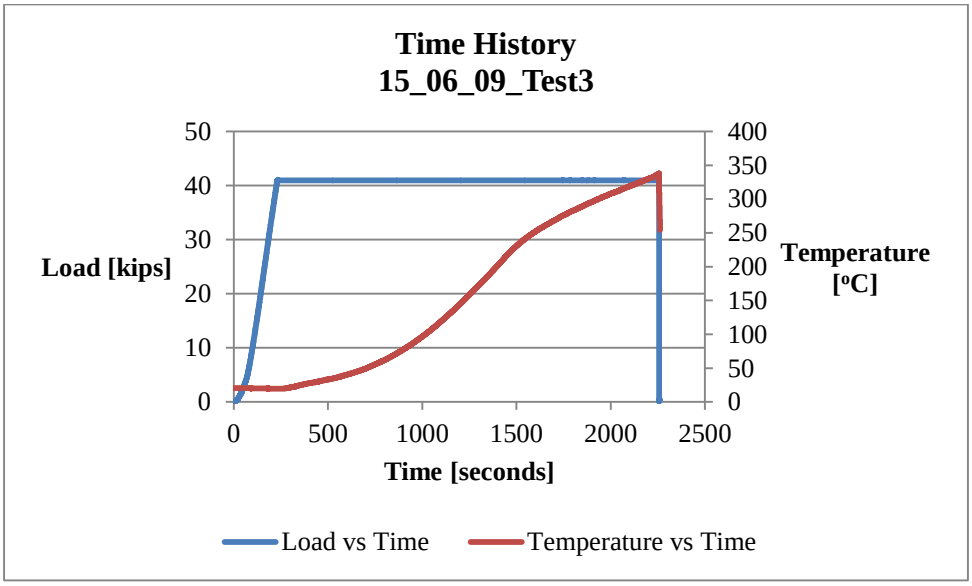

Figure 71: Time-history Specimen 15_06_09(3)

Figure 72: 70% Stress Test 4

Figure 73: Elastic Modulus Test 1 Strand

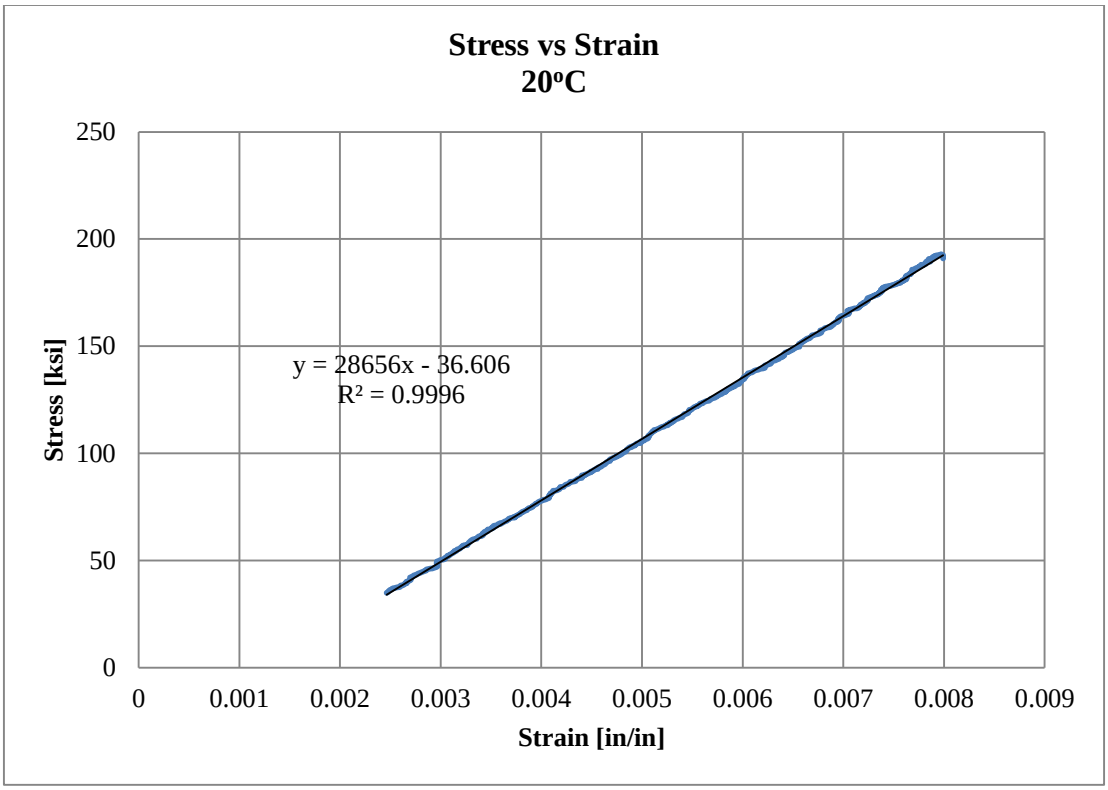

Figure 74: Elastic Modulus Test 1 20C

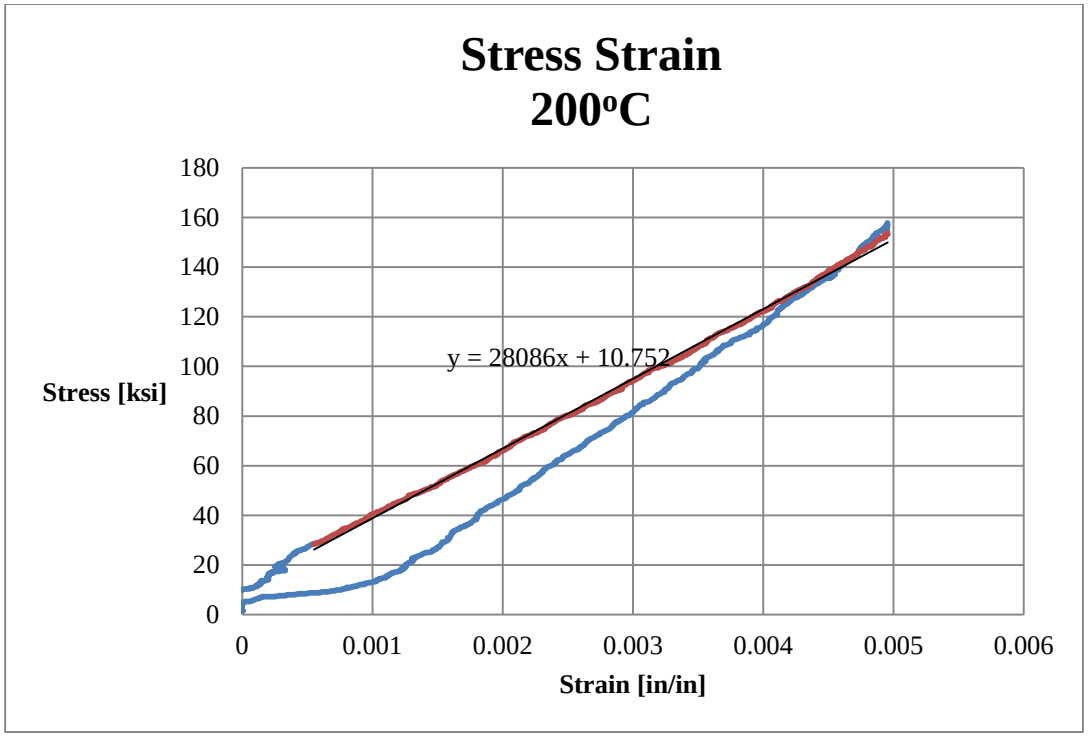

Figure 75: Elastic Modulus Test 1 200C

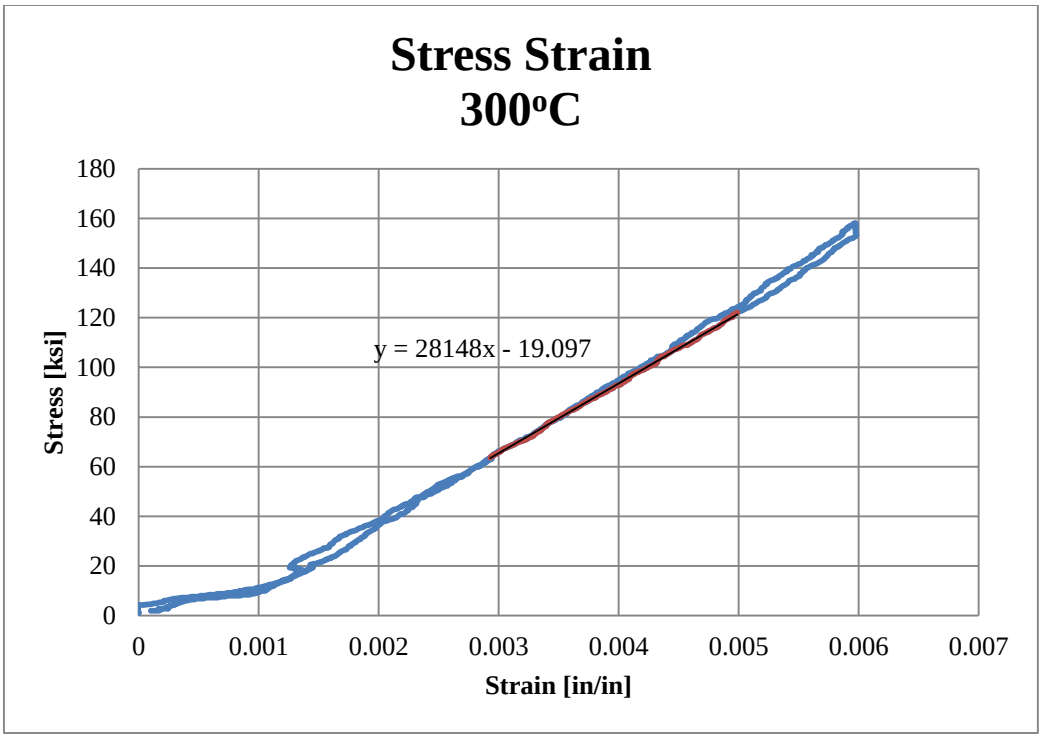

Figure 76: Elastic Modulus Test 1 300C

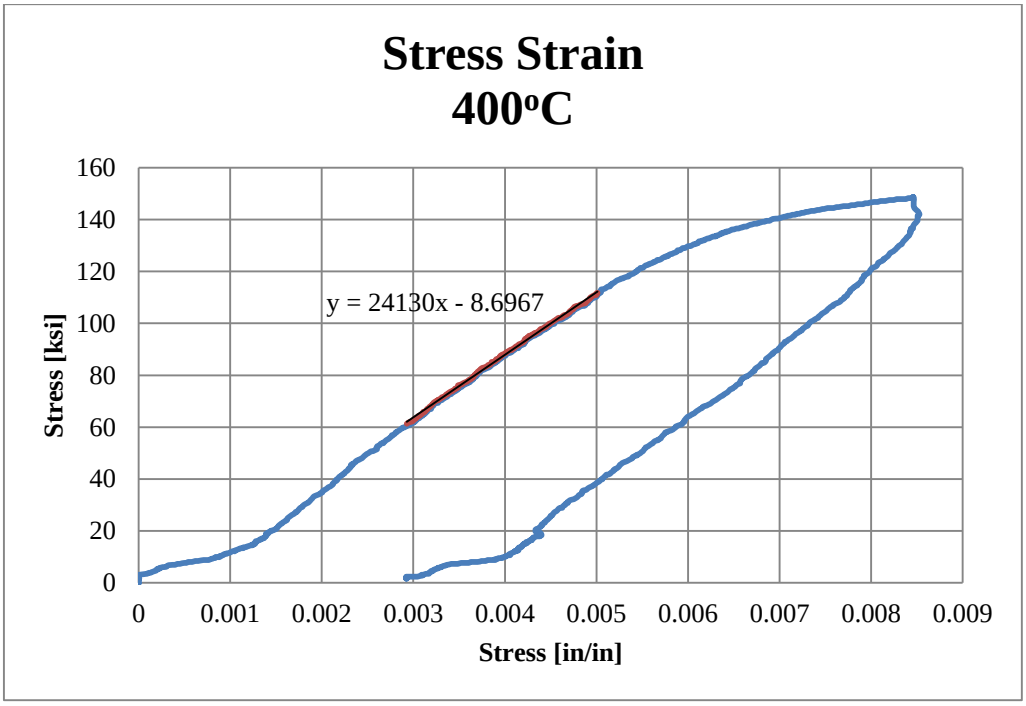

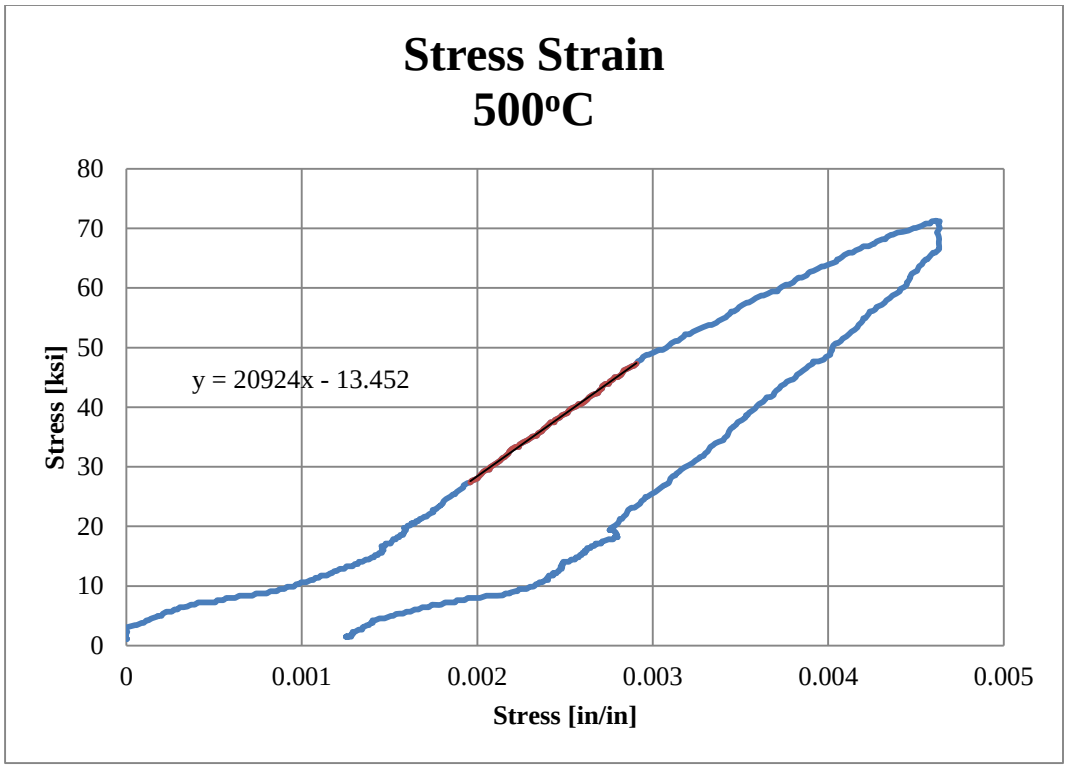

Figure 77: Elastic Modulus Test 1 400C

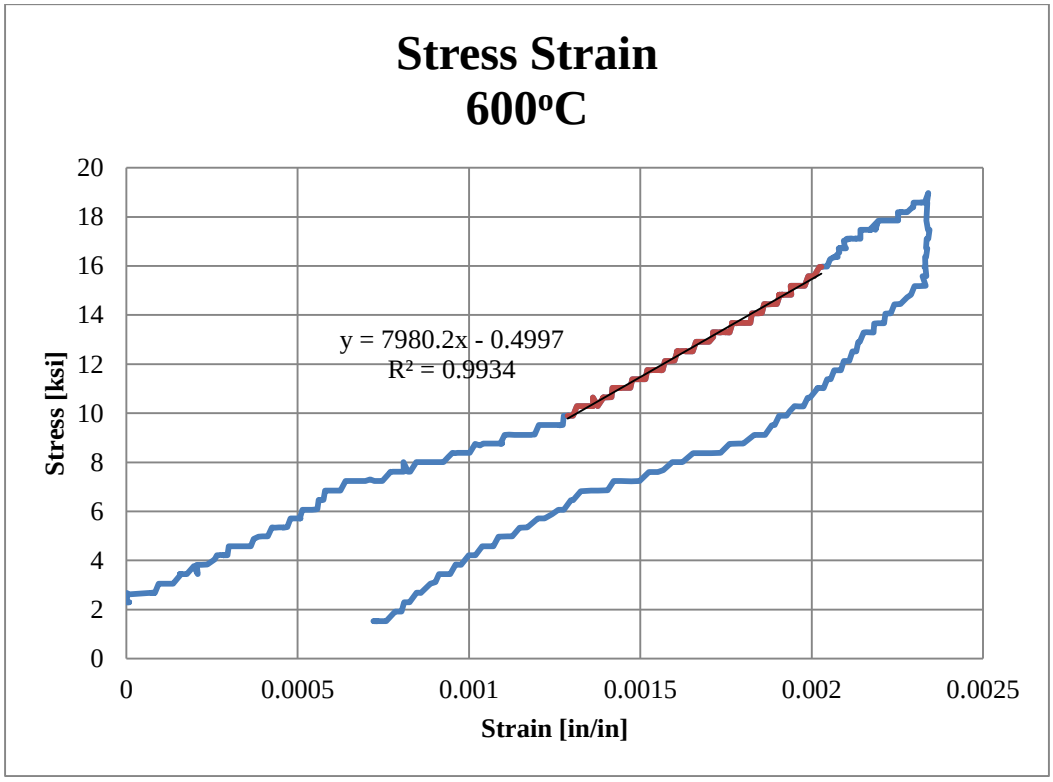

Figure 78: Elastic Modulus Test 1 500C

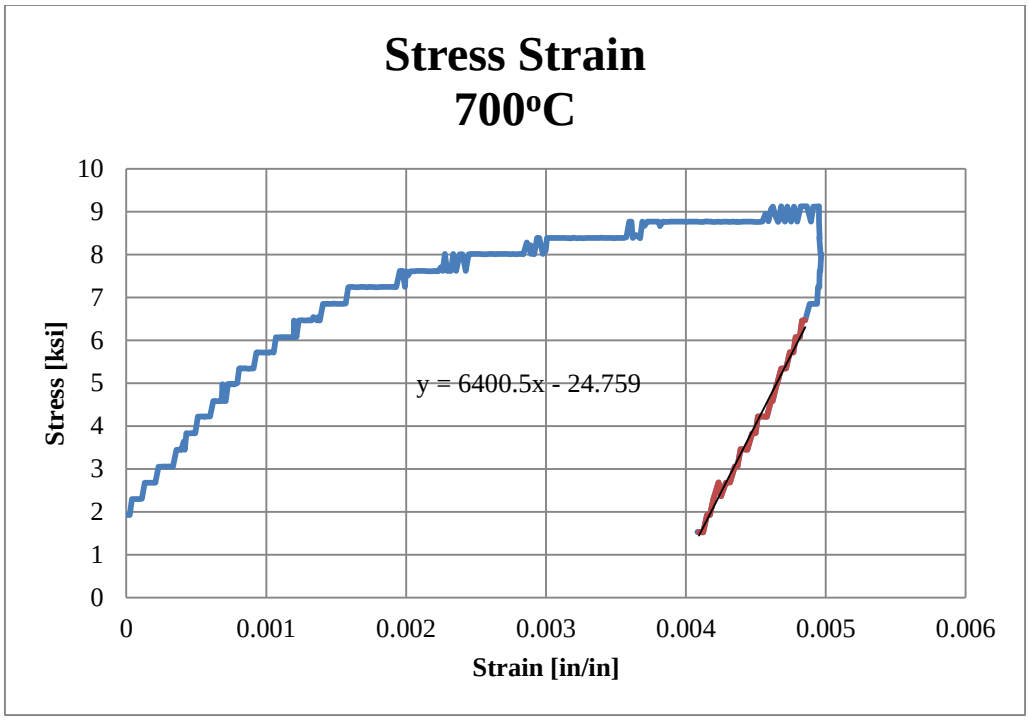

Figure 79: Elastic Modulus Test 1 700C

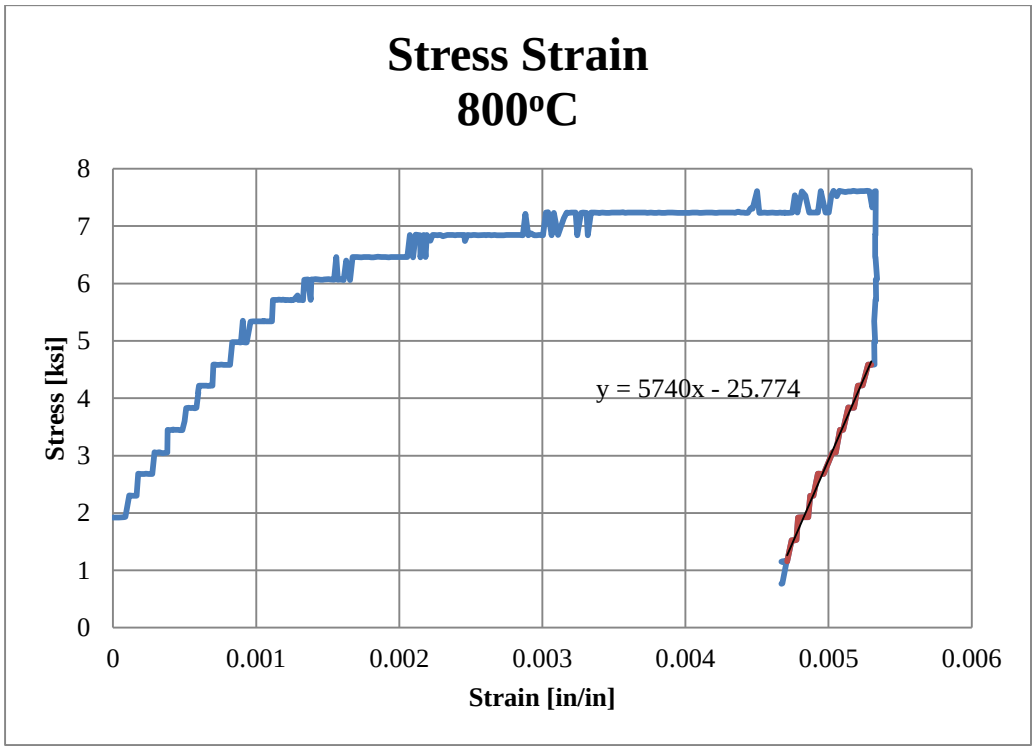

Figure 80: Elastic Modulus Test 1 800C

Figure 81: Elastic Modulus Test 2 Strand

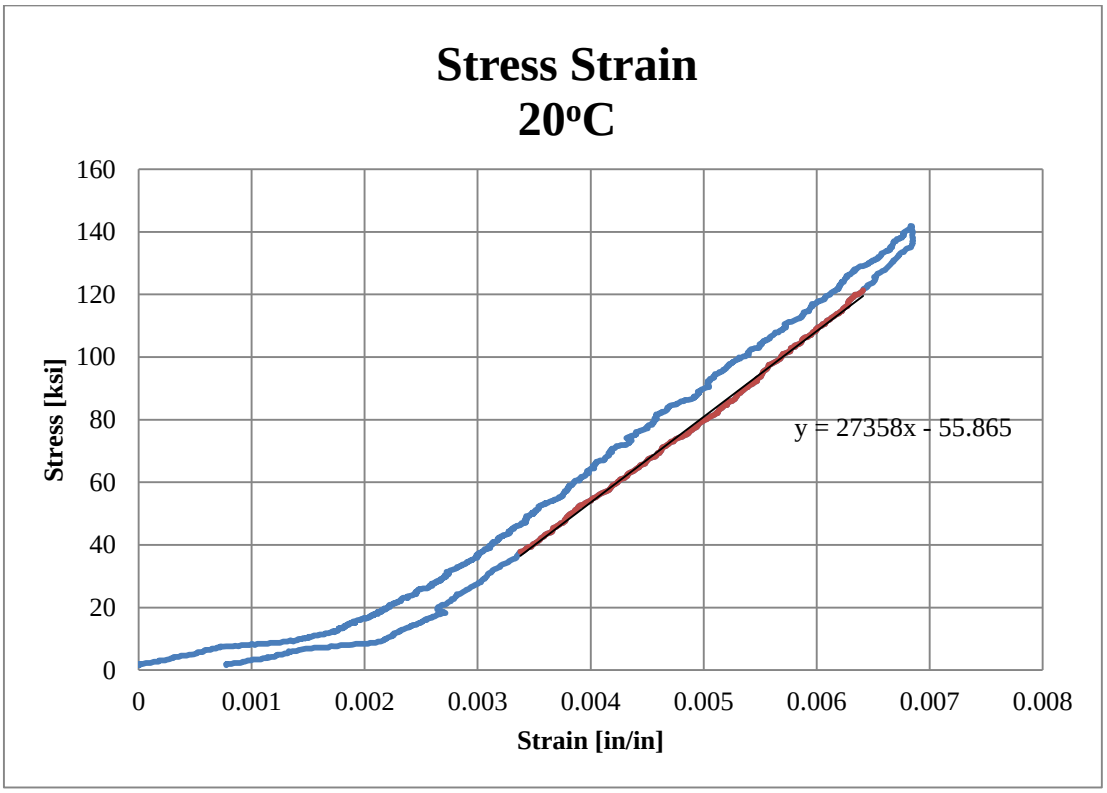

Figure 82: Elastic Modulus Test 2 20C

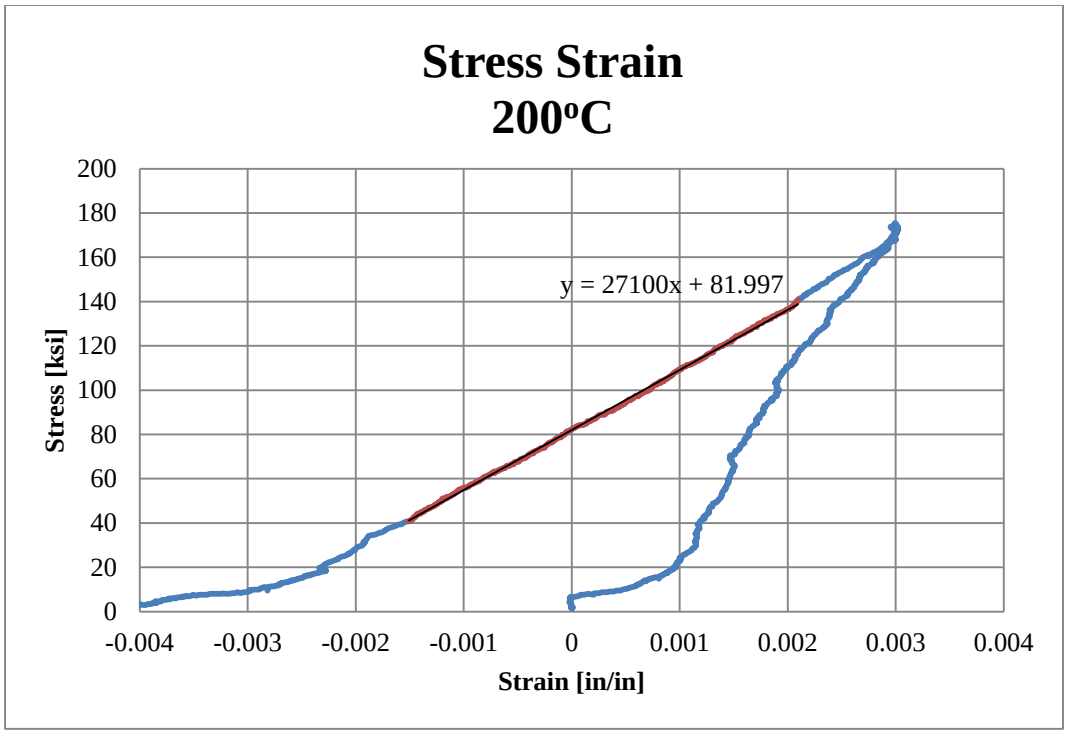

Figure 83: Elastic Modulus Test 2 200C

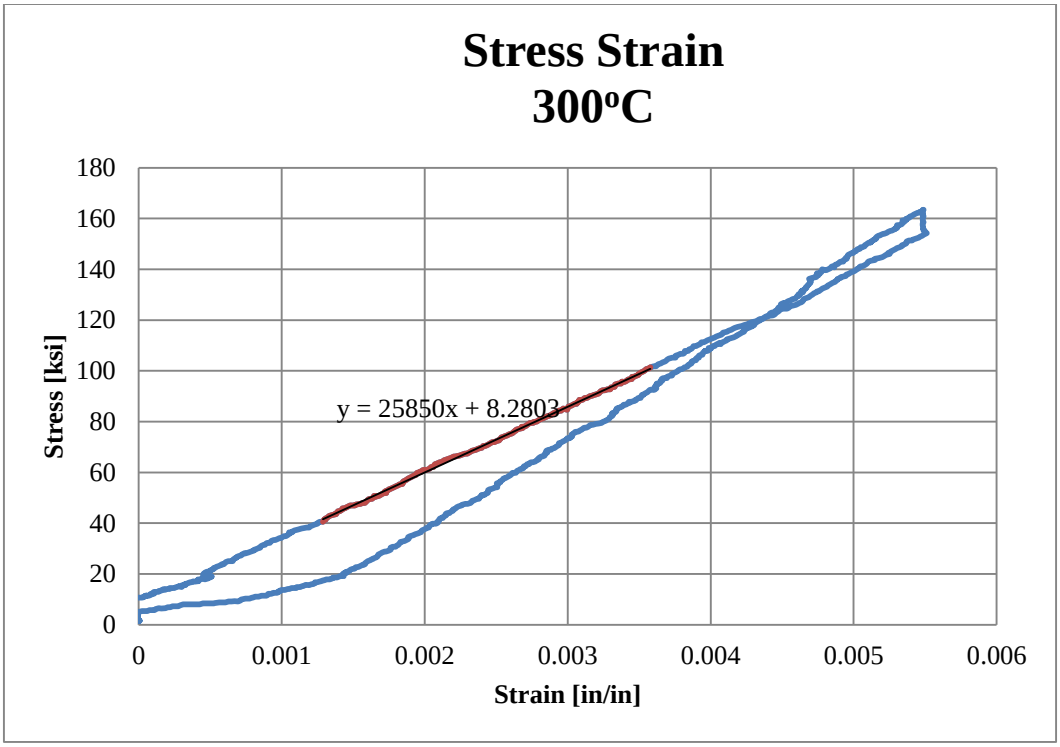

Figure 84: Elastic Modulus Test 2 300C

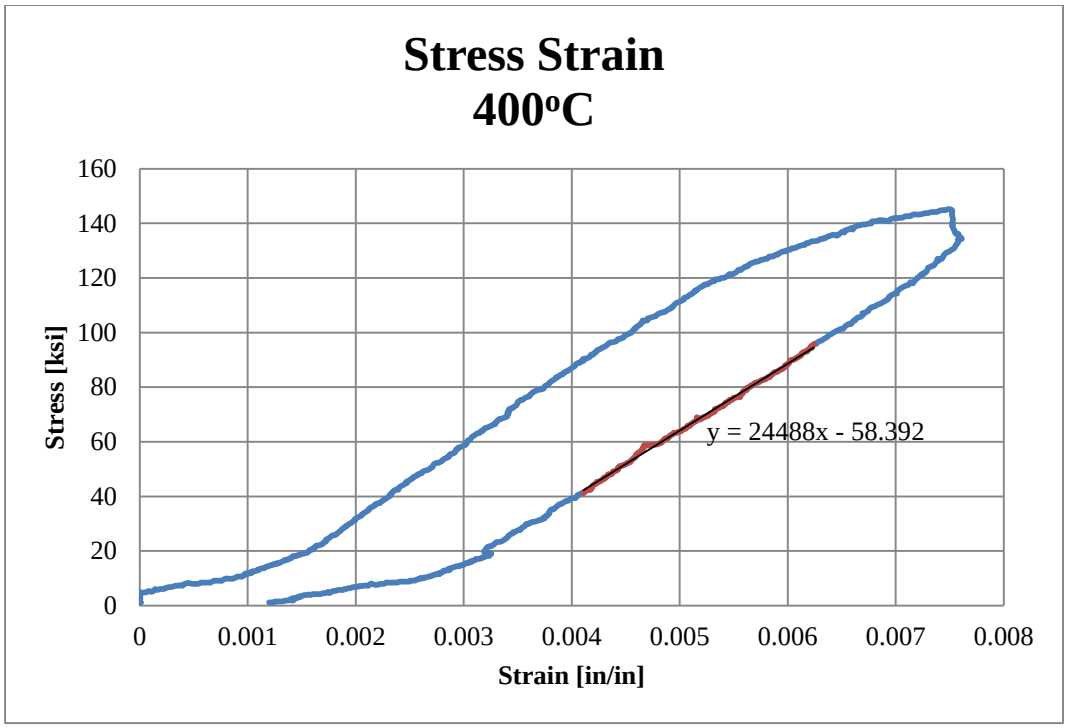

Figure 85: Elastic Modulus Test 2 400C

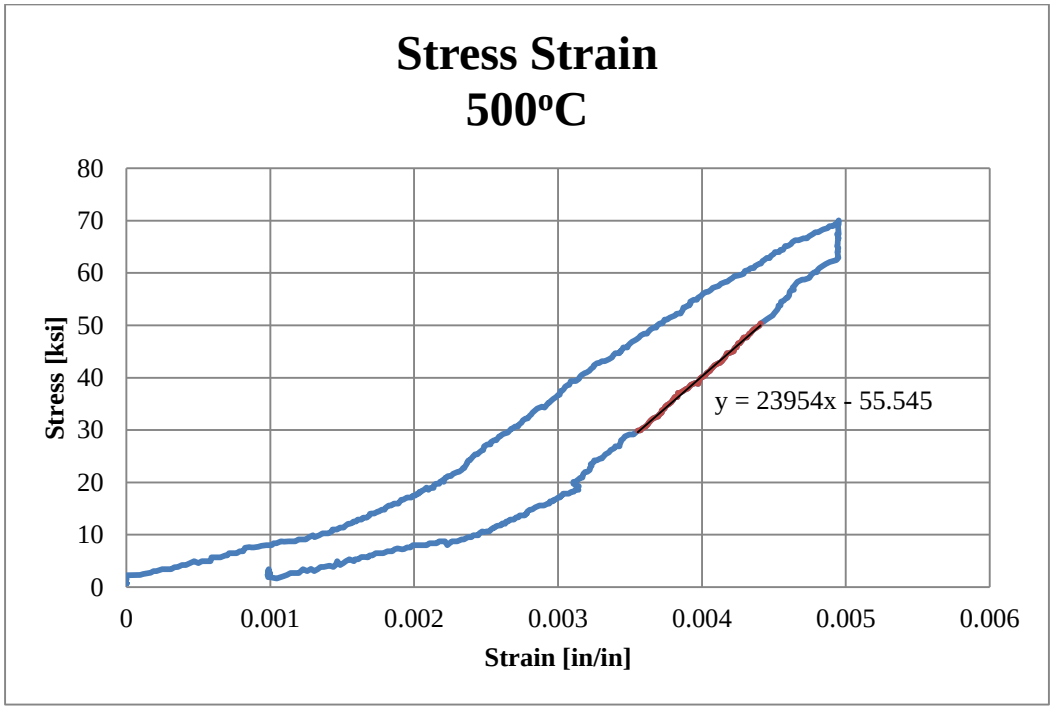

Figure 86: Elastic Modulus Test 2 500C

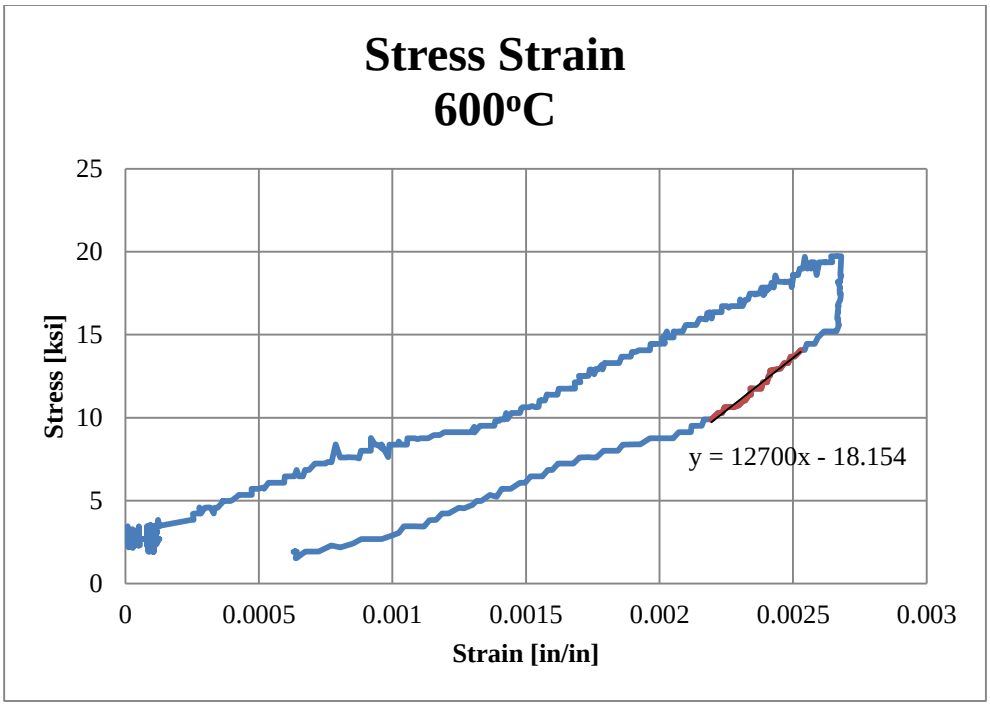

Figure 87: Elastic Modulus Test 2 600C

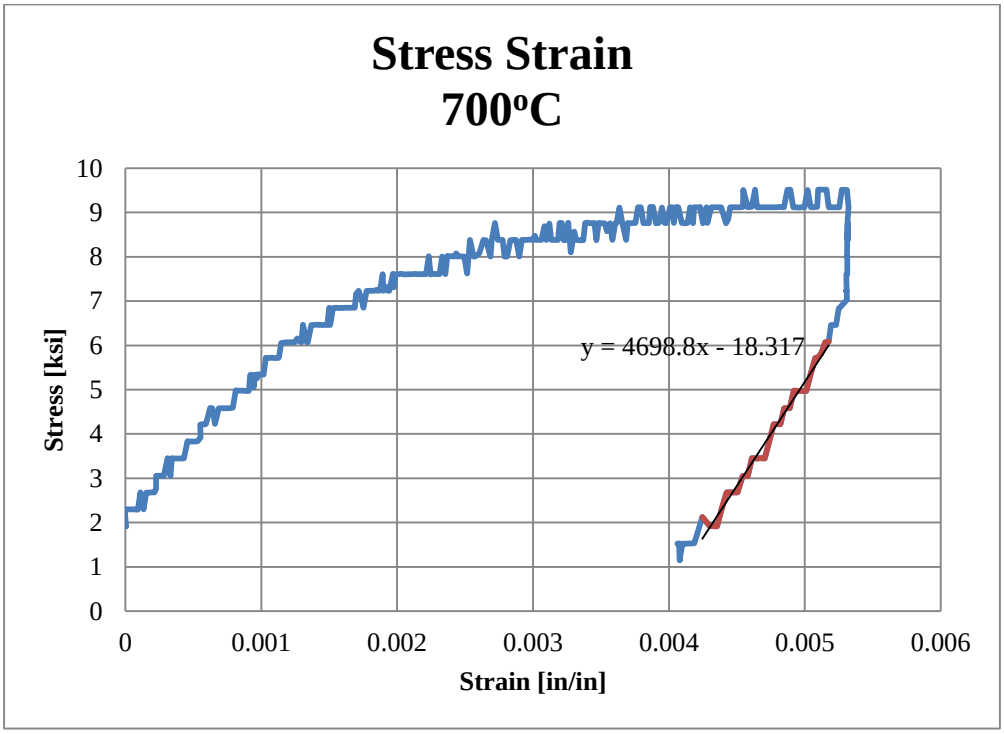

Figure 88: Elastic Modulus Test 2 700C

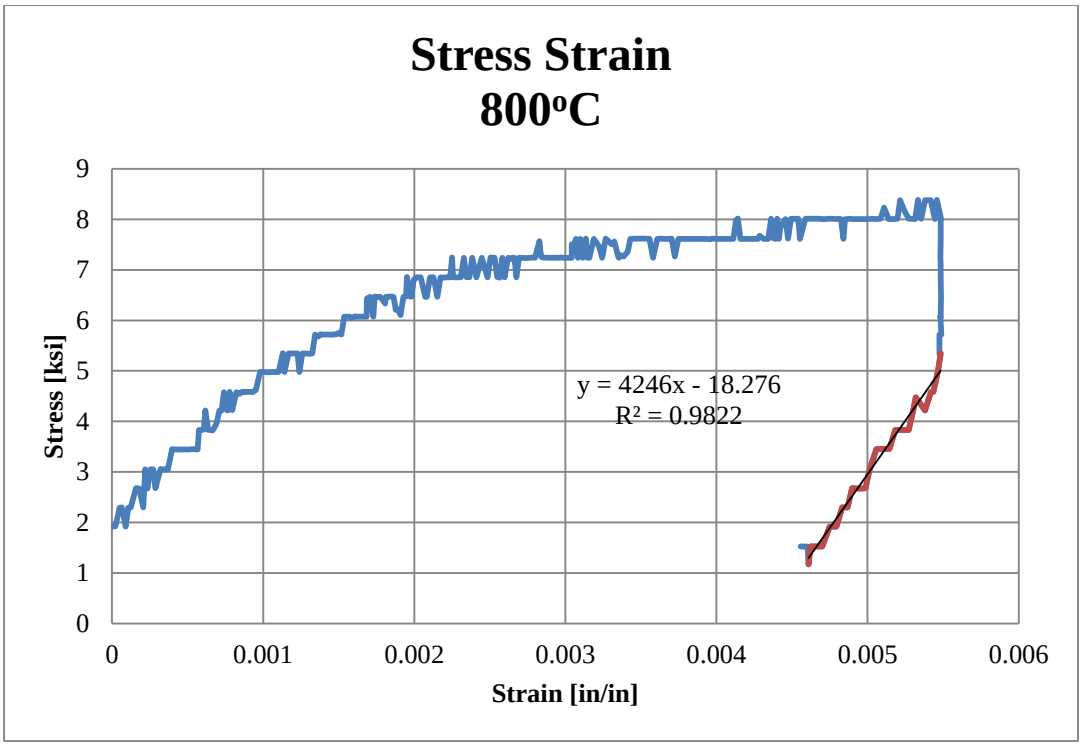

Figure 89: Elastic Modulus Test 2 80

Chapter 5 Evaluation of Test Results

5.1 General

Chapter 5 presents the evaluation and interpretation of the laboratory test results. First, a brief study was performed to evaluate the distribution of temperature during the tests both through the cross-section and over the length of the experimental specimen. Then, from the constant temperature test results, the load displacement curves are presented along with the reduction of ultimate strength at elevated temperatures. The elastic modulus test data is presented alongside the Eurocode elastic modulus reduction. Combined with the new data for proportional limit, modifications to the Eurocode stress strain model for cold-drawn strand are then presented. The transient test data is plotted and compared to the constant temperature test results. And finally, the microstructure analysis from the constant temperature test specimens are presented and discussed.

5.2 Heat Transfer Studies

A heat transfer study was performed to illustrate the temperature distribution both through the cross-section and over the length of the specimens. A comparison of finite element and analytical lumped mass models to the experimental data provides verification of the uniformity of temperature through the critical cross-sections. During the constant temperature tests, the specimen has time to reach steady state and the temperature distribution is assumed uniform. For the transient temperature testing, the specimen temperature is increasing while a constant load is applied. For this reason, the cross section temperature profile must be examined to determine if the entire cross section can be simplified to a uniform temperature. If the cross section temperature is found to be uniform, then more simplified heat transfer analysis can be carried out.

For steel sections exposed to fire, it is common to assume that the cross section behaves as a lumped mass and develops a relatively uniform temperature. For large cross sections, irregular shapes, and non-uniform heating, this assumption should always be verified through a more rigorous heat transfer analysis. In order to verify that the lumped mass assumption was correct for the 0.6 inch diameter 7-wire strand, a 2-D heat transfer analysis was performed using ABAQUS finite element software.

The thermocouple data from the 42% MUTS fast heating rate transient temperature test was used to create the boundary temperature for the perimeter of the exposed 7-wire strand. The 7-wire strand was modeled as shown in Figure 90(A and C) and then as a simplified circular cross section with equivalent area in Figure 90(B and D). The cross section is analyzed at two points in time. Figure 90 A and B show the results approximately 33 minutes into the heating phase. The cross section temperature is approximately equal to the rupture temperature of the 70% MUTS prestressed transient test specimen. For Figure 90A there is a 5^{o}C temperature difference between the perimeter of the strand and the center of the strand. In Figure 90B, this temperature gradient is reduced to 1^{o}C. The results are the same for Figure 90 C and D. Figure 90C and D show the cross section at approximately 37 minutes. At this time, the strand has reached the approximate rupture temperature of the 45% MUTS prestressed transient test specimen. The realistic 7-wire model shows that there is a temperature differential of approximately 5^{o}C between the exposed perimeter and the center-most portion of the strand. This 5^{o}C differential is not significant in terms of the mechanical properties of the strand, but it could explain why the central wire never ruptured during the transient temperature testing (note that the central wire showed significant necking and was at the edge of rupture). When the equivalent circular section was analyzed, the temperature was uniform across the section and equal to the maximum temperature obtained from

the realistic 7-wire model. The results of the ABAQUS HTA indicate that lumped-mass approach, or a one-dimensional HTA, can provide an acceptable and conservative calculation of cross-sectional temperature for these strands. In a one-dimensional HTA, the entire cross section is assumed to behave as a lumped mass in terms of heat transfer (i.e. the entire cross section temperature is represented by a single 'point'). This allows the assumption that the thermocouple data represents the temperature of the entire cross section at the thermocouple location.

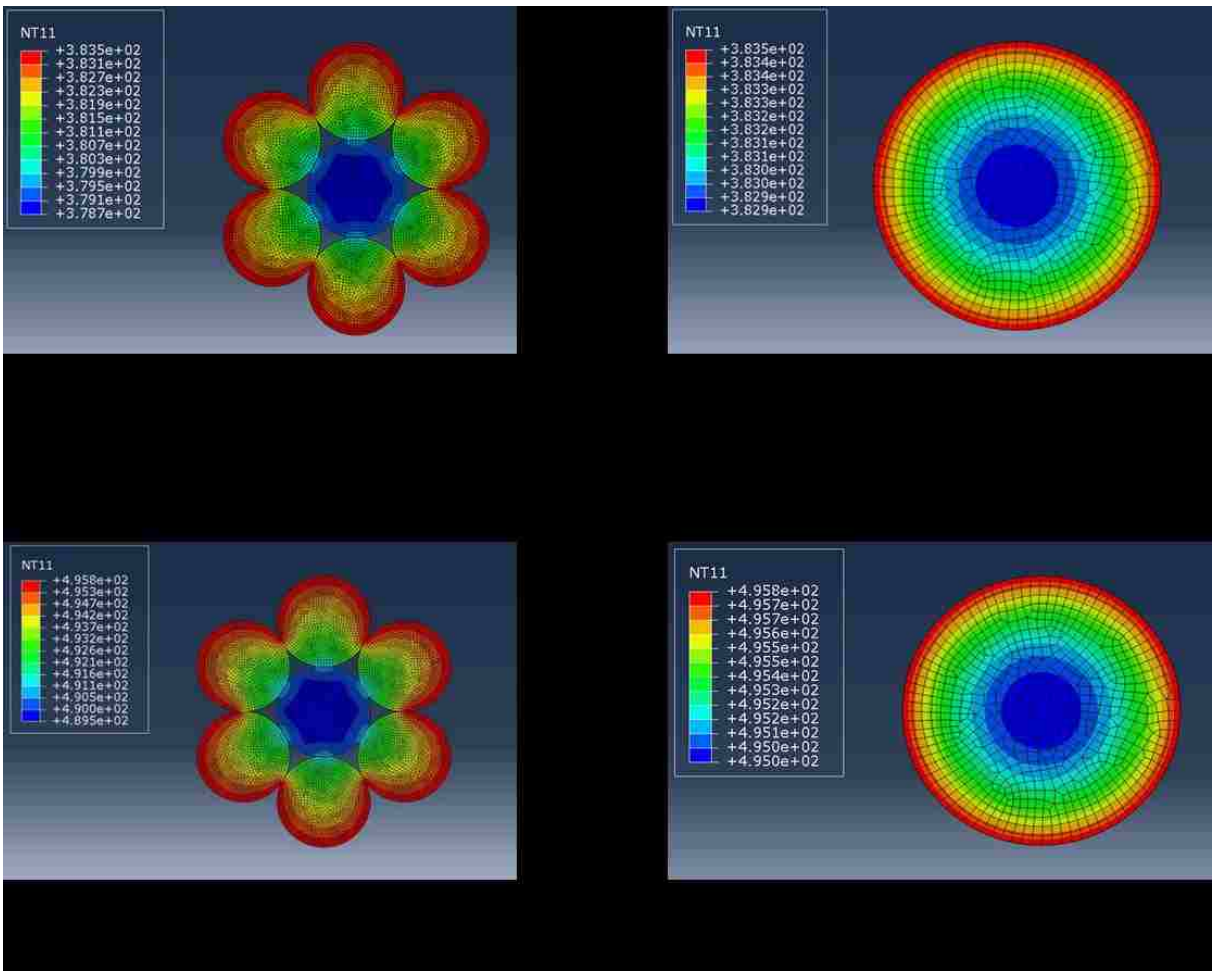

Figure 90: 2D ABAQUS Heat Transfer Analysis

Once the lumped mass cross-sectional approach was verified, a MATLAB script (shown in the appendix) was created for one-dimensional HTA along the length of the strand specimens using a multiple lumped mass approach. This analytical code was created to show that a simple heat transfer analysis approach can produce results that are in agreement with more complex finite element heat transfer analysis. The MATLAB script was created using a one-step lag approach (Quiel and Garlock 2010). This approach assumes that the current step's heat transfer properties are a function of the steel temperature at the previous time step. The equations used to determine the temperature increase are presented below.

$$\dot{h}_{conductuion_i} = \frac{K_{T_i} \cdot (T_i - T_{i-1})}{L} \tag{3}$$

$$\dot{h}_{radiation_i} = e \cdot \sigma \cdot ({T_{applied}}^4 - {T_i}^4) \tag{4}$$

$$\dot{h}_{conveciton_i} = h \cdot K_{T_i} \cdot (T_{applied} - T_i) \tag{5}$$

The heat fluxes are calculated for conduction, radiation, and convection for each element at each time step as shown by **Error! Reference source not found.**, **Error! Reference source not und.**, and **Error! Reference source not found.** respectively. The heat fluxes are multiplied by the area of heat transfer (for conduction this is the cross sectional area, for convection and radiation this is the surface area of the individual element) and the time step to transfer for the heat flux into units of Watt now represented by capitol letter Q. To convert the heat flux to units of temperature the heat fluxes are summed (which now have units of Watt) and then divided by the product of the specific heat, the density of the material, and the volume of the individual

elements. The result is the incremental temperature change of the element. This is shown in **Error! Reference source not found.**.

$$\Delta Temp = \frac{(Q_{conduction}+Q_{radation}+Q_{convection})}{c_{T_i} \cdot V \cdot \rho} \quad (6)$$

The thermal conductivity, K, and the specific heat, c, are functions of temperature and thus they are updated at each time step based on the current temperature of the individual element. (The functions used for the conductivity and specific heat are taken from Franssen and Zaharia (2005) and shown in the appendix) This incremental temperature change is computed for each element at each time step using a one directional approach.

For the analytical model, the specimen length was chosen as the length of the 7-wire strand (approximately 5 feet), and the heated length was chosen as the heated length of the furnace (approximately 12 inches). The individual finite elements each had a height of approximately .25 inches. When a small time step (less than 5 seconds) was chosen, this approach produced results that showed good agreement when compared to an ABAQUS one dimensional HTA (using the simplified cross-sectional model shown in Figure 90(B).

To further compare the ABAQUS HTA and the MATLAB code, a constant temperature test comparison was performed using a desired furnace temperature of 520^{o}C. This comparison between the MATLAB script and the ABAQUS results is displayed in Figure 91. In this analysis the temperature was measured at the center of the furnace which produces the maximum temperature in the specimen. The MATLAB script conservative with respect to the ABAQUS results, and both results eventually approach the desired furnace temperature.

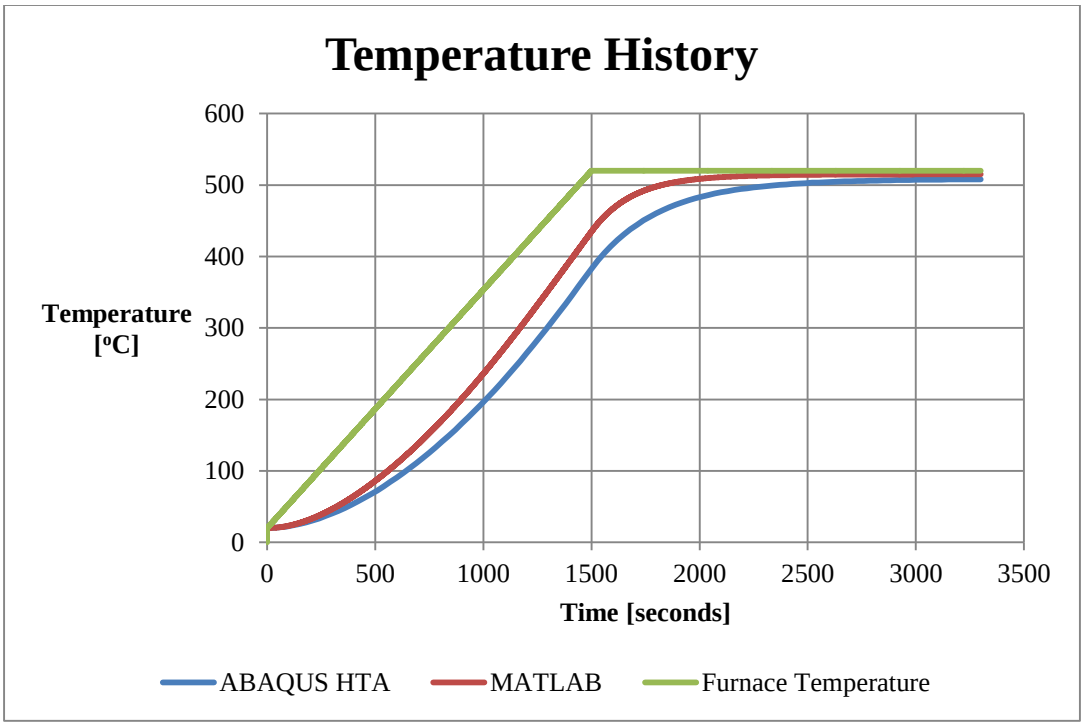

Figure 91: Finite Element Heat Transfer Time-history

One of the assumptions made in the constant temperature testing is that the strand outside of the heated zone is relatively unaffected by the heat from the furnace. To show that the MATLAB script and the test results are agreeable, the outside thermocouple time history data was plotted for the 500°C test. In Figure 92 it is shown that the MATLAB script over-predicts the temperature at the thermocouple locations. The MATLAB model uses the lumped mass approach and therefore the strand surface area is reduced to the circular cross section assumption. For this reason, the MATLAB model is not able to remove as much heat from the unheated portions of the strand. Both the model and the physical test results show that the temperature does not reach above 60°C for the model and 35°C for the test results. At such low temperatures, it is assumed that the mechanical properties of the strand are unaffected by the temperature increase.

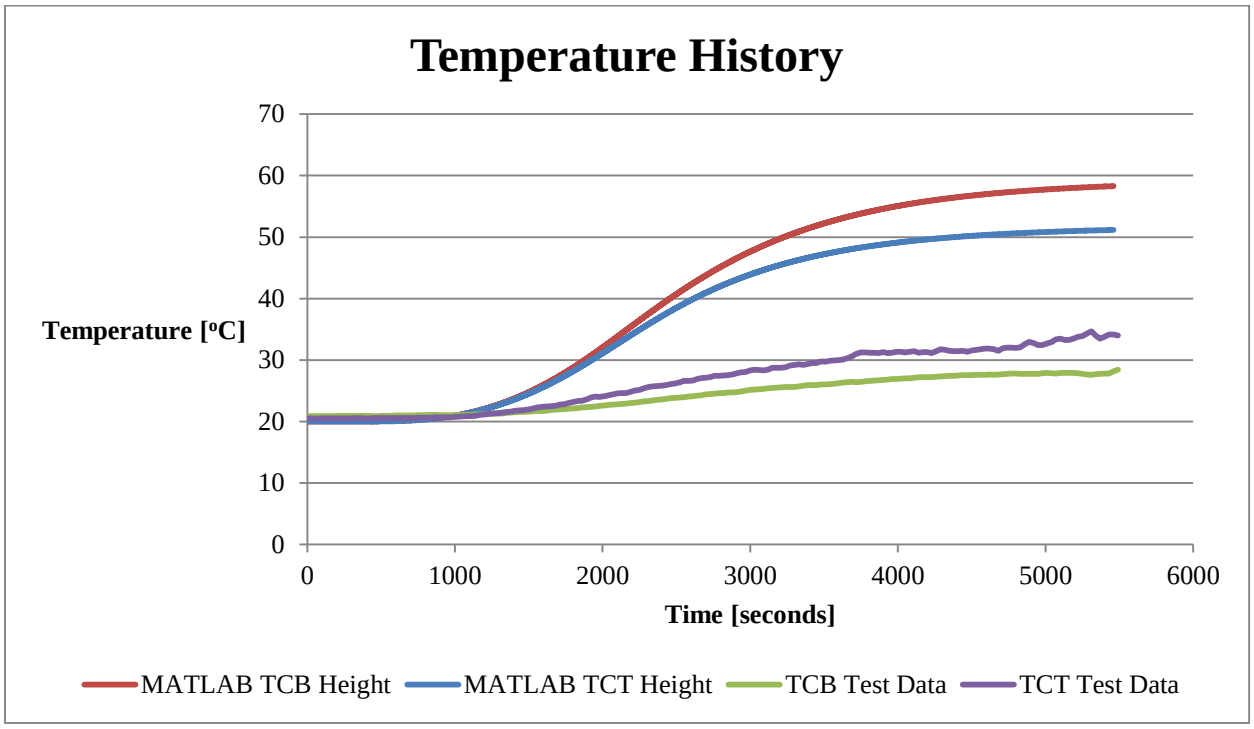

Figure 92: Temperature History of Outside Thermocouples

A comparison between the ABAQUS HTA and the MATLAB script is shown in Figure 93, which shows the temperature profile after the 30 minute heat soak. This comparison shows that

while a slight discrepancy exists during the heating phase, the ABAQUS and MATLAB model are almost identical once the strand has reached its final temperature. This analysis was conducted to show that a simplified MATLAB code is capable of producing results that agree with the more complex heat transfer analysis in a software package like ABAQUS. The thermocouple from the 500°C constant temperature test are included in this plot to show that while there are discrepancies between the model and the physical test specimen, the model provides an agreeable prediction of the strand temperature. In reality, the hot air created by the furnace rises upwards and the hottest part of the specimen is found above the true center of the furnace. The heat transfer model does not account for this action, and therefor develops a temperature profile that is symmetric about the furnace center.

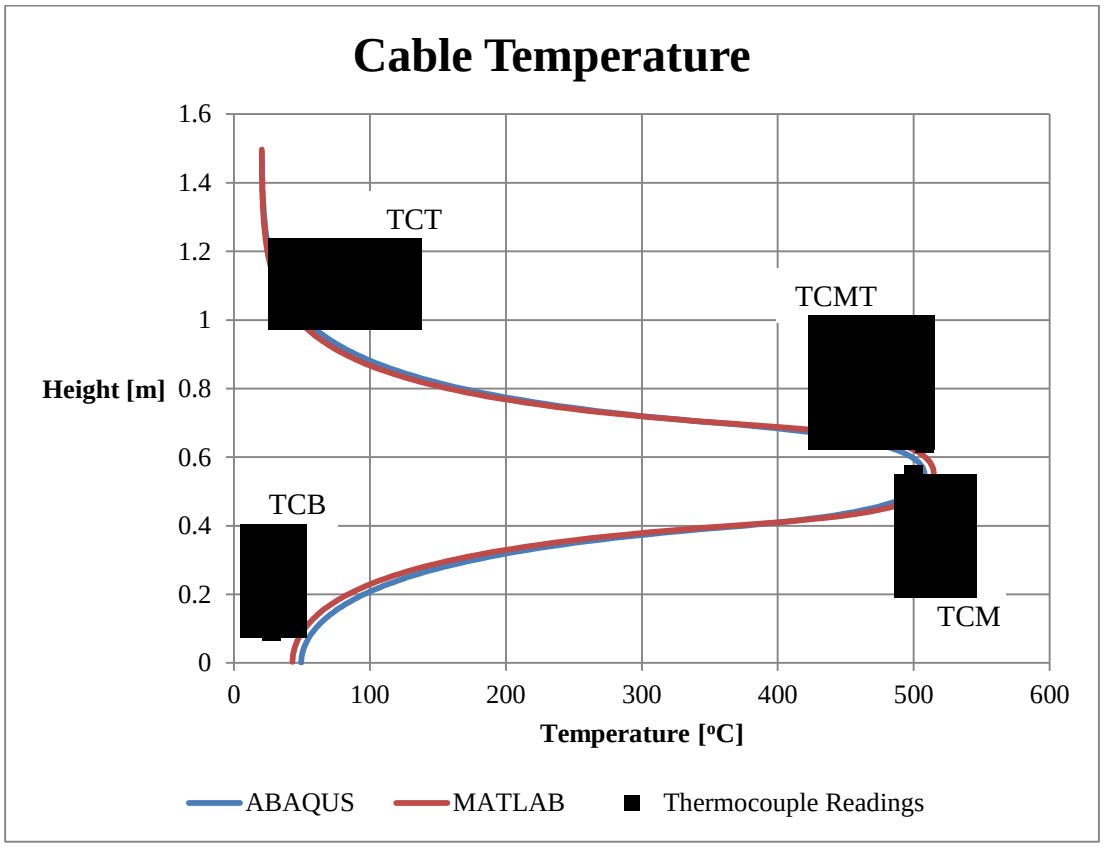

Figure 93: Comparison of ABAQUS and MATLAB HTA

5.3 Constant Temperature Test

The constant temperature test data was used to determine the ultimate strength at elevated temperature. The data was also used to create a modified Eurocode material model that captures the stress strain behavior of ASTM-A416 grade 270 cold-drawn steel at elevated temperature. The new material model is proposed because the current Eurocode model does not accurately predict the behavior of the A416 cold drawn steel strand. While the modulus of elasticity and the ultimate strength parameters are in agreement with the Eurocode model, the proportional limit and the strain-hardening behavior of the current study do not agree with the Eurocode model. The elastic-perfectly plastic model used for hot-rolled steel does not fit the performance model for cold-drawn steel strand. The Eurocode model uses the same stress-strain equation for both cold-drawn and hot-rolled steel but utilizes different reduction factors. The proposed model modifies the equation and the reduction factors to fit the data from the current study. The results are compared to the current standards, ACI 216 and Eurocode 2 part 1-2, for ultimate strength and stress strain behavior respectively, as well as the strength reduction equation presented by Hertz (2004). Further constant temperature testing was conducted in order to determine the elastic modulus of the strand at elevated temperatures.

5.3.1 Ultimate Strength

The entire suite of load displacement curves are plotted together in Figure 94 and shows the degradation of mechanical properties as the temperature increases. These curves were obtained by shifting the raw test data presented in Chapter 4 to remove the initial grip set region, which showed a smaller stiffness that is not indicative of the strand performance. In their modified form, the load-displacement curves start from zero load and zero displacement, and then immediately follow the elastic displacement trajectory until the steel reaches the proportional

limit. The modified load-displacement curves for the individual test results can be found in Figure 104 through Figure 111. While there appears to be a large decrease in ductility at elevated temperature (300-600ºC) it is important to remember that at 20ºC the entire cable acted as the gauge length. At elevated temperature, the length of the furnace acted as the equivalent gauge length. This value is conservative for the model. From the finite element study, approximately 8 inches of the strand will be at the desired temperature, while 2 inches above and below will be at a lower temperature. While it is shown that the cables at 300-500ºC ruptured after only ~1/4 of the total displacement compared to the 20ºC, the displacement was occurring over a length of 12 inches, where at 20ºC the displacement occurred over 60 inches. At 600ºC and 700ºC the cable develops a bi-linear load displacement curve and the cable becomes extremely ductile. At 800ºC the load displacement curves are more representative of the ambient temperature curves, where there is a more defined yield plateau.

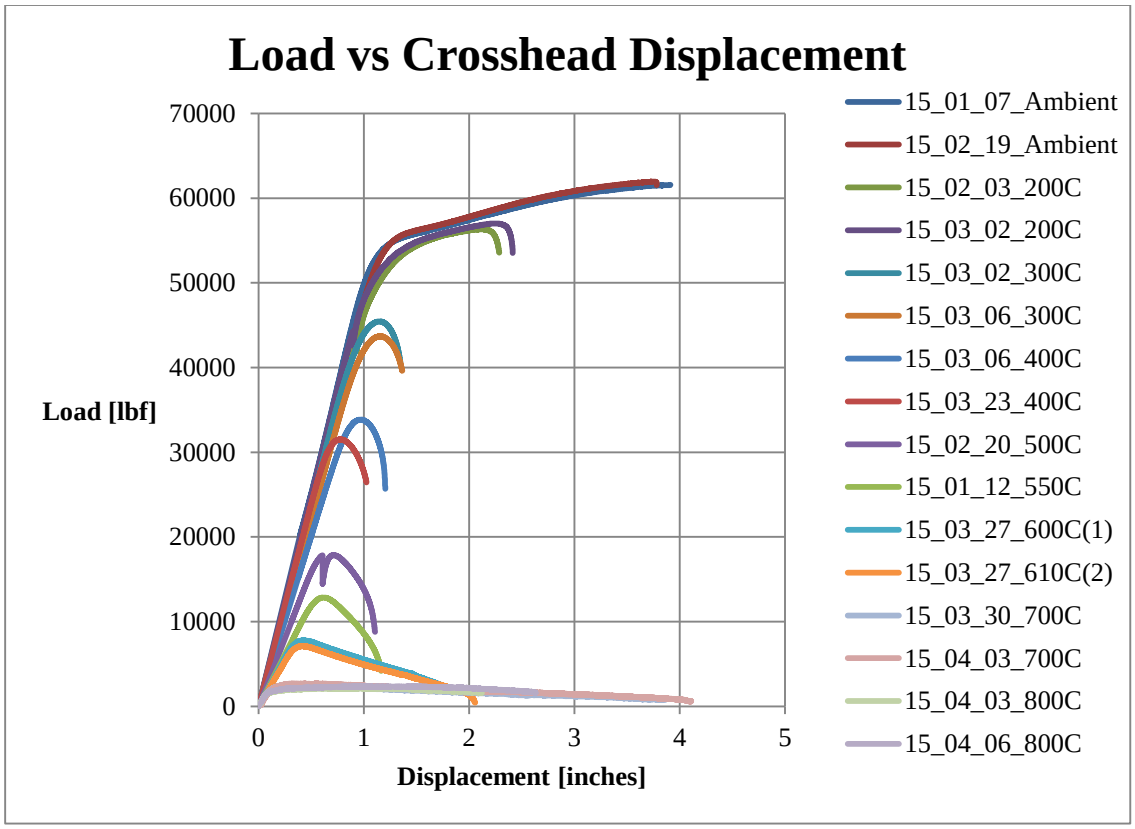

Figure 94: Load-displacement curves (modified to remove initial grip set)

The peak loads from the load-displacement curves were recorded with the temperature of the cable at rupture. The data can be found in Table 5 and is represented graphically in Figure 95 and Figure 96. Figure 95 also shows the ACI 216 curve (ACI 2014) for cold-drawn steel at elevated temperature and the strength reduction model from Hertz (2004) which are derived from a number of studies (one being Harmathy and Stanzak 1970). The ACI 216 curve originated from the Abrams and Cruz (1961) study. The current study agrees well with both the ACI 216 standard and the Hertz model. Note that the data from the current study is expressed as a percentage of the ultimate strength of the cable obtained from the ambient tensile tests, and not as a percentage of the listed MUTS. To use the curve as a percentage of the MUTS, simply multiply the data points by the ultimate strength divided by the MUTS.

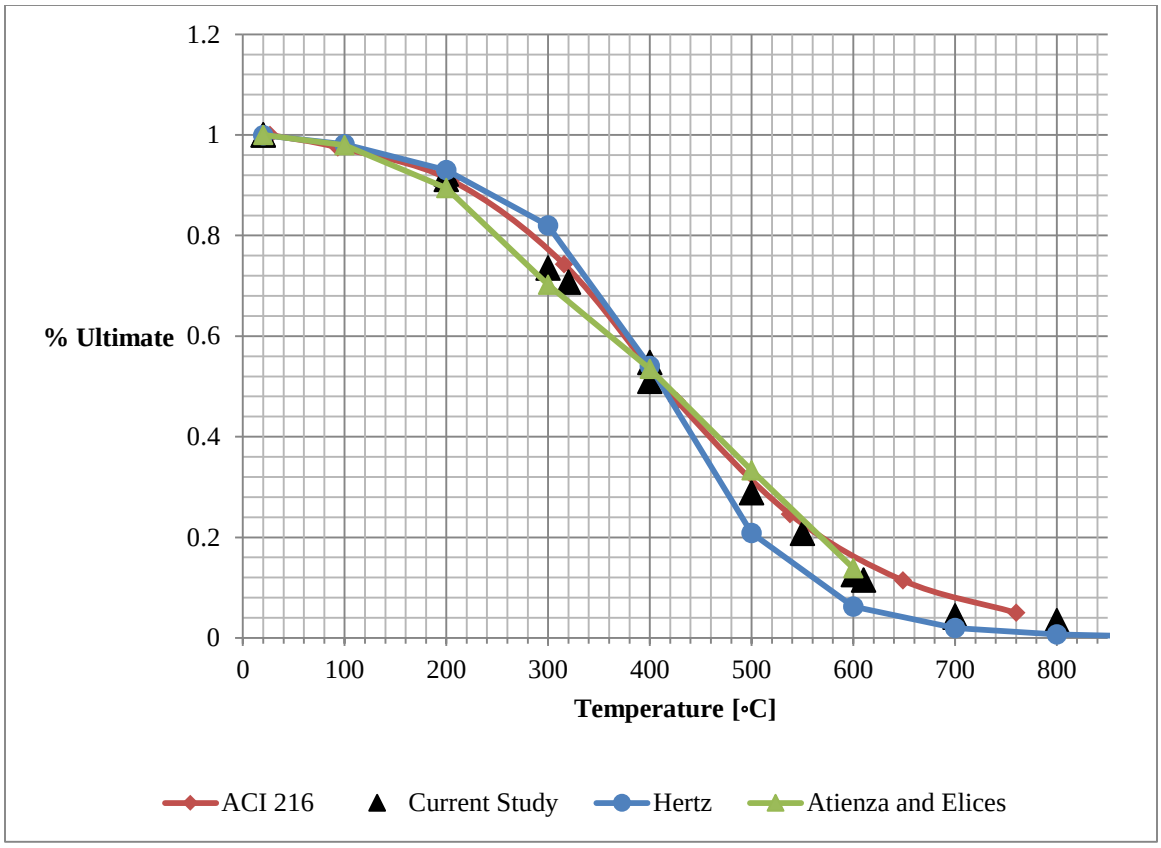

Figure 95: Ultimate Strength Comparison

The Eurocode reduction values are also compared to the current study. Again, the current study agrees well with the reduction factors from Eurocode 2 part 1-2 (2004) for cold-drawn steel. Figure 96 shows that there is significant difference between the behavior of cold drawn steel and mild steel at elevated temperature. The current study data further emphasizes the need for using appropriate reduction values for cold-drawn steel when analyzing steel cables rather than those for mild steel.

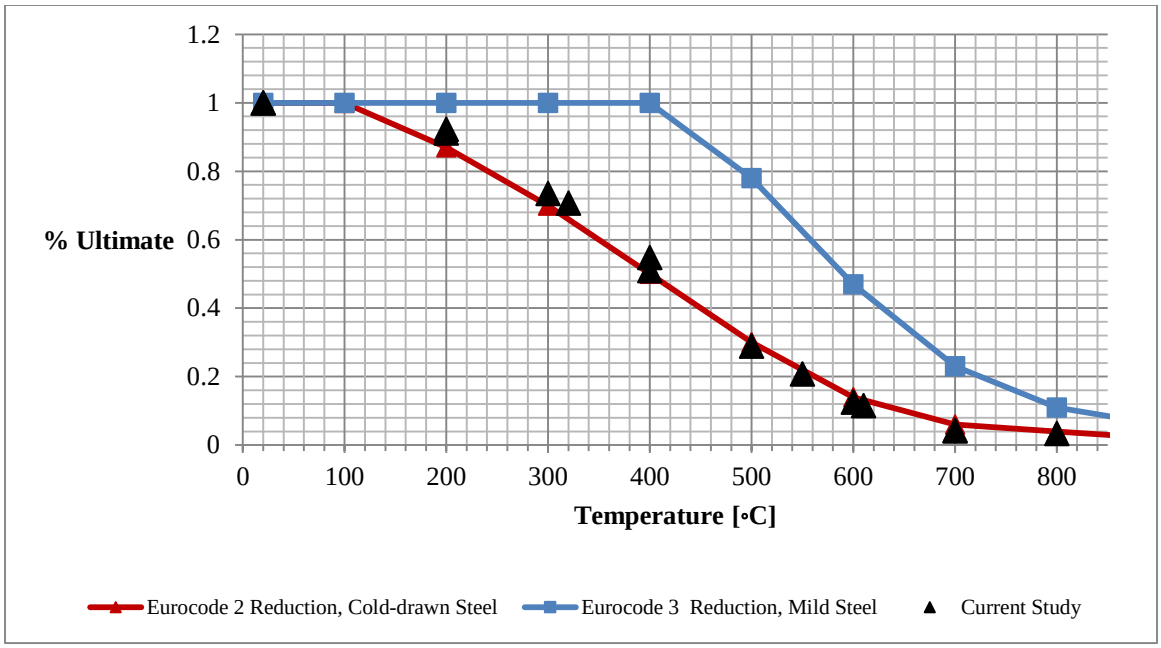

Figure 96: Ultimate Strength Eurocode Comparison

The proportionality limit measured in the current study is compared to the Eurocode model for proportionally reduction in Figure 97. In the current study the proportionality limit was determined through visual inspection of the first non-linear behavior during the load displacement curves. It is important to note that the Eurocode model normalizes the proportionality limit by the ambient temperature yield strength. Initially, the proportionality limit is 1.0 for Eurocode because it is assumed that it yields at the ultimate strength at room temperature (elastic perfectly plastic) – this model does not account for strain hardening at ambient temperature. The current study shows that between 200ºC and 500ºC, the tested specimens showed more linear elastic behavior than the Eurocode equation prediction. The current data shows better agreement with the Eurocode model for cold drawn steel from 600ºC to 800ºC.

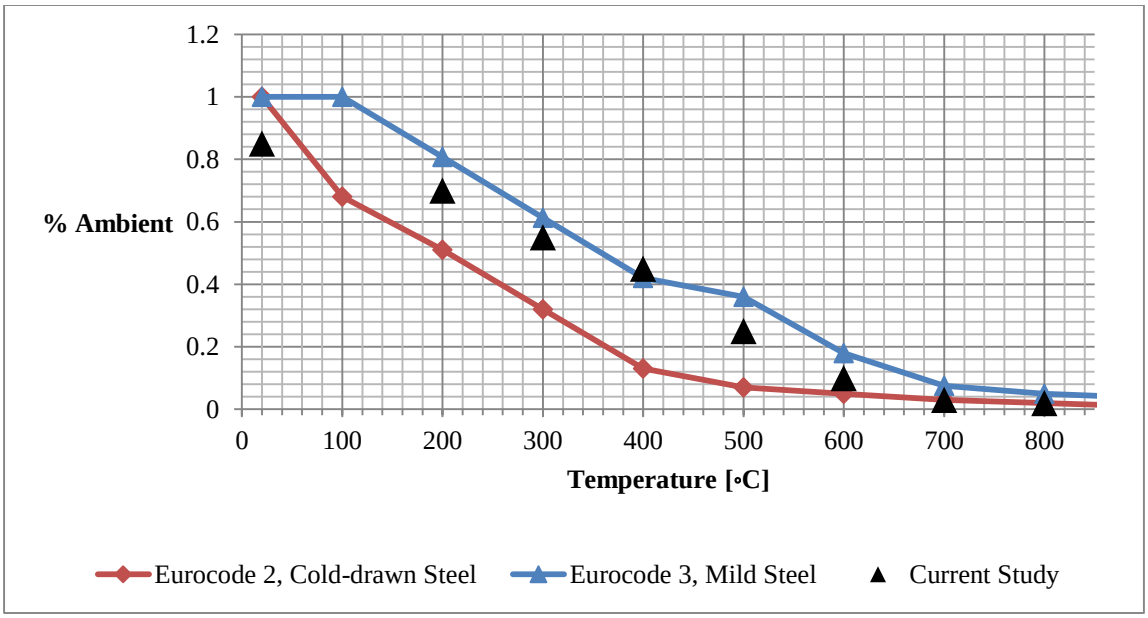

Figure 97: Proportionality Limit Eurocode Comparison

5.3.2 Elastic Modulus Tests

The elastic modulus test data is presented in Table 7 and Table 8. The test data follows a similar trend to the reduction factor provided by the Eurocode material model for cold-drawn steel. The elastic modulus is relatively unaffected at 200°C and 300°C. At 400°C a slight reduction is noticeable. At 600°C a large drop occurs. The 700 and 800°C tests result in approximately the same elastic modulus as the curve begins to level out. The elastic modulus curve follows the same S-shaped curve as the Eurocode model and is compared in Figure 98. The current test data shows that the Eurocode model is conservative at all elevated temperatures. It is worth noting that in the current study the elastic modulus was determined using two stringpots and was not measured with a strain gauge or extensometer. It is recommended that a more accurate measurement is performed before any change or modification to the Eurocode model is suggested. It is also worth noting that at higher temperatures, the strand exhibited non-linear behavior as soon as the load was increased from the holding load of less than 1% MUTS. This made it difficult to accurately

determine the elastic modulus during the loading phase. The elastic modulus was measured as the more conservative slope from either the loading or unloading phase. The unloading phase usually produced more conservative results.

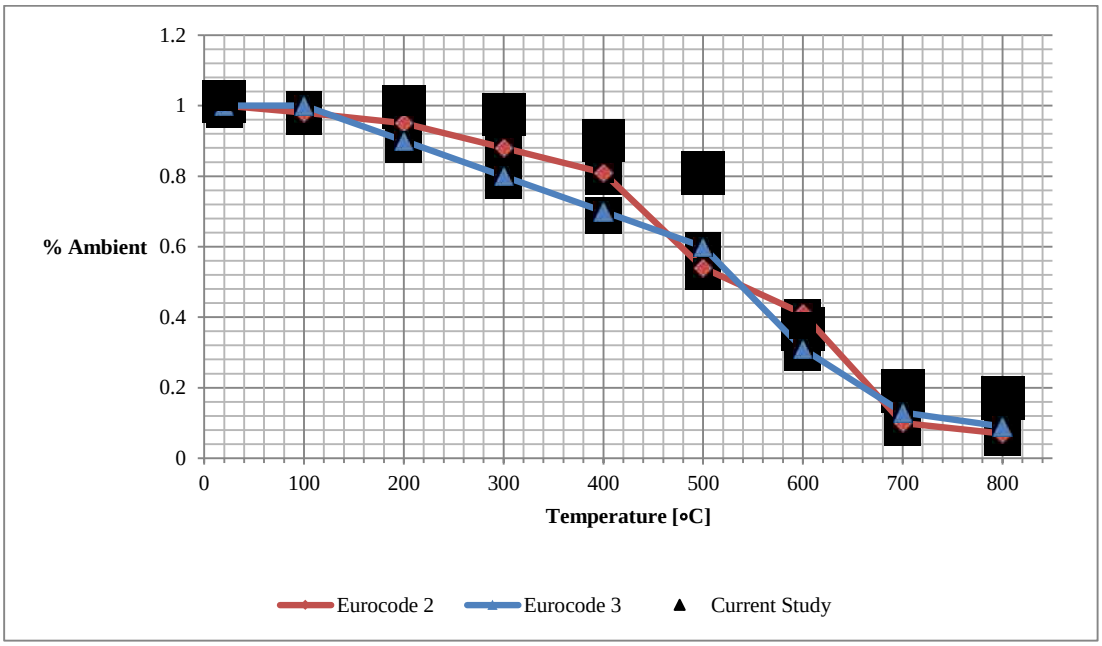

Figure 98: Elastic Modulus Results

5.3.3 Material Model

The material model for cold-drawn steel presented in Eurocode 2 part 1-2 uses a similar form to that used in Eurocode 3 for mild steel. At ambient temperature, the material is assumed to be elastic-perfectly-plastic; at elevated temperature, the model has a nonlinear transition between the elastic region and a yield region. It is worth noting that the Eurocode model uses the MUTS and a suggested β reduction value. For 'Class A' steel the β value of 0.9 is used. Using this reduction value the ultimate strength is represented as the yield strength of the material. This model captures the yield limit and does not account for any strain hardening that takes place after yield.

For this reason, the Eurocode model parameters were modified in order to better predict the behavior of the test data from the current study. Table 9 shows the values presented by the Eurocode, and Table 10 suggests the updated parameters. In the new model, the same equation presented in Figure 5 is used, but some of the parameters are renamed: $k_{y,T}$ (the yield stress reduction) becomes $k_{u,T}$ (the ultimate stress reduction factor), e_y (the yield strain) becomes e_{max} (the strain at the maximum stress level). The new model includes the non-linear stress-strain behavior up to the maximum stress and then the model declines linearly from maximum stress to zero stress at the recorded ultimate strain. The data from the constant temperature tests were used to extrapolate approximate stress strain curve at elevated temperature. The process used the Eurocode reduction factors for the modulus of elasticity and the cable elastic modulus to create the linear elastic region of the curve because these values were found to be conservative. The linear elastic region ends when the proportional limit was reached. At this point, the load displacement data was converted to stress-strain using the furnace height of 12 inches as the strain gauge length. Based on the results of the heat transfer study, it is assumed that the temperature profile is fairly uniform inside the furnace zone and that the deformation is occurring in the region of elevated temperature. In order to produce a conservative model, the more conservative load displacement data was used from each of the constant temperature tests. The new model is presented in Figure 112 through Figure 119.

Table 9: Values for Eurocode Stress-strain Relation of Cold-drawn Steel

Temp [°C]	$k_{y,t}$	$k_{p,t}$	$k_{E,t}$	e_t	e_u	e_y
20	1.00	1.00	1	0.05	0.1	0.02
100	0.99	0.68	0.98	0.05	0.1	0.02
200	0.87	0.51	0.95	0.05	0.1	0.02
300	0.72	0.32	0.88	0.055	0.105	0.02
400	0.46	0.13	0.81	0.06	0.11	0.02
500	0.22	0.07	0.54	0.065	0.115	0.02
600	0.1	0.05	0.41	0.07	0.12	0.02
700	0.08	0.03	0.1	0.075	0.125	0.02
800	0.05	0.02	0.07	0.08	0.13	0.02

Table 10: Proposed values for Eurocode Model

Temp [°C]	$k_{u,t}$	$k_{p,t}$	$k_{E,t}$	e_t	e_u	e_{max}
20	1.00	0.85	1	0.06	0.06	0.06
200	0.90	0.7	0.95	0.06	0.06	0.04
300	0.73	0.55	0.88	0.04	0.06	0.04
400	0.52	0.45	0.81	0.025	0.05	0.025
500	0.28	0.25	0.54	0.025	0.06	0.025
600	0.12	0.1	0.41	0.015	0.14	0.015
700	0.04	0.03	0.1	0.025	0.35	0.02
800	0.03	0.02	0.07	0.1	0.185	0.085

The proposed values for the ultimate strength, proportionality limit, and elastic modulus are shown in Figure 99. The new values show that the proportional limit always trends below the ultimate strength, ensuring that the new model captures the effects of strain-hardening. As stated, the elastic modulus reduction is taken from the Eurocode reduction values. The proportional limit and the ultimate strength reduction factors are normalized by the ultimate strength.

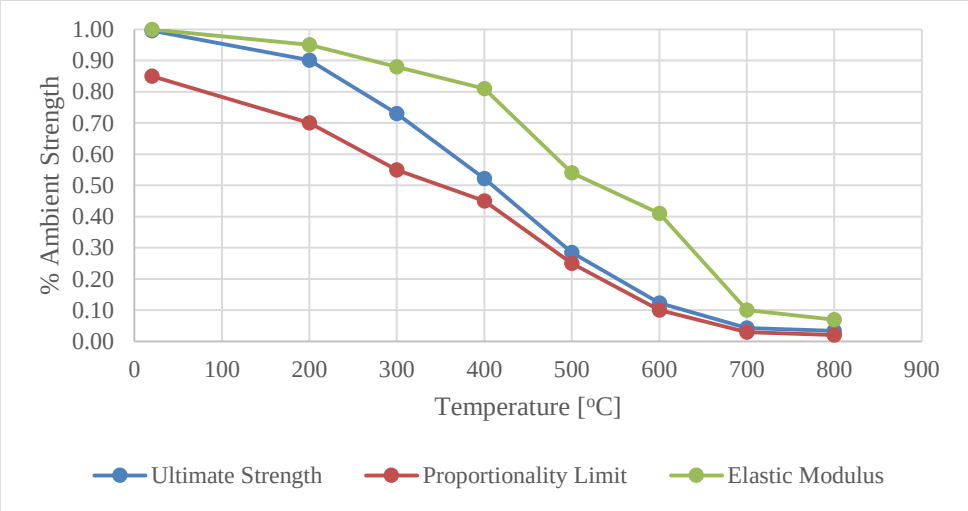

Figure 99: Proposed Strength Reduction Factors

The modifications to the strain values in the Eurocode material model are shown below in Figure 100. The rupture strain remains approximately .006 for temperatures between 20ºC and 500ºC. At 600 and 700ºC the rupture strain shows a large increase. The rupture strain then decreases at 800ºC. The strain at maximum strength and the limit strain for the yield plateau are approximately equivalent at all temperatures. This represents a lack of yield plateau for cold drawn steel.

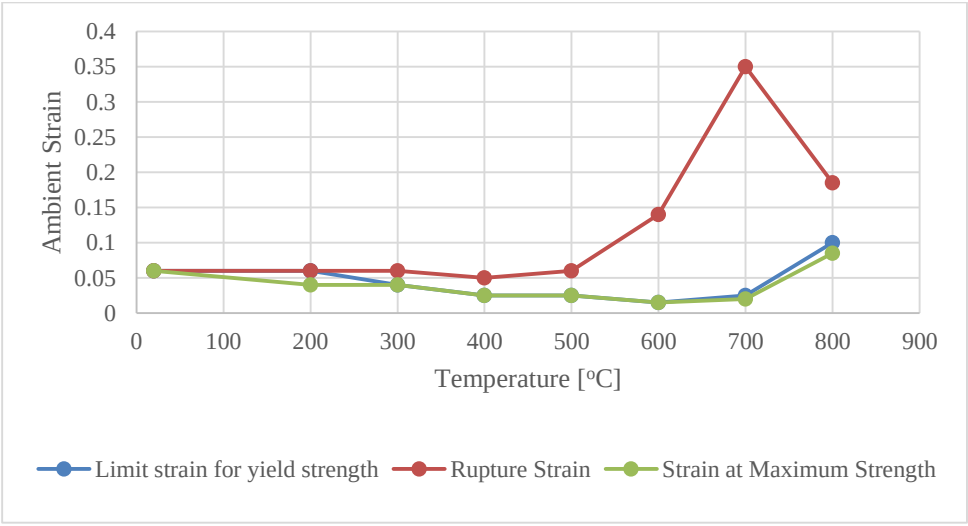

Figure 100: Proposed Strain Reduction Factors

5.4 Transient Temperature Test

The transient test results show that a faster heating rate can lead to a higher rupture temperature relative to the constant temperature test results. The test data presented in Table 6 shows that for both the 45% MUTS and 70% MUTS tests, the faster heating rate lead to ~40°C higher rupture temperature when compared to the slower heating rates. The strands held to 45% MUTS and heated at a slower heating rate (7-9°C/minute) ruptured at approximately 460°C. When that heating rate was increased to 25-26°C, the strands ruptured at 500°C. The same was true for the 70% MUTS test. The strands heated at 6-7°C/minute ruptured between 337 and 350°C while the strands heated at 18-19°C/minted ruptured between 386-395°C.

Two possible explanations to the dependency on heating rate: 1) the mechanical property degradation is a time-dependent function, or 2) faster heating rates lead to a non-uniform temperature gradient across the strand cross section. In regards to the mechanical property being time-dependent, Callister, and Rethwisch (2011) discuss recovery (the process of removing the properties gained through cold-working) as a time-dependent process. When the strand is heated at a faster heating rate, the recovery is incomplete relative to tests using a constant temperature soak, and the material is thus able to withstand a higher rupture temperature. The finite element heat transfer study discussed in Section 5.2 verified that for the 0.6 inch diameter 7-wire strand, the temperature was relatively uniform through the cross section. This suggests that the time-dependency of recovery is the primary factor contributing to the increase in strength for the transient tests.

The results of the 42% and 45% MUTS transient temperature tests are shown in Figure 101. The constant temperature test results are displayed as a function of the MUTS. This comparison shows that at lower heating rates, the transient rupture temperature is close to the constant

temperature ultimate strength prediction. When tested at 42% MUTS the rupture temperature appears to follow a similar slope to that of the constant temperature testing. However, not enough data was created to suggest a correlation between the constant temperature data and the transient temperature data at ever temperature/load point.

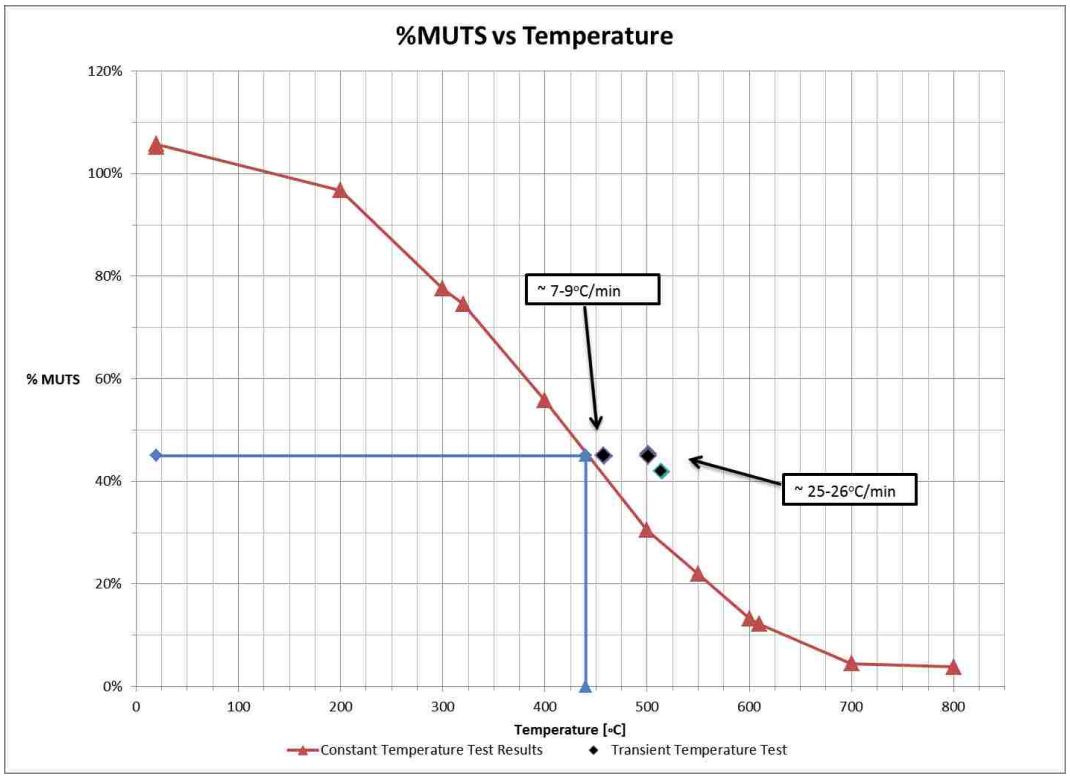

Figure 101: 45% MUTS Transient Test Plot

A similar trend is found in the 70% MUTS test shown in Figure 102. The strands tested at the slower heating rate are close to the constant temperature curve and are slightly conservative. When the strand was heated at higher rate, the constant temperature curves provide increasing conservatism in the rupture temperature estimate.

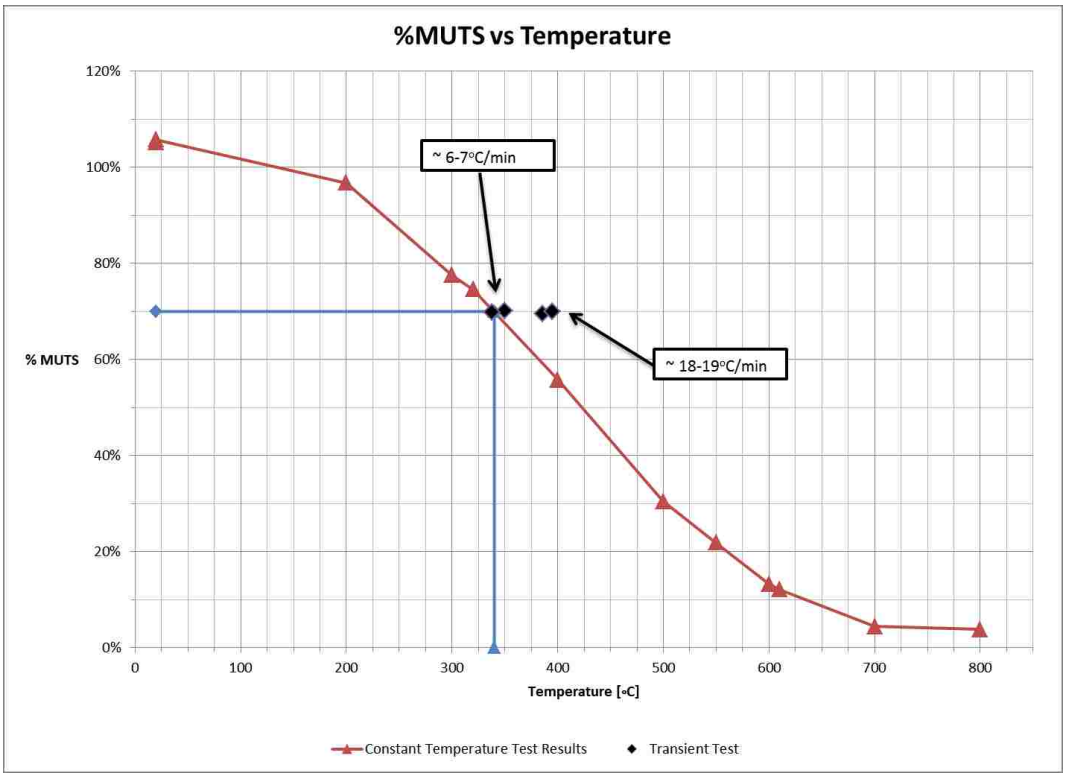

Figure 102: 70% MUTS Transient Temperature Plot

5.5 Steel Microstructure

Using light optical microscopy, a microstructure analysis was conducted through the Material Science department at Lehigh University. Specimen samples were cut from the constant temperature tested strands using bolt-cutters. The samples were then sent to the Material Science Department at Lehigh University for polishing and microscopy. The results are displayed on the following page in Figure 103 (Also shown in larger scale in Appendix A3). The microstructure does not noticeably change from 20°C to 200°C, which show the steel composition of ferrite (the light part of the microstructure) and cementite (the dark part of the microstructure). At 300°C, more iron carbides (i.e. cementite) form throughout the microstructure at the grain boundaries. The iron carbides appear as small dark spots and can be seen throughout the microstructure.

There is also a noticeable lightening of the microstructure as the recovery and recrystallization process begins. This process is even more pronounced at 400°C as the image becomes increasingly lightened with an increasing number of small, dark-colored cementite globules. At 500°C the cementite globules are found throughout the steel microstructure. At 600°C the color and composition of the microstructure has undergone a significant change from 20°C. Recovery and recrystallization are functions of time and temperature. At higher temperatures, the recovery process is accelerated. This leads to more significant changes at higher temperatures. The 700°C sample shows spheroidization, which is the process where the pearlite lamella is broken down and the cementite forms in small rounded dark-colored particles (larger than the dark specks shown in the previous several temperature steps). Spheroidite is more ductile and has a lower strength than pearlite. At 800°C the microstructure shows that a new pearlitic structure has started to form in between the cementite globules (Bramfitt and Benscoter 2001).

The microstructure analysis provides further insight to the mechanical study of the cold-drawn steel cable. Significant changes to the microstructure were discovered in the samples held at high temperature. During the constant temperature testing, the 20°C and 200°C samples both exhibited strain-hardening after reaching the proportionality limit since the microstructure was relatively unchanged. At 300°C, the samples no longer showed that strain-hardening behavior (with the exception of 800°C). The microstructure analysis has shown that the recovery phase begins at 300°C. This finding is consistent with the recent study by Callister and Rethwisch (2008), which showed that at temperatures above recrystallization, the strain hardening phenomena will not occur. The samples tested at 400°C -600°C are very similar to the 300°C sample as the recovery and cementite globule formation progresses. The 700°C sample showed extreme amounts of ductility, and the failure surface was necked down to a point. This behavior is a result of the development of spheroidite formations shown in the microstructure analysis. This was not the

case in the 800°C sample, which showed necking that was closer to the 500°C sample. At 800°C the formation of the new pearlitic structure can explain how the steel reverted to a more brittle behavior.

5.6 Summary

This chapter discussed the results of a heat transfer study, the test results, and the microstructure analysis of the tested specimens. The heat transfer study was performed to examine the distribution of temperature across the strand section and over its length when tested in the previously discussed setup. The study used a simple example to show that a one dimensional lumped mass approach can be used to model the heat transfer for truss elements. The ABAQUS heat transfer analysis was compared to a simplified 'one-step lag' approach created in MATLAB. The MATLAB code was more conservative for the time-temperature-history and the temperature-height curves showed good agreement with ABAQUS. The ultimate strengths obtained from the constant temperature test results were consistent with the past research of Abrams and Cruz (1961), which is currently used as the standard for the ultimate strength cold-drawn steel in ACI. The transient test results show that at higher heating rates, the constant temperature curves are conservative due to incomplete recovery of the cold-drawn properties, and at lower heating rates, the constant temperature curves provide a good prediction of the rupture temperature. The microstructure analysis has shown that the steel microstructure is very sensitive to temperature and shows unique microstructures for each temperature in the study. Recovery of the cold-working begins at 300°C. This effect is increasingly more pronounced as the temperature increases. At 700°C the microstructure resembles spheroidite (increasing ductility), and at 800°C new pearlite begins to form (which results in similar ductility to specimens tested at 500°C and 600°C).

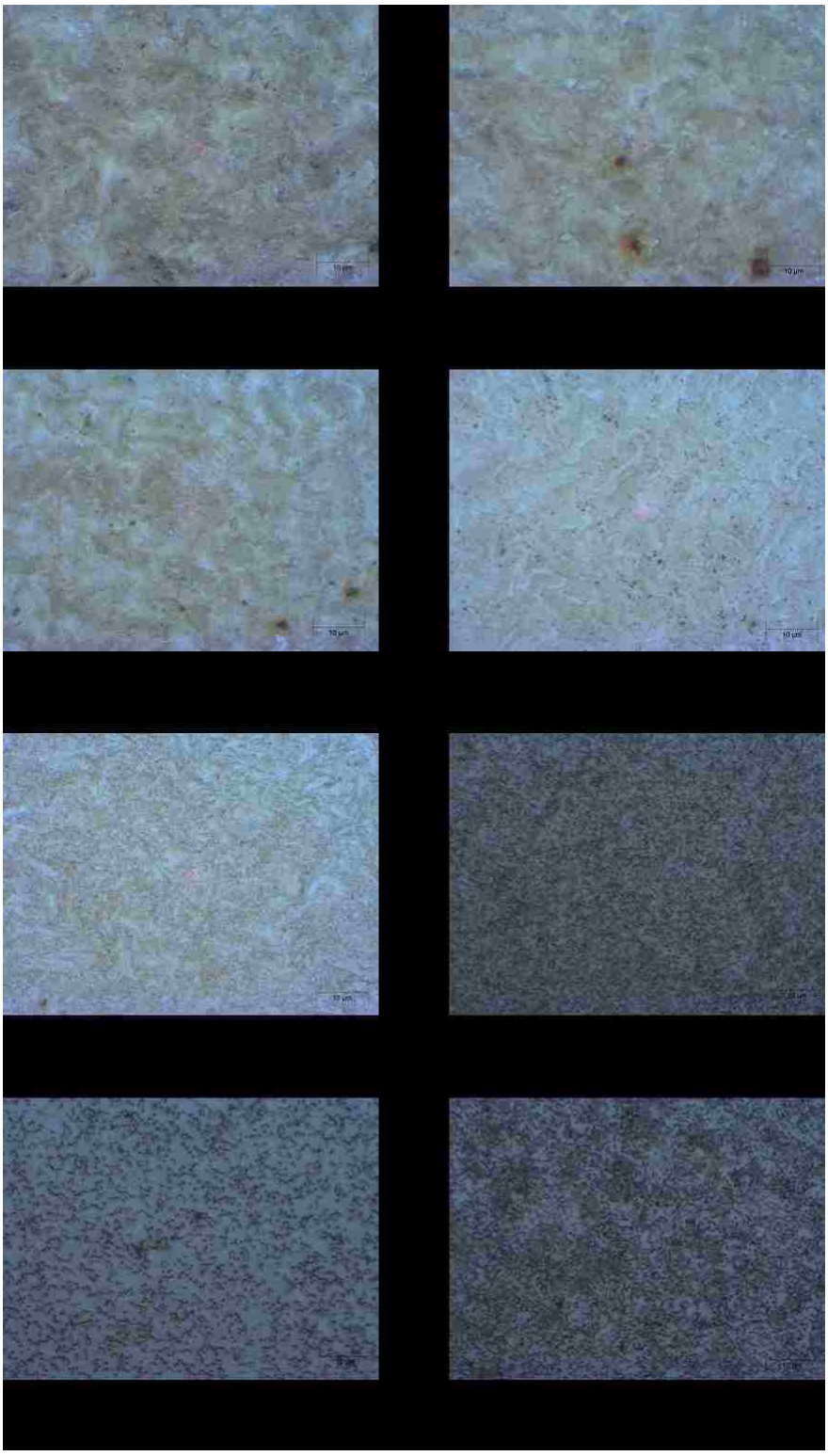

Figure 103: Microstructure Analysis

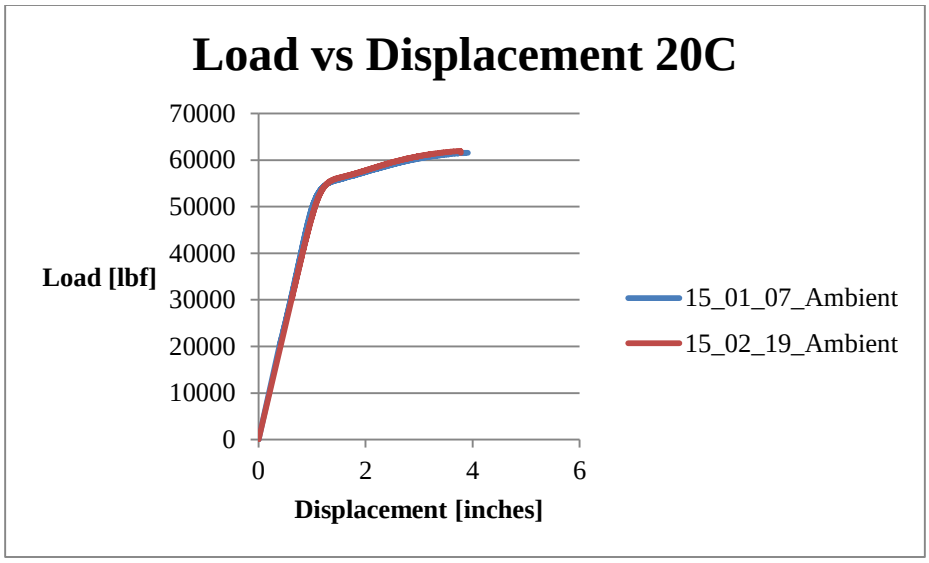

Figure 104: Load-displacement 20C Shifted

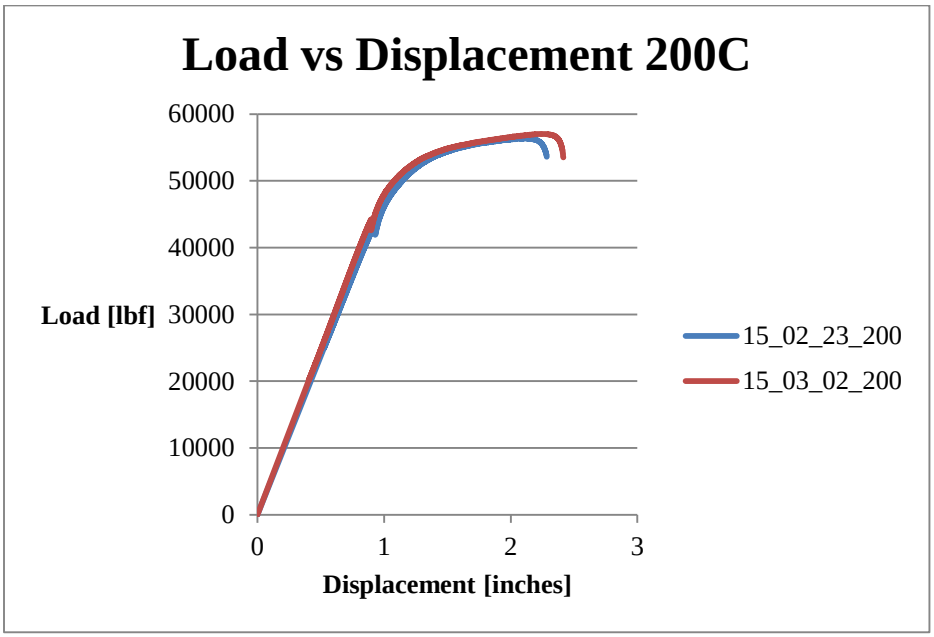

Figure 105: Load-displacement 200C Shifted

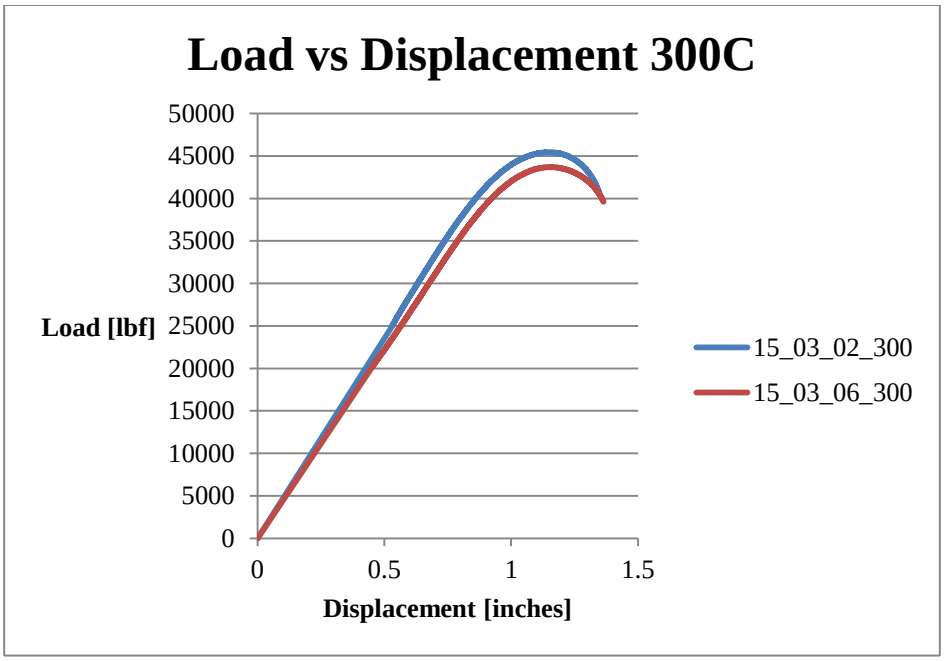

Figure 106: Load-displacement 300C Shifted

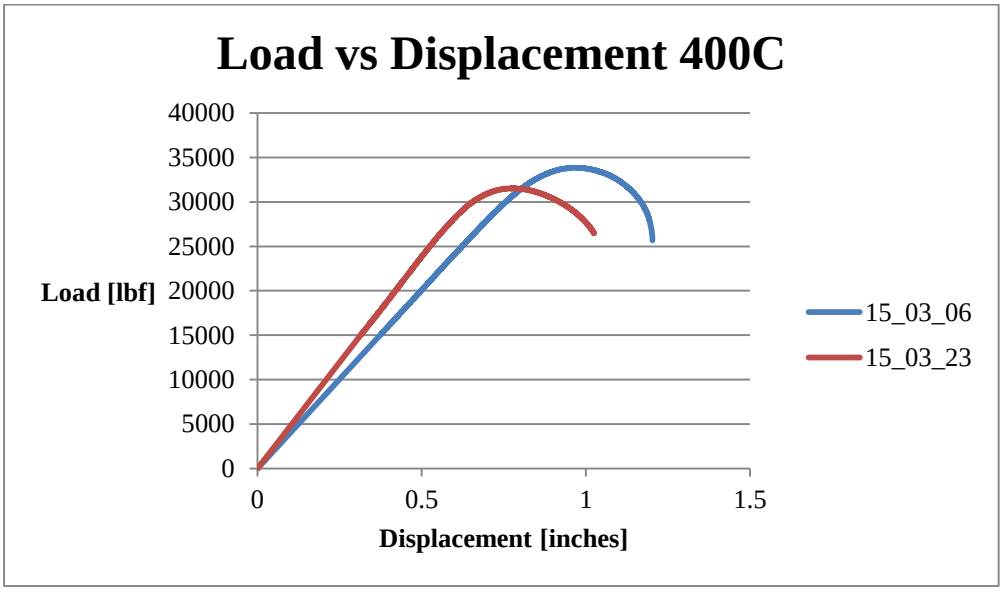

Figure 107: Load-displacement 400C Shifted

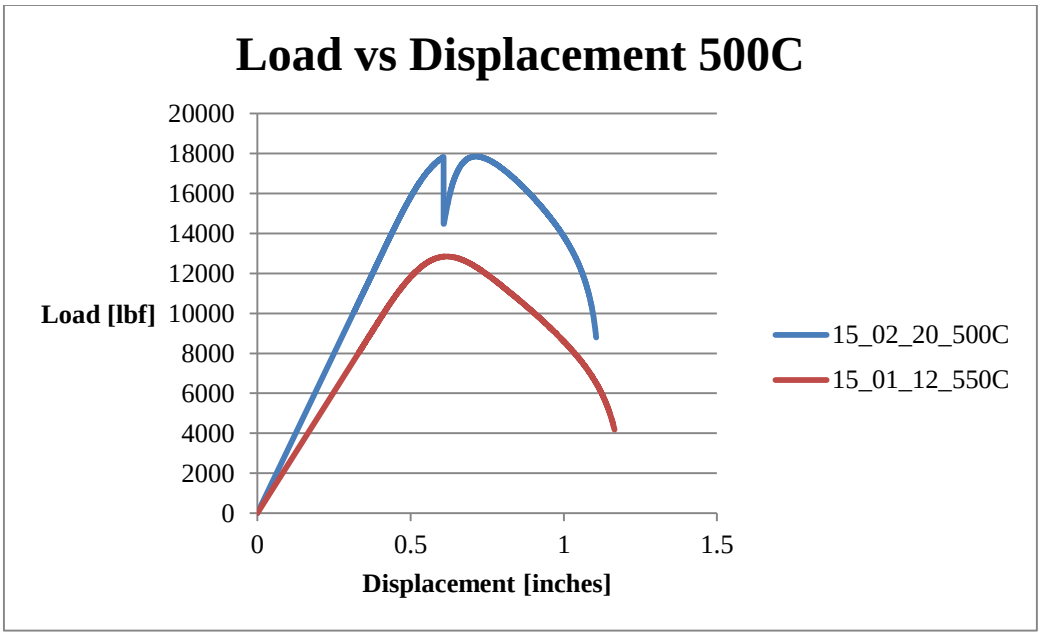

Figure 108: Load-displacement 500C Shifted

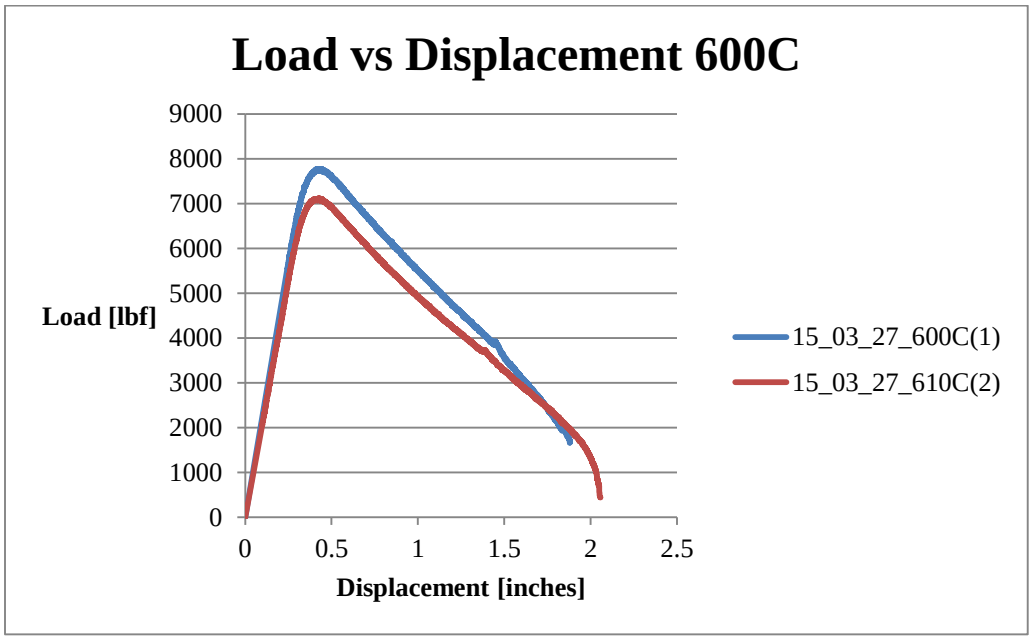

Figure 109: Load-displacement 600C Shifted

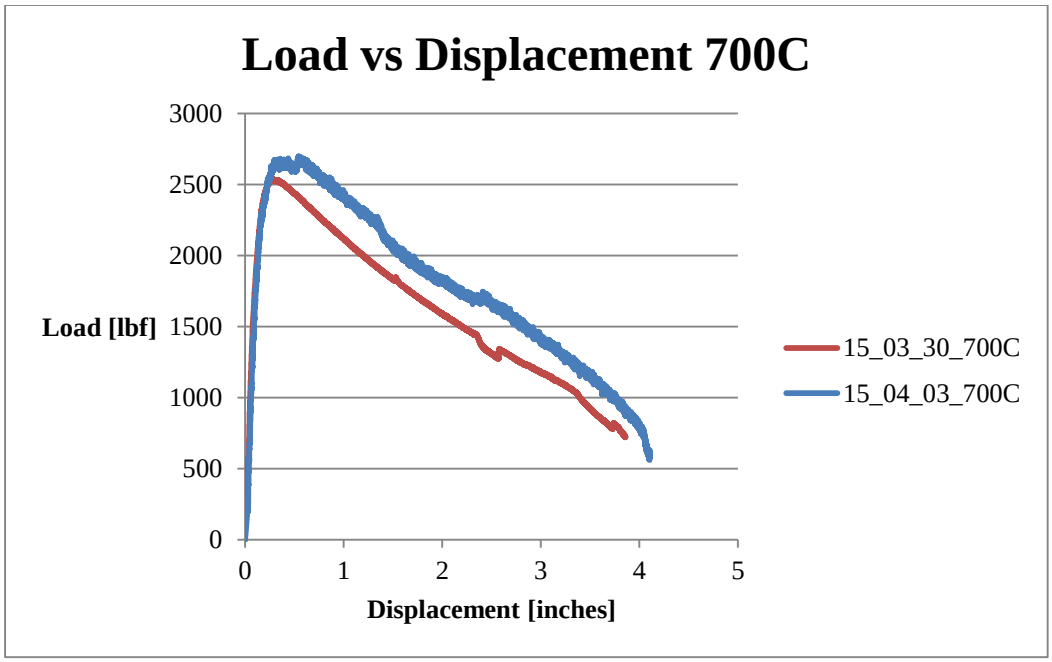

Figure 110: Load-displacement 700C Shifted

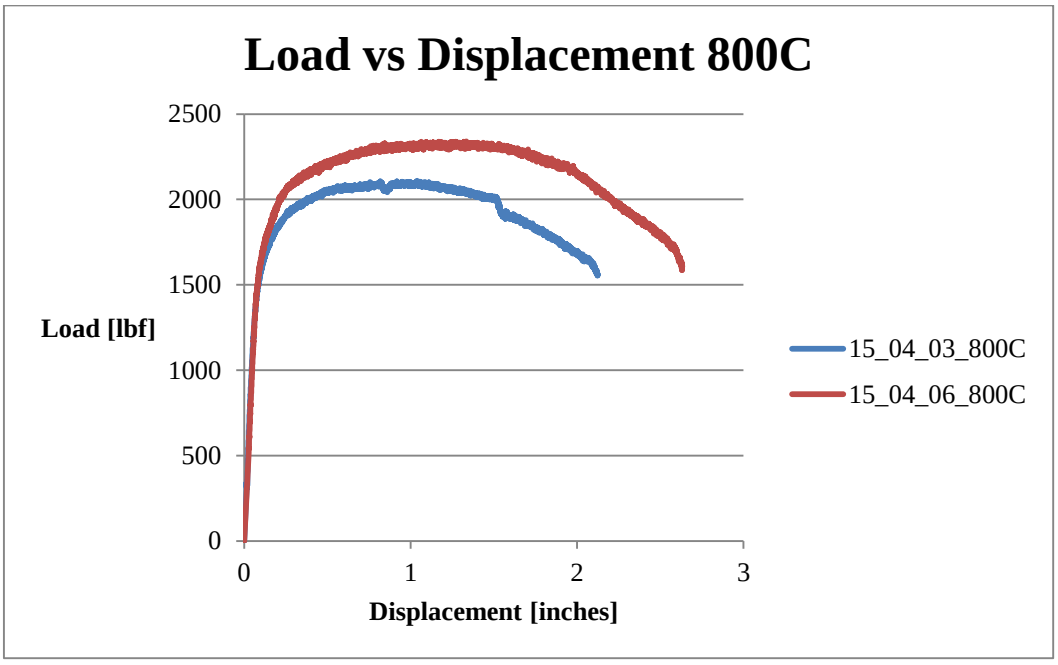

Figure 111: Load-displacement 800C Shifted

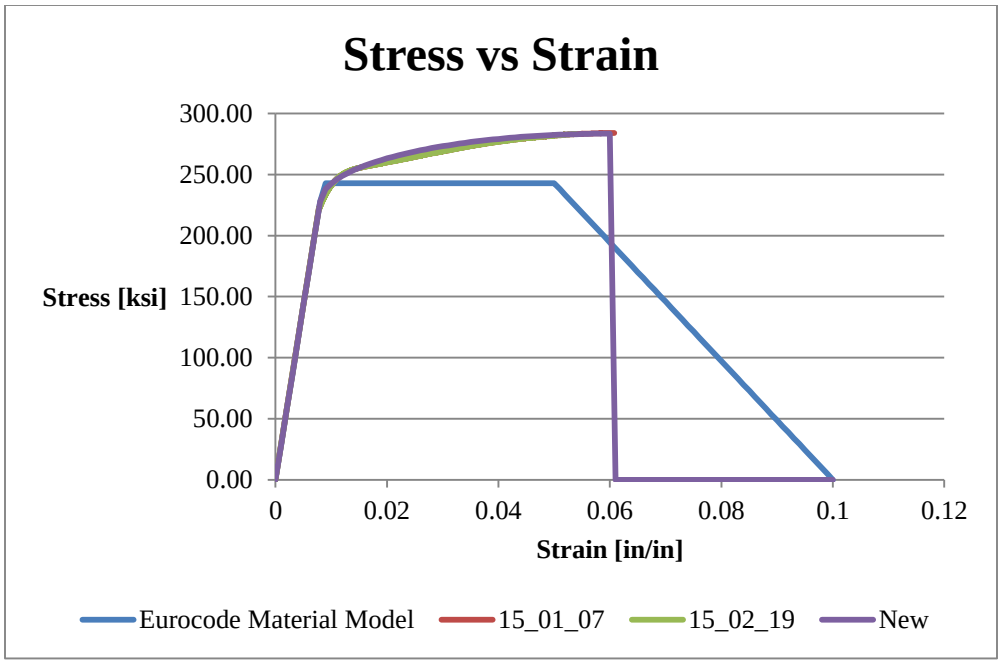

Figure 112: Eurocode Model-Stress/Strain Comparison 20C

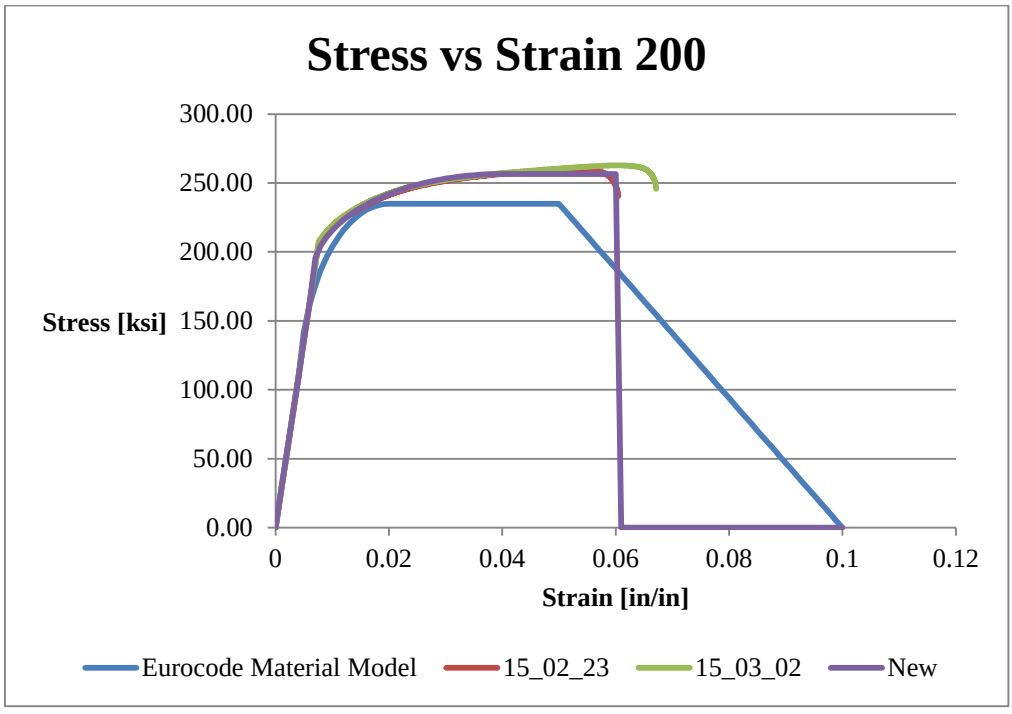

Figure 113: Eurocode Model-Stress/Strain Comparison 200C

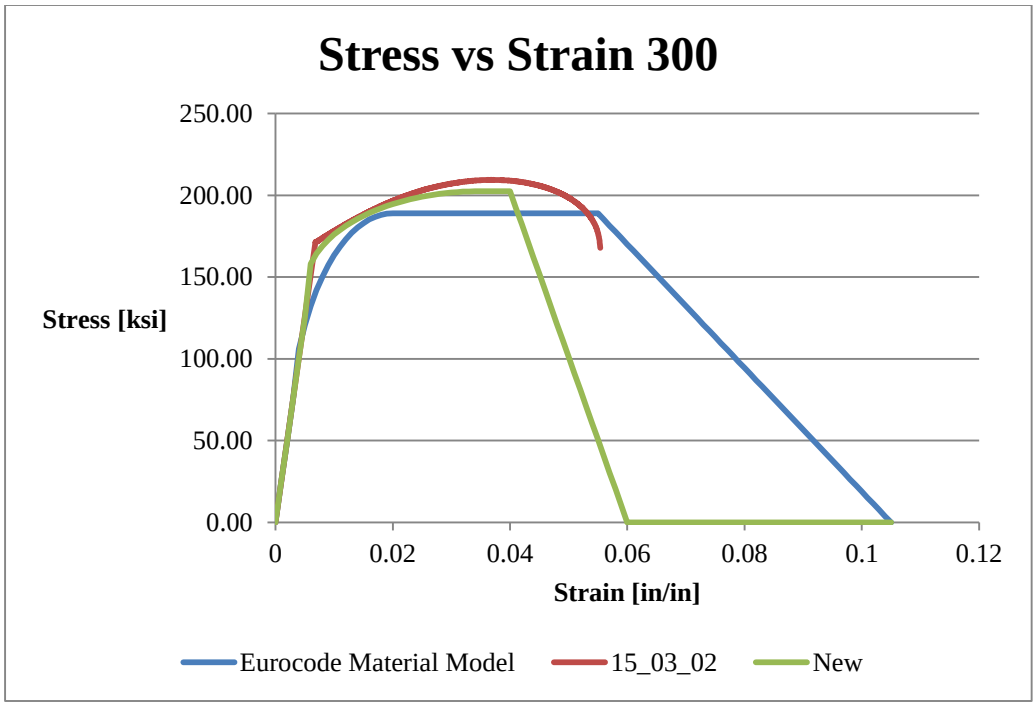

Figure 114: Eurocode Model Stress/Strain Comparison 300C

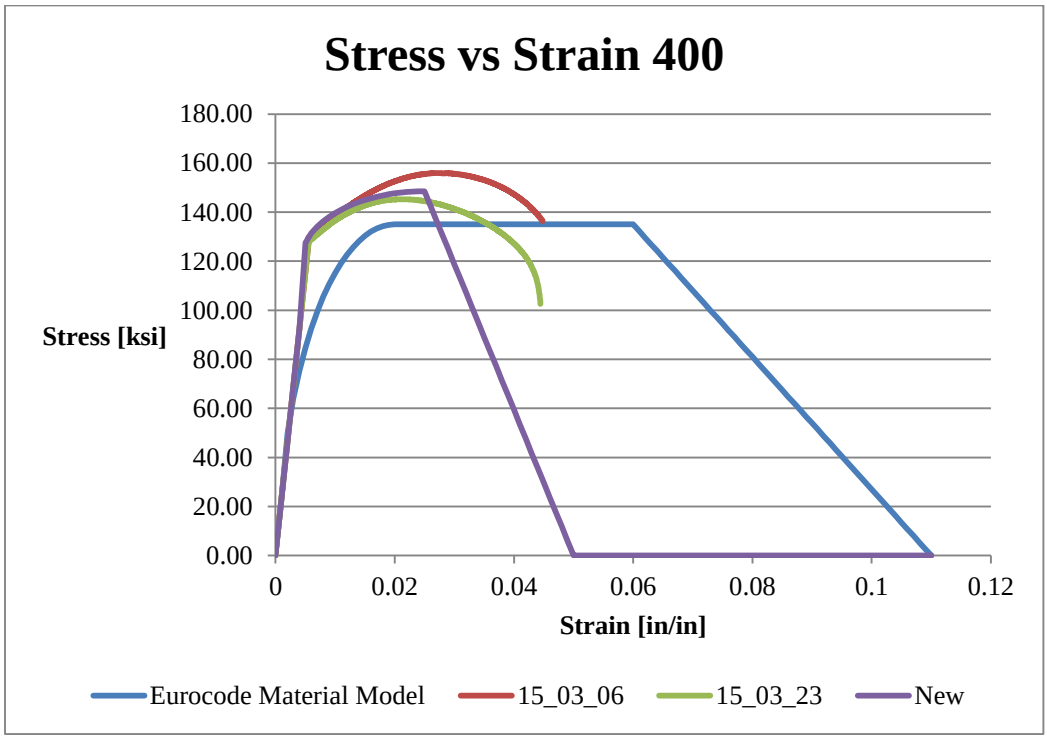

Figure 115: Eurocode Model Stress/Strain Comparison 400C

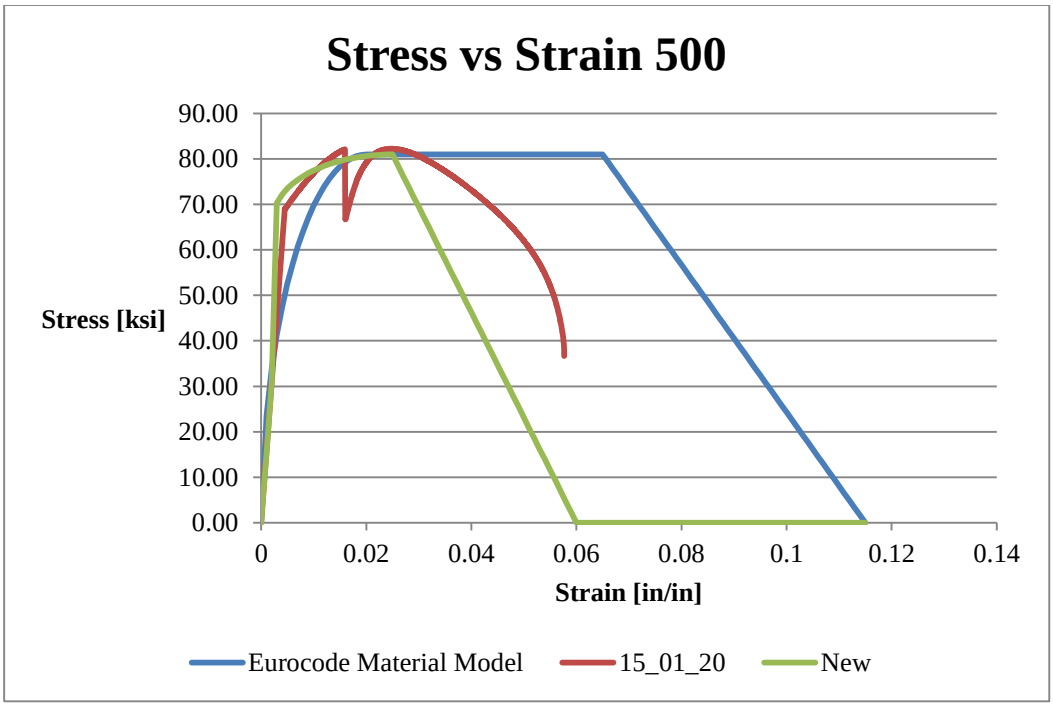

Figure 116: Eurocode Model Stress/Strain Comparison 500C

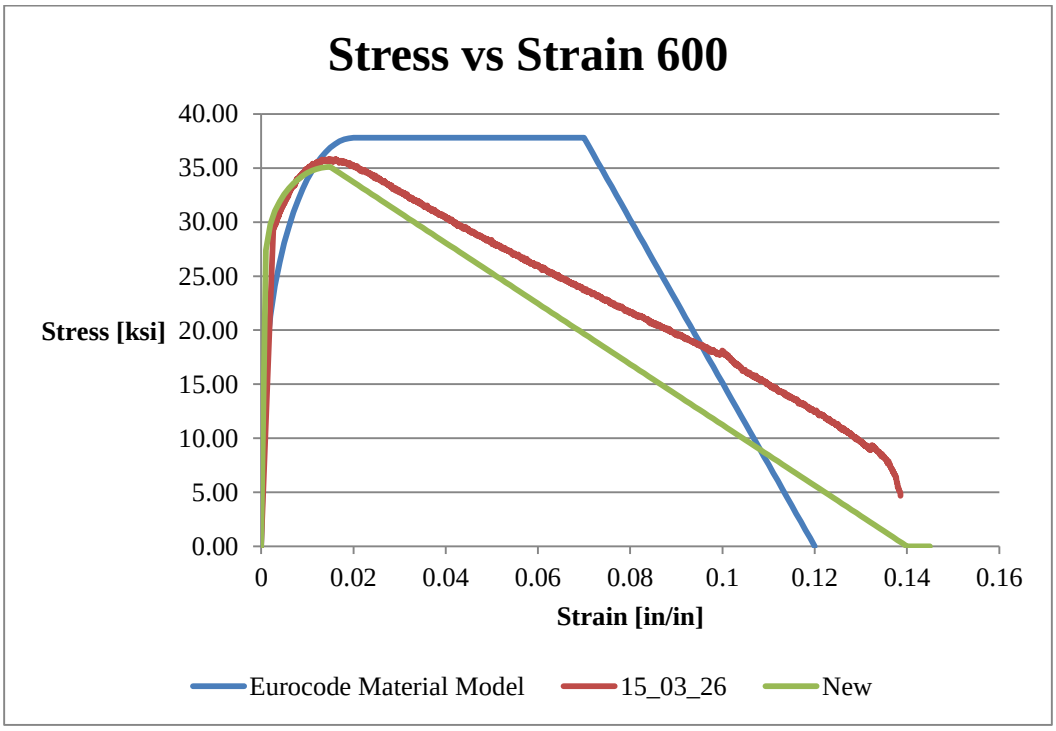

Figure 117: Eurocode Model Stress/Strain Comparison 600C

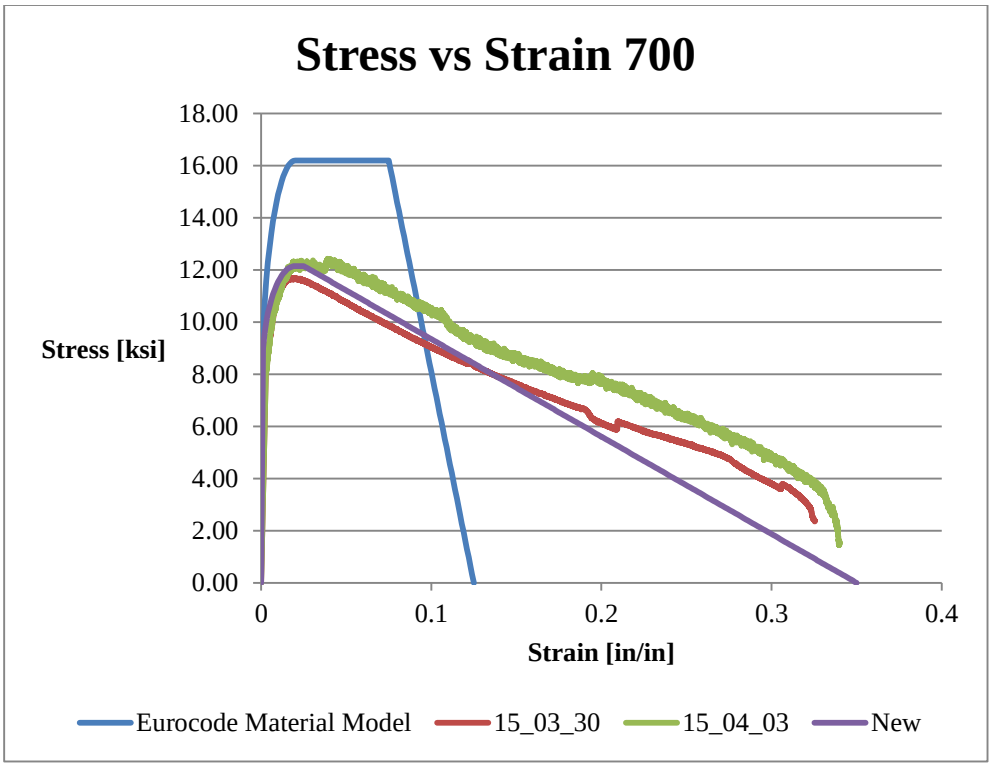

Figure 118: Eurocode Model Stress/Strain Comparison 700C

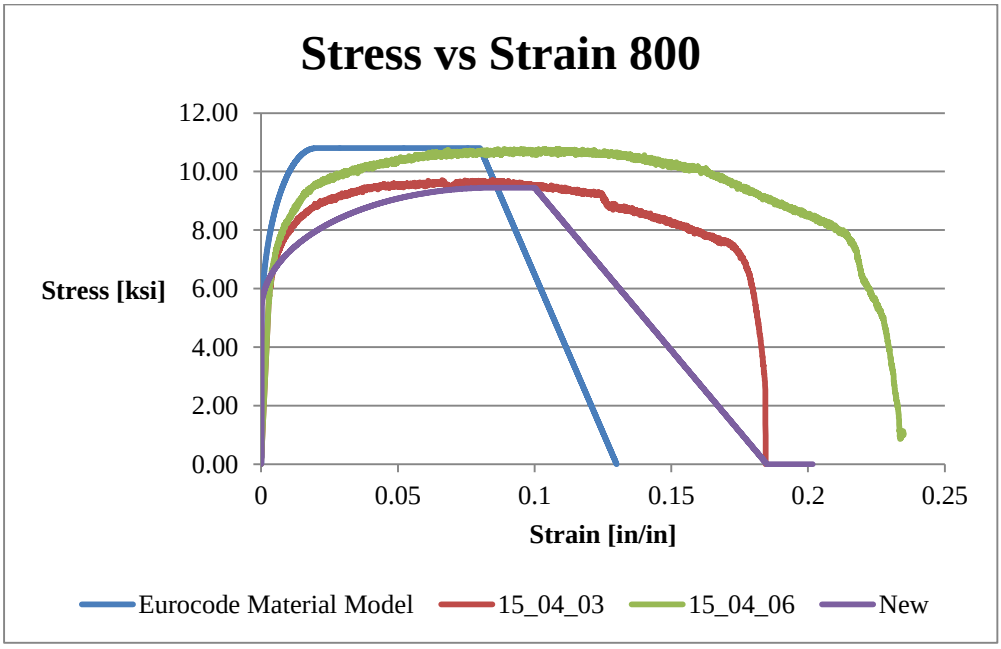

Figure 119: Eurocode Model Stress/Strain Comparison 800C

Chapter 6 Summary, Conclusions, and Recommendations

6.1 General

This chapter presents an overview of the experimentation and results from the laboratory testing performed at Lehigh University's ATLSS Lab. Conclusions are drawn from the test program and recommendations are made for future work.

6.2 Summary

The goals of this project were to:

1. Create a repeatable test program
2. Determine the mechanical properties of 7-wire strand
3. Determine the effect of the heating rate during a transient temperature test
4. Investigate the microstructure of the steel strand after cooling from elevated temperature

To accomplish the goals a literature review was conducted to determine the methods used in past studies on this topic. A test matrix was created based on the literature review and the available testing equipment at Lehigh University.

Testing was carried out using a 600 kip SATEC universal testing machine and an Instron SF-16 split tube ceramic furnace. 0.6 inch diameter 7-wire strand manufactured by SWPC were gripped using custom built aluminum grips. Three types of tests were carried out: constant temperature, transient temperature, and elastic modulus. The basic set-up for each test was identical. The 7-wire strand was placed in the testing machine using the aluminum grips. The strand was loaded to approximately 1%

MUTS to keep the strand taut. Four type-K thermocouples were used to record the temperature data, and the load cell and cross head displacement of the universal testing machine were used to capture the load-displacement data. A Campbell Scientific CR9000X data acquisition system recorded the data. 7-wire strand is known to rupture in a violent manner. In order to protect the fragile ceramic furnace tiles a stainless steel pipe machined and placed around the cable during testing.

The constant temperature test was carried out by heating the strand to an elevated temperature (200^{o}C through 800^{o}C at intervals of 100^{o}C) and holding the temperature for 30 minutes. After the 30 minute thermal soak, the strand was tensioned until rupture. The maximum strength at temperature was recorded and the load-displacement curves were used to develop stress-strain curves at elevated temperature. Observations were made in regards to the failure surface, heat-tinting, ductility, and behavior of the strand at rupture. Once the strand was cooled to room temperature, samples were cut and labeled for microstructure analysis. Scanning electron microscopy was carried out at the Material Science Department at Lehigh University in order to determine any changes to the microstructure at elevated temperature.

In the transient temperature test, the 7-wire strand was restressed to typical service level loads for cable-stay bridge design (45% MUTS) and for post-tensioned concrete construction (70% MUTS). Once the strand was loaded to the prescribed load, the furnace was turned on and the stress was maintained throughout the test. The temperature was increased until the strand ruptured. The rupture temperature was recorded and the thermocouple data was used to determine the strand heating rate. Tests were carried out at slow heating rates (5-9^{o}C/minute) and fast heating rates (18-26^{o}C/minute). The rupture temperature at stress level was compared to the constant temperature ultimate strength curves. Observations during testing included the failure surface, ‘suddenness’ of rupture, necking of non-rupture strands, and behavior of the strand at rupture.

The elastic modulus test required two string pot displacement sensors in order to measure the deformation inside the heated zone. Slotted rods were attached to the strand using circular clamps. The clamps were surrounded by temperature resistant fabric in order to ensure a proper grip on the strand. The slotted rods were located approximate 1 inch and below the furnace. The string pots were placed on the bottom head of the universal testing machine and attached to one of the slotted rods. This set-up created a gauge length that was approximately the height of the furnace. The strand was then heated to the desired temperature, heat-soaked for 30 minutes, and then placed in tension. During the testing, attempts were made to keep the load below the proportional limit. The load-displacement data was analyzed to create the stress-strain relationship and to determine the elastic modulus at elevated temperature. There were no observations made during the elastic modulus testing.

Microstructure analysis was carried out at Lehigh University. Samples were cut from the constant temperature test specimens in order to determine any changes to the microstructure due to elevated temperature. The samples were taken from the strand after it returned to room temperature.

The results from the constant temperature were compared to both the ACI 216 and Eurocode reduction values for cold-drawn steel at elevated temperature. The current study showed good agreement with both reduction models for ultimate strength. The transient temperature testing results show that at slower heating rates, the constant temperature test data is a good predictor of the ultimate strength. When the heating rate was increased from ~6-9ºC/minute to ~20-25ºC/minute the constant temperature prediction of ultimate strength was conservative and the rupture temperature was approximately 40ºC above the predicted value. The elastic modulus test provided reduction values for the modulus at elevated temperature. The results generally compared well with the Eurocode reduction values for mild and cold-drawn steel.

6.3 Conclusions

The conclusions based on the test results are presented in this section.

6.3.1 Constant Temperature Tests

The mechanical properties of cold-drawn steel are significantly affected by increased temperature. The cold-drawing process gives the 7-wire strand high-strength properties at room temperature; however, that same process makes the strand more susceptible to high temperature than mild steel. The data collected during the laboratory testing strongly agrees with the ACI-216 curve for the percentage of ultimate strength at elevated temperature. When plotted, percentage of ultimate strength as a function of temperature forms an S-shaped curve. The strength is relatively unaffected at 200ºC, and the strength begins to decline rapidly at 300ºC. At 700ºC the curve flattens out almost all of the room temperature strength is removed.

6.3.2 Transient Temperature Tests

When the ultimate strength data is normalized with respect to the MUTS, this new curve provides a good prediction of the rupture temperature of strands held at constant stress. For slower heating rates, the rupture temperature was approximately equal to the predicted temperature. When the heating rate was increased, the rupture temperature also increased. The rupture was also found to be sudden for both slower and faster heating rates.

A heat transfer analysis was conducted using a 2-D approach. The 2-D HTA confirmed that the temperature is approximately uniform throughout the cross section for a heating rate of ~25ºC/minute. This led to the use of a lumped mass approach in a 1-D HTA. A MATLAB script was created and

matched the results obtained through an ABAQUS HTA. This heat transfer analysis ruled out the possibility that non-uniform temperature throughout the cross section led to the increase in ultimate strength. It is more likely that the rupture temperature, along with the reduction of mechanical properties, is a time-dependent property based on the degree of recovery in the cold-drawn steel.

6.3.3 Elastic Modulus Tests

It was difficult to measure the elastic modulus without using a proper strain gauge. The results did trend with the Eurocode reduction factors for cold-drawn steel. The Eurocode reduction factors were found to be conservative. The testing also demonstrated that at higher temperatures, above 700^{o}C, the steel strand has an extremely low proportional limit, increasing the difficulty to precisely measure the modulus.

6.4 Recommendations

Based on the results of the study the following recommendations are made:

- Engineers should continue to use the ACI 216 curve for reduction of ultimate strength as a function of temperature. The current study agrees with the data from Abrams and Cruz 1961 test.
- The Dynamic increase factor for cable loss due to fire should be reevaluated
    - The PTI Recommendations for Stay Cable Design, Testing, and Instillation, 6th Ed (2012) suggests using a dynamic increase factor of 0.0 for cable loss due to fire. The manual states that cable loss due to fire is a gradual process. The results of this study show that this may only apply for certain temperature ranges, and cable failure will be sudden and violent for others.

- A simple one-dimensional heat transfer analysis is accurate for the 0.6 inch diameter 7-wire strand. A lumped mass approach is an adequate approximation for the heat transfer analysis at relatively fast rates of heat increase.
- The Eurocode model for cold-drawn steel found in Eurocode 2 part 1-2 does not accurately model the behavior of ASTM A416 grade 270 ksi cold-drawn 7-wire strand. New parameters have been proposed to modify the existing Eurocode model for stress-strain behavior of cold-drawn steel strand.

The current study has also demonstrated need for further work:

- Repeat the current study using other types of bridge cables, including ASTM A586 structural-strand
- Conduct a microstructure analysis on the transient test specimens
- Measure the elastic modulus of the strand during the constant temperature testing rather than during a separate suite of tests
- Investigate a high-temperature strain gauge that will work for multi-wire steel strand
- Include more thermocouples to ensure that the temperature across the gauge length is the desired temperature

Works Cited

Abrams, M.S. & Cruz, C.R. (1961). "The behavior at high temperature of steel strand for prestressed concrete." *Journal of the PCA Research and Development Laboratories*, 3(3), 8-19.

ACI (2014), *ACI 216.1-07/TMS-0216-07: Code requirements for determining fire resistance of concrete and masonry construction assemblies*, American Concrete Institute, Farmington Hills, Michigan, USA.

AISC (2011). *Steel Construction Manual 14th Edition.* American Institute of Steel Construction, Chicago, IL.

ASTM (2010). *A421 / A421M-10, Standard Specification for Uncoated Stress-Relieved Steel Wire for Prestressed Concrete*, ASTM International, West Conshohocken, PA, <www.astm.org>

ASTM (2012). *A416 / A416M-12a, Standard Specification for Steel Strand, Uncoated Seven-Wire for Prestressed Concrete*, ASTM International, West Conshohocken, PA, <www.astm.org>

ASTM (2013). *A931 / A931M-08, Standard Test Method for Tension Testing of Wire Ropes and Strand*, ASTM International, West Conshohocken, PA, <www.astm.org>

ASTM (2014). *E119-14, Standard Test Methods for Fire Tests of Building Construction and Materials*, ASTM International, West Conshohocken, PA, <www.astm.org>

Atienza, J., and Elices, M. (2009). "Behavior of prestressing steels after a simulated fire: Fire-induced damages." *Construction and Building Materials*, 23(8), 2932-2940.

Bramfitt, B. L., and Arlan O. Benscoter. (2001). *Metallographer's Guide: Practice and Procedures for Irons and Steels.* ASTM International, West Conshohocken, PA, <www.astm.org>

Callister, W., and Rethwisch, D. (2008). *Fundamentals of materials science and engineering*. 3rd Ed. Wiley, Hoboken, N.J.

DeGarmo, E., Black, J., and Kohser, R. (1988). *Materials and processes in manufacturing*. Macmillan Pub. Co., New York.

CEN (2004) .*Eurocode 2: Design of Concrete Structures: Part 1-2: General rules - Structural fire design.* British Standards Institution.

Franssen J.M., Zaharia R., (2005) *Design of Steel Structures subjected to Fire, Background and Design Guide to Eurocode 3*, University of Liège, Belgium.

Gales, J., Bisby, L., MacDougall, C., and MacLean, K. (2009). "Transient high-temperature stress relaxation of prestressing tendons in unbonded construction." *Fire Safety Journal*, 44(4), 570-579.

Garlock, M., Paya-Zaforteza, I., Kodur, V., and Gu, L. (2012). "Fire hazard in bridges: Review, assessment and repair strategies." *Engineering Structures*, 35, 89-98.

Gross, J.L. and Cauffman, S.A. (2011). "Bridges: The next generation of experimental research in structural fires." *Proceedings of the 27th US-Japan Bridge Engineering Workshop*.

Harmathy, T.Z. and Stanzak, W.W. (1970). “Elevated-temperature tensile and creep properties of some structural and prestressing steels.” *ASTM STP-464: Fire Test Performance*, 186-208.

Hertz, K. (2004). “Reinforcement data for fire safety design.” *Magazine of Concrete Research*, 56(8), 453-459.

Holmes, M., Anchor, R.D, Cook, G.M.E, and Crook, R.N. (1982) “The effects of elevated temperatures on the strength properties of reinforcing and prestressing steels.” *The Structural Engineer*, 60(1), 7-13.

IBC. (2012). *2012 International Building Code.* International Code Council,Inc, Country Club Hills, IL.

MacLean, K.J.N., Bisby, L.A., MacDougall, C.C. (2008). “Post-fire deterioration and prestress loss in steel tendons used in post-tensioned slabs.” *ACI SP-255: Designing Concrete Structures for Fire Safety*, pp. 147-174.

Neves, I., Rodrigues, J., and Loureiro, A. (1996). “Mechanical Properties of Reinforcing and Prestressing Steels after Heating.” *Journal of Material Science and Civil Engineering*, 8(4), 189–194.

NFPA (2011). *NFPA 502: Standard for Road Tunnels, Bridges, and other Limited Access Highways*, 2011 edition, National Fire Protection Association, Quincy, MA.

PTI (2006). *Post-Tensioning Manual, 6th Ed*, Post-Tensioning Institute Phoenix, AZ.

PTI (2012). *Recommendations for Stay Cable Design, Testing, and Instillation, 6th Ed*, Post-Tensioning Institute, Phoenix, AZ.

Preston, H. K. (1990). "Testing 7-Wire Strand for Prestressed Concrete – State of the Art," *PCI Journal*, 30(3), pp. 134-155.

Quiel, S.E., Garlock, M.E.M. (2010) "Closed-form prediction of the thermal and structural response of a perimeter column in a fire." *Open Construction Build Technology Journal*, 4, pp. 64–78.

SWPC (2015). "Production Preocess for ASTM A416 Low-Relaxtion PC Strand." *Sumiden Wire Products Corporation*, <http://www.sumidenwire.com> (June 18, 2015).

Zoli, T.P. & Steinhouse, J. (2007). "Some considerations in the design of long span bridges against progressive collapse." *Proceedings of the 23th US-Japan Bridge Engineering Workshop*.

Appendix 1: MATLAB FEM Program

Thermal Analysis

```
%This matlab code is used to determine the time temperature history of
%steel cable in an electric furnace
%Metric units used
%Result is a plot of the time temperature history



%User input locations:
% Furnace Input
%   Includes set temperature and heating rate

close all;
clear all;
clc;
```

Furnace Constants

```
To=20; %ambient temeprature
Furnace_Begin=0.4;   %Height from cable end to bottom of furnace
Furnace_Height=0.30;
Furnace_End=Furnace_Begin+Furnace_Height;  %location of the top
```

Furnace Input

```
TDesired=520;  %Final furnace temperature | Celsius
HEATRATE=20;% Heating rate of furnace | oC/minute
EndTime=3300; %End of heating in seconds
```

Thermal Properties

```
h_cold_air=4; %Convection coefficeint room air | units [W/(m^2*K)]
h_hot_air=20; %Convection coefficeint furnace air  These values form Table 3-1 (Franssen and
Zaharia 2005)
p=7850; %mass density of steel | units [kg/m^3]
ksh=1.0; %Correction factor for shadow effect see page 49 (Franssen and Zaharia 2005)
```

```
emiss=0.7; % Surface emissivity of steel
SBc=5.67*10^-8; %Stephan Boltzmann constant units [W/(m^2*K^4)]
ABZero=-273;    %Abosulte zero, used to convert C to K
```

Geometric Properties of Cable

```
%User Defined
N_elems=250;          %Number of elements
Lo=1.5;             %Total length [m]
Le=Lo/N_elems;        %Element length using equal subdivisions
r=6.679*10^-03;       %equivalent cable radius [m]

%Constant
A=pi()*r^2;           %Equivalent cross sectional area [m^2]
Pe=2*pi()*r;          %Perimeter of element [m]
V=Le*A;               %volume [m^3]
Am=Pe*Le;             %Surface area [m^2]
Am_V=Am/V;            %Surface Area to volume parameter [m^-1]
```

Finite Element Analysis

```
% Nodal Coordinates
Nodes=zeros(N_elems+1,2); %allocates Nodal matrix
N_nodes=length(Nodes);
Nodes(1,:)=[0,0];
if N_elems>1;
    for i=2:N_elems+1
        Nodes(i,:)=Nodes(i-1,:)+[Le,0];
    end
end

%Defining heated zone
for i=1:N_elems;
    Elems(i,:)=[i,i+1];
    if Nodes(Elems(i,1),1)>Furnace_Begin && Nodes(Elems(i,2),1)<Furnace_End
            con_coef(i)=h_hot_air;
    else
            con_coef(i)=h_cold_air;
   end
end


% Heat Transfer Analsysis
%the applied heat is based on the desired furnace and heat rate
%Initial Parameters
inc=1;
```

```
int=2;
t(1)=0;


To=To-ABZero;
T_Furnace(1)=To;
TDesired=TDesired-ABZero;

T_Applied(:,1)=To*ones(N_elems,1);
c(:,1)=S_heat(To)*ones(N_elems,1);




dt=.1; %Time step for integration in secods
while T_Furnace<TDesired
    t(int)=t(int-1)+dt;
    T_Furnace(int)=T_Furnace(int-1)+HEATRATE*dt/60;

    for i=1:N_elems %For loop determines if the element is inside the furnace and then
assigns furnace temperature
        if Nodes(Elems(i,1),1)>Furnace_Begin && Nodes(Elems(i,2),1)<Furnace_End
               T_Applied(i,int)=T_Furnace(int);
        else T_Applied(i,int)=To;
        end
    end
    int=int+inc;
end
Heated_Time=t(int-1)/60; %Time required to heat furnace to desired temp


% Determining element heat
T_elems(:,1:2)=To*ones(N_elems,2);
for j=2:40000
    int=int+inc;
    t(j)=t(j-1)+dt;
    if t(j)>EndTime
        t(j)=[]; % Break added an extra time step
        j=j-1; % Break in for loop added additional +1 to j
        break
    end
    if t(j)>=Heated_Time*60
        for i=1:N_elems %For loop determines if the element is inside the furnace and then
assigns furnace temperature
        if Nodes(Elems(i,1),1)>Furnace_Begin && Nodes(Elems(i,2),1)<Furnace_End
               T_Applied(i,j)=TDesired;
        else T_Applied(i,j)=To;
        end
        end
    end
  for i=1:N_elems
    c(i,j)=S_heat(T_elems(i,j-1));
```

```
    K(i,j)=Thermal_Con(T_elems(i,j-1));
    h_rad(i,j)=emiss*SBc*(T_Applied(i,j)^4-T_elems(i,j-1)^4);
    h_conv(i,j)=con_coef(i)*(T_Applied(i,j)-T_elems(i,j-1));
    if i==1
        h_cond(i,j)=A*K(i,j)*(-T_elems(i,j-1)+T_elems(i+1,j-1))/Le;
        %|Units Joules/Sec=W
    elseif i~=1 && i~=N_elems
        h_cond(i,j)=A*K(i,j)*((T_elems(i-1,j-1)-T_elems(i,j-1))+(T_elems(i+1,j-1)-
T_elems(i,j-1)))/Le;
    elseif i==N_elems
        h_cond(i,j)=A*K(i,j)*(T_elems(i-1,j-1)-T_elems(i,j-1))/Le;
    end

    h_net(i,j)=(h_rad(i,j)+h_conv(i,j)); %net heat flux convection and radiation | Units
[W/m^2]
    dT(i,j)=(h_net(i,j)*Am+h_cond(i,j))/(c(i,j)*p*V)*(t(j)-t(j-1));  %Change in temperature |
Units [C/K]
    T_elems(i,j)=T_elems(i,j-1)+dT(i,j);
  end
  Tfinal=T_elems(:,j);
  f=i;
end



T_elems=T_elems+ABZero;  %Back to C

%Determine which element is at the center of furnace
hottest=T_elems(1,j);
for i=1:N_elems
    if T_elems(i,j)>hottest
        hottest=T_elems(i,j);
        hot=i;
    end
    height(i,1)=(Nodes(i,1)+Nodes(i+1,1))/2; %Element height, used later
end


%Plot temperature time history
figure
plot(t,T_elems(hot,:))
hold on
ylabel('Element Temperature [oC]')
xlabel('Time [sec]')
title('Temperature-Time History')


%Plot Temperature along height

figure
plot(T_elems(:,j),height)
title('Cable Temperature')
```

```
ylabel('Height [m]')
xlabel('Temperature [oC]')
```

Specific Heat

```
%Function used to determine the temperature dependent specific heat of steel
%Units return in [J/kgK] Temperature input in Celsius
%(Franssen and Zaharia 2005) Annex I, I.1.2
%Data from Eurocode 3
function [c]=S_heat(T_elems)


T_elems=T_elems-273; %Convert to C

if T_elems<600
    c=425+0.773*T_elems-1.69*10^-3*T_elems^2+2.22*10^-6*T_elems^3;
elseif 600<=T_elems && T_elems<735
    c=666+13002/(738-T_elems);
elseif 735<=T_elems && T_elems<900
    c=545+17820/(T_elems-731);
elseif T_elems>=900
    c=650;
end
```

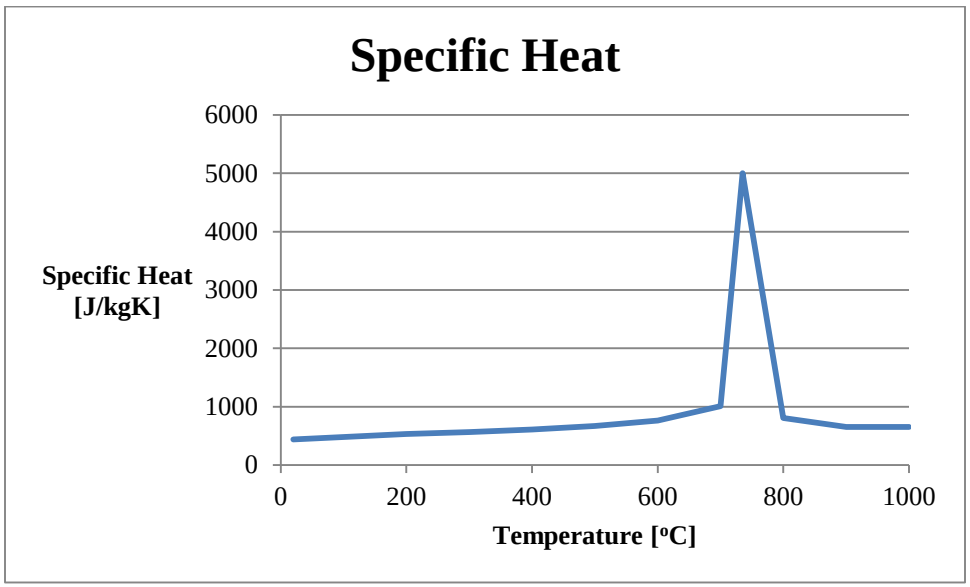

Thermal Conductivity

```
%Function used to determine the temperature dependent thermal conductivity
%Input units of K |output  units [W/mK]
%(Franssen and Zaharia 2005) Annex I, I.1.1
%Data from Eurocode 3
function [K]=Thermal_Con(T_elems)

T_elems=T_elems-273; %Convert to C

if T_elems<800
    K=54-T_elems/30;
elseif 800<=T_elems
    K=27.3333;
end
```

Published with MATLAB® R2014a

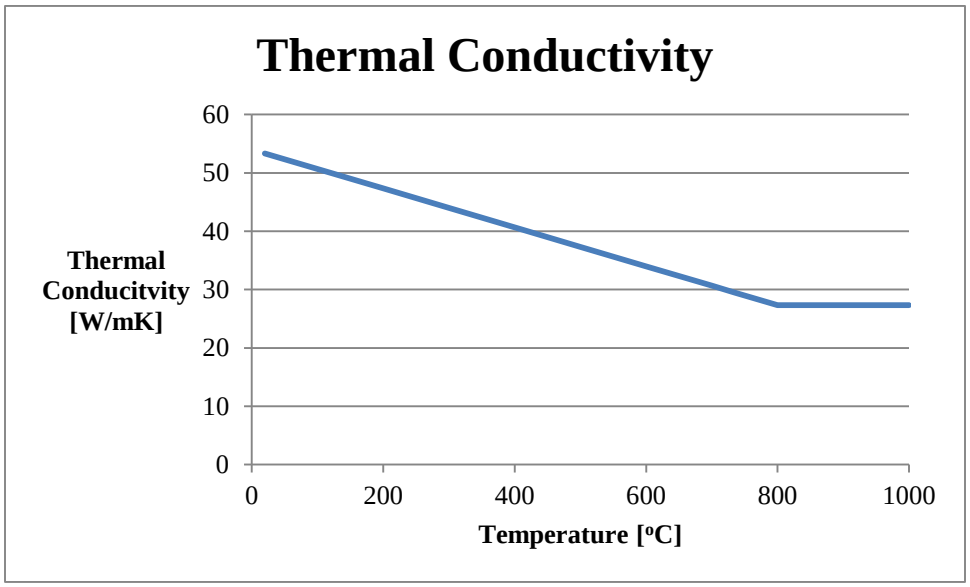

Appendix 2: Microstructure Results

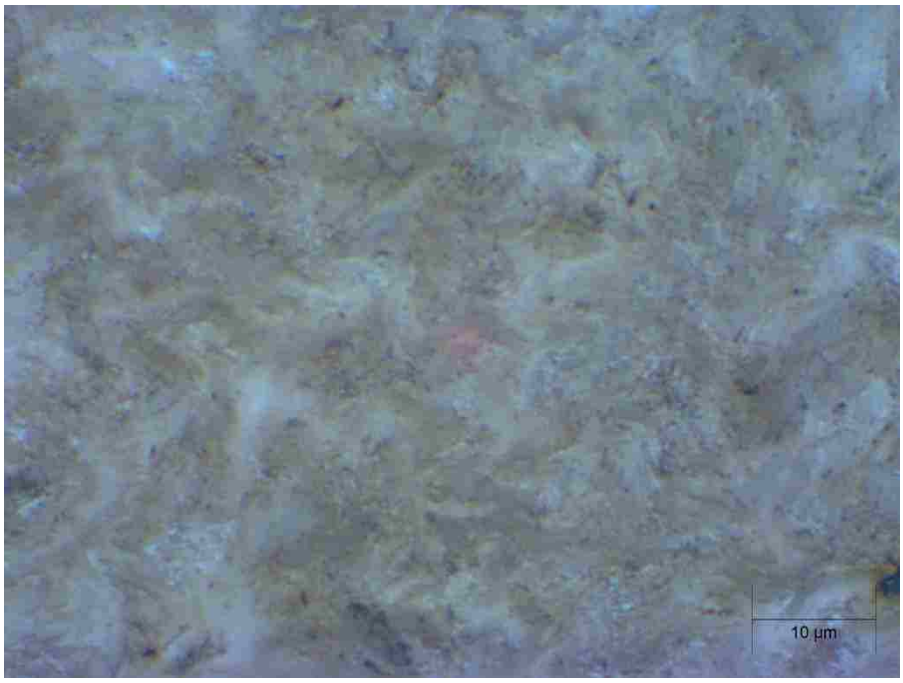

Figure 120: Microstructure of 20ºC Sample

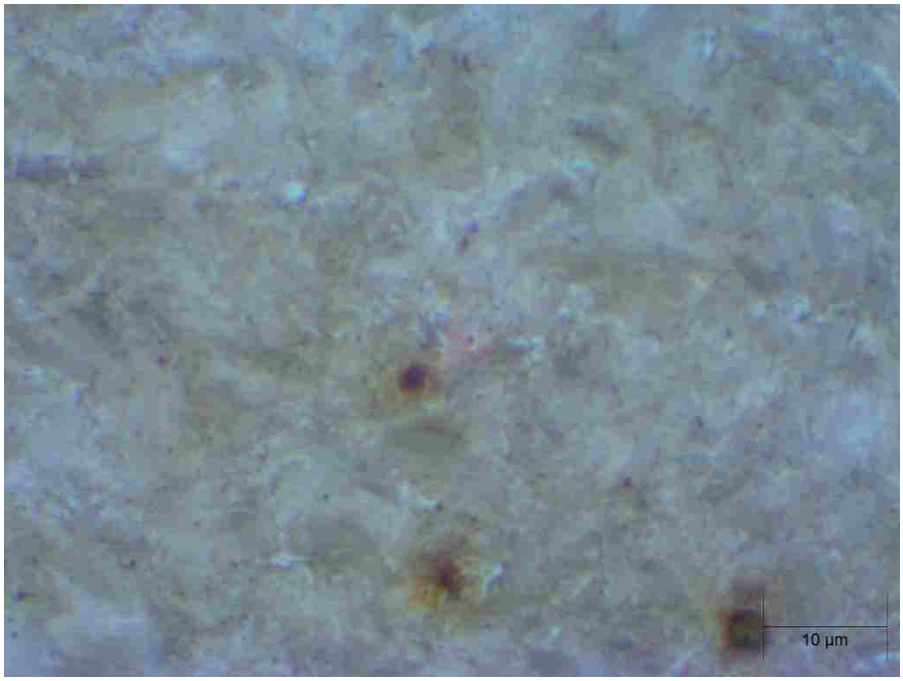

Figure 121: Microstructure of 200ºC Sample

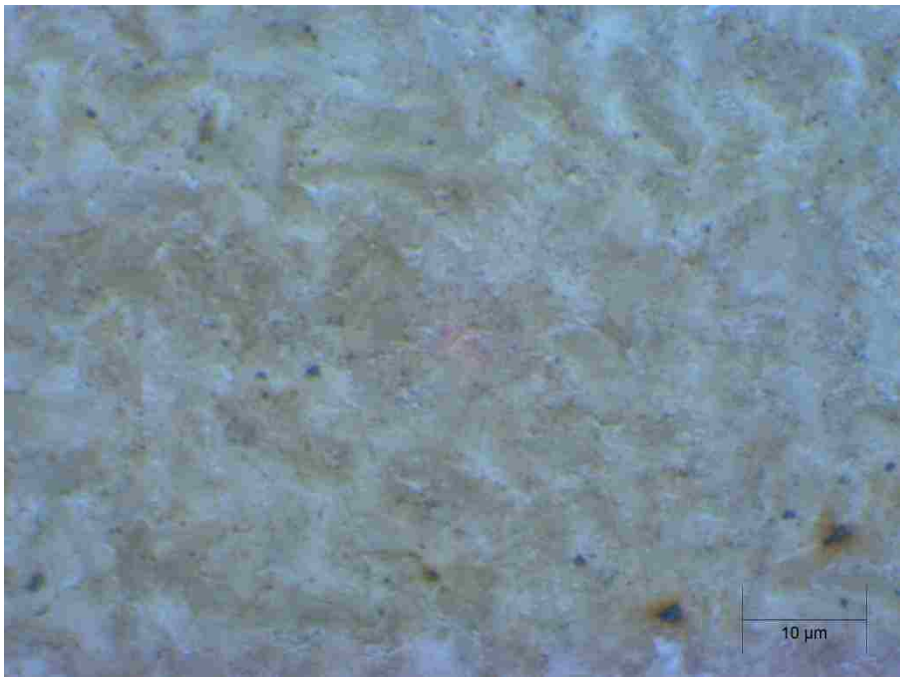

Figure 122: Microstructure of 300ºC Sample

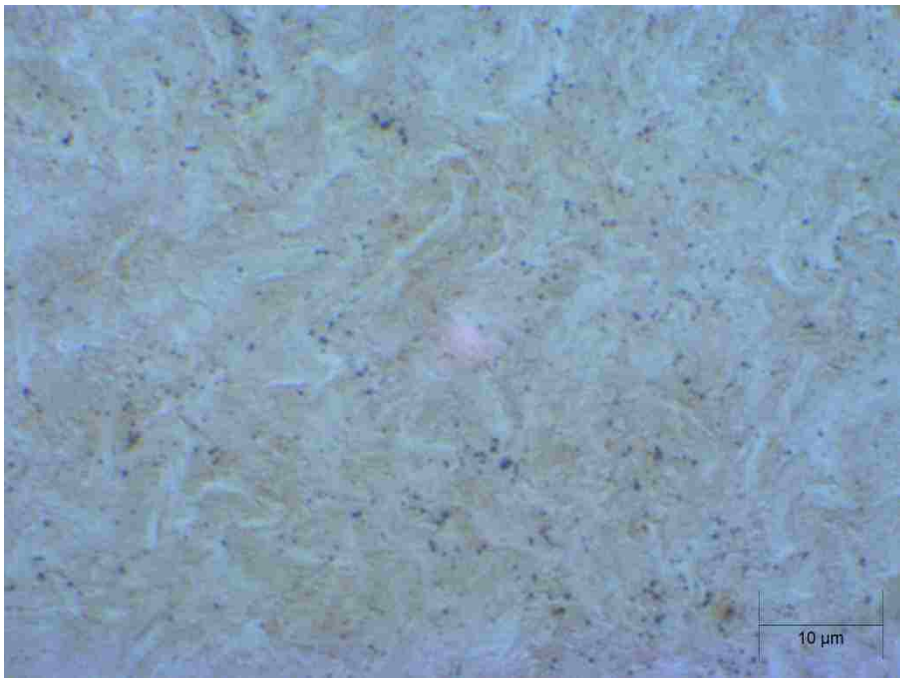

Figure 123: Microstructure of 400ºC Sample

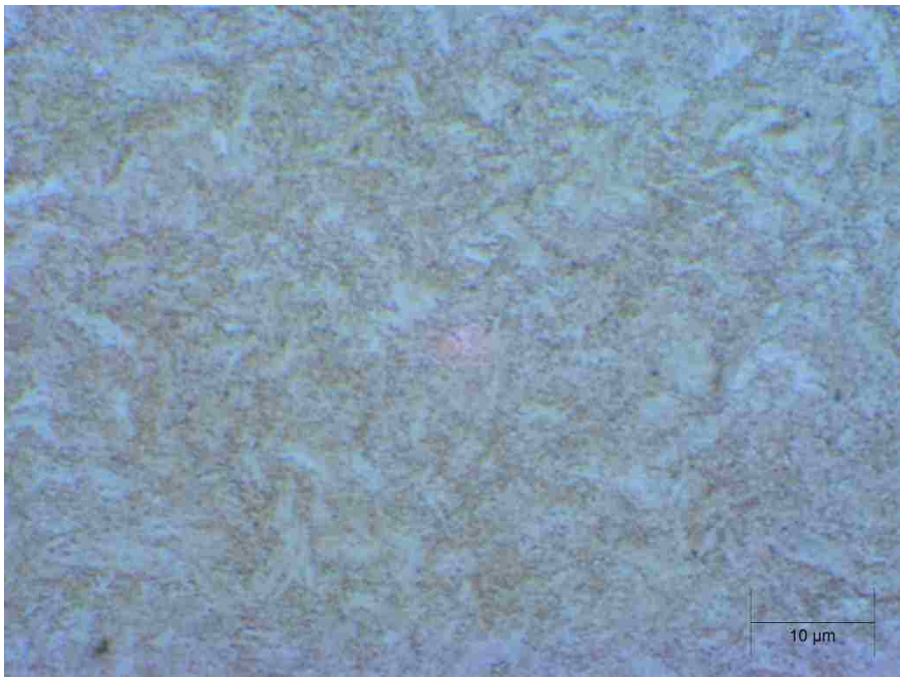

Figure 124: Microstructure of 500ºC Sample

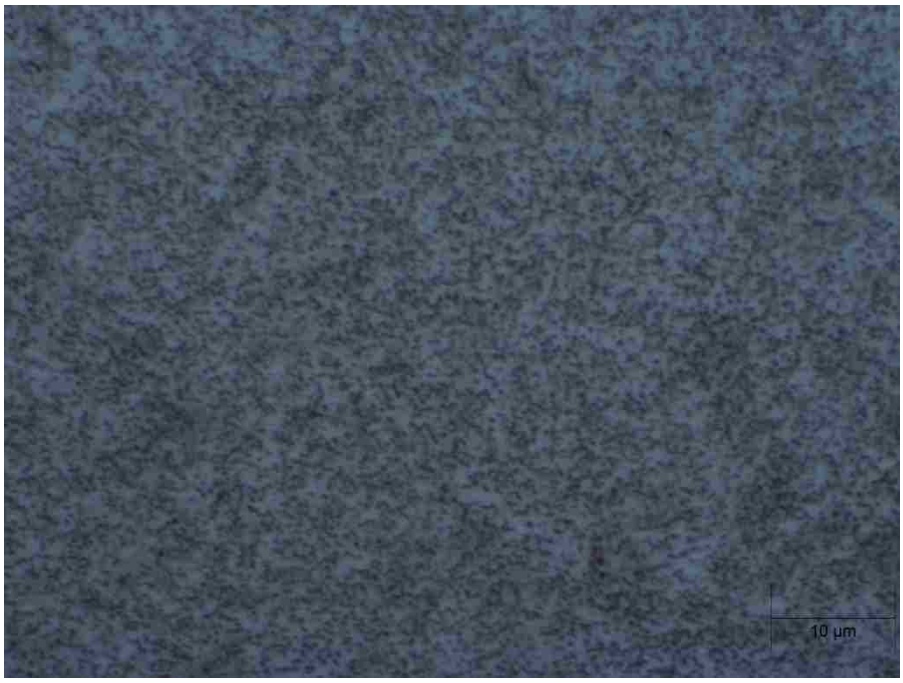

Figure 125: Microstructure of 600ºC Sample

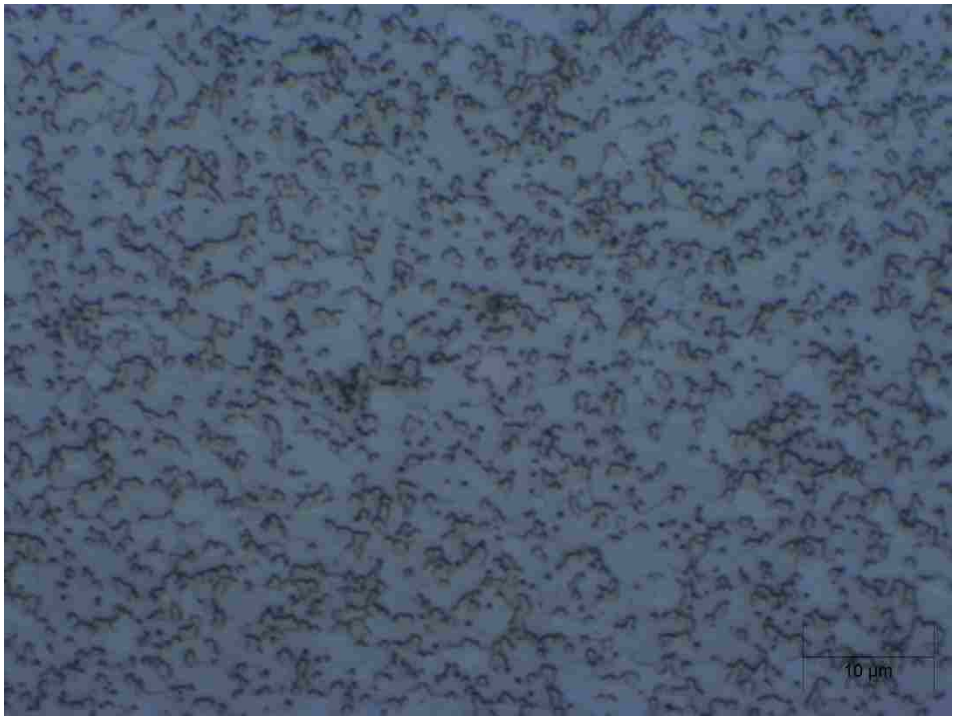

Figure 126: Microstructure of 700ºC Sample

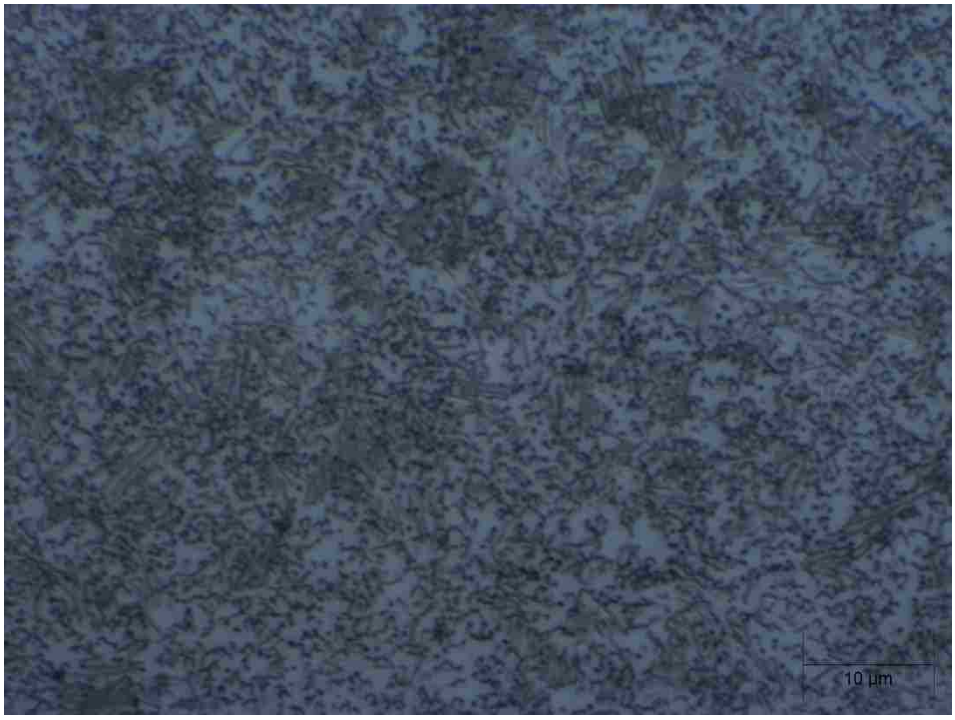

Figure 127: Microstructure of 800ºC Sample

Vita

Conor Thompson, son of Drs. William and Kathleen Thompson, was born December 9th 1991 in Somerset, Pennsylvania. He graduated summa cum laude from Lehigh University in May 2014 with a Bachelor of Science Degree in civil engineering. He will graduate with a Master of Science Degree in structural engineering from Lehigh University in September 2015. After graduation he plans to move to Philadelphia and will begin working at Thornton Tomasetti.